INSTITUTE OF AERONAUTICAL ENGINEERING

(Autonomous)
Dundigal, Hyderabad -500 043

AEROSPACE ENGINEERING

COURSE LECTURE NOTES

Course Name	**ADVANCED COMPUTATIONAL AERODYNAMICS**
Course Code	BAEB05
Programme	M.Tech
Semester	I
Course Coordinator	Ms. D. Anitha, Assistant Professor
Course Faculty	Ms. D. Anitha, Assistant Professor
Lecture Numbers	1-45
Topic Covered	All

COURSE OBJECTIVES (COs):

The course should enable the students to:	
I	Explain the concept of panel methods, analyze various boundary conditions applied and demonstrate several searching and sorting algorithms.
II	Describe the initial methods applied in the process of CFD tools development their advantages and disadvantages over modern developed methods.
III	Demonstrate different methods evolved in analyzing numerical stability of solutions and evaluate the parameters over which the stability depends and their range of values.
IV	Understand advanced techniques and methods in time marching steps and identify different boundary conditions for different cases in CFD techniques.

COURSE LEARNING OUTCOMES (CLOs):

Students, who complete the course, will have demonstrated the ability to do the following:

S. No	Description
BAEB05.01	Understand the concept of flux approach and its formulations.
BAEB05.02	Explain the Euler equations for the aerodynamic solutions computationally.
BAEB05.03	Emphasize on basic schemes to solve the differential equations.
BAEB05.04	Understand the stability of the solution by time dependent methods.
BAEB05.05	Explain the implicit methods for the time dependent methods to solve computationally.

Source from Computational Fluid Mechanics and Heat Transfer by Tannehill John C, Anderson Dale A, Pletcher Richard H

BAEB05.06	Develop the approximate factorization schemes for time dependent methods.
BAEB05.07	Illustrate to apply concepts of discretization and its application for implicit difference equation.
BAEB05.08	Distinguish implicit and explicit discretization and differentiation equations for the stability of solution.
BAEB05.09	Explain the flow gradients at boundaries of unstructured grids.
BAEB05.10	Understand the concept of philosophy of method of characteristics
BAEB05.11	Explain supersonic nozzle design using method of characteristics.
BAEB05.12	Differentiate the domain of dependence and range of influence.
BAEB05.13	Understand the basic formulation and boundary conditions.
BAEB05.14	Explain the reduction of a problem to a set of linear algebraic equations.
BAEB05.15	Discuss the preliminary considerations prior to establishing numerical solution.

SYLLABUS

Unit-I	NUMERICAL SOLUTIONS
Euler equations: Flux approach, Lax-Wendroff method, basic principles of upwind schemes, flux vector splitting, Steger Warming flux vector splitting, Van Leer flux vector splitting, Upwind reconstruction, evolution, Godunov's first order upwind method, Roe's first order upwind method.	
Unit-II	**TIME DEPENDENT METHODS**
Stability of solution, explicit methods, FTFS, FTCS, FTBS, Leapfrog method, Lax method. Implicit methods: Euler's FTCS, Crank Nicolson method, description of Lax- Wendroff scheme, McCormack two step predictor corrector methods, description of time split methods, approximate factorization schemes.	
Unit-III	**BOUNDARY CONDITIONS**
Boundary Layer Equations: Setting up the boundary layer equations, flat plate boundary layer solution, boundary layer transformations, explicit and implicit discretization, solution of the implicit difference equations, integration of the continuity equation, boundary layer edge and wall shear stress, Keller-box scheme. Concept of dummy cells, solid wall inviscid flow, viscous flow, farfield concept of characteristic variables, modifications for lifting bodies inlet outlet boundary, injection boundary, symmetry plane, coordinate cut, periodic boundaries, interface between grid blocks, flow gradients at boundaries of unstructured grids.	
Unit-IV	**METHOD OF CHARACTERISTICS**
Philosophy of method of characteristics, determination of characteristic lines, two dimensional irrotational flow, determination of compatibility equations, unit processes, supersonic nozzle design by the method of characteristics, supersonic wind tunnel nozzle, minimum length nozzles, domain of dependence and range of influence.	
Unit-V	**PANELMETHODS**
Basic formulation, boundary conditions, physical considerations, reduction of a problem to a set of linear algebraic equations, aerodynamic loads, preliminary considerations prior to establishing numerical solution, steps toward constructing a numerical solution, solution of thin airfoil with lumped vortex filament, accounting for effects of compressibility and viscosity.	
Text Books:	
1. Tannehill John C, Anderson Dale A, Pletcher Richard H, "Computational Fluid Mechanics and Heat Transfer", Taylor & Francis, 2nd Edition, 1997. 2. Chung T G, "Computational Fluid Dynamics", Cambridge University Press, 2nd Edition, 2010. 3. Katz Joseph and Plotkin Allen, "Low-Speed Aerodynamics", Cambridge University Press, 2nd Edition, 2006.	

Reference Books:
1. Anderson J D, “Modern Compressible Fluid Flow”, McGraw Hill 2nd Edition, 1990. 2. Anderson J D, “Fundamentals of Aerodynamics”, Tata McGraw Hill, 5th Edition, 2010. 3. Anderson J D, “Computational Fluid Dynamics”, McGraw Hill, 1995. 4. Rathakrishnan E, “Gas Dynamics”, Prentice-Hall India, 2004.

UNIT - I
NUMERICAL SOLUTIONS

Euler Equations

Euler equations For incompressible flow the inviscid 1D Euler equations decouple to:

$$\rho_t + u\rho_x = 0$$

$$u_t + \frac{p_x}{\rho} = 0$$

$$e_t + ue_x = 0$$

The 3D Euler equations are given by

$$\begin{pmatrix} \rho \\ \rho u \\ \rho v \\ \rho w \\ E \end{pmatrix}_t + \begin{pmatrix} \rho u \\ \rho u^2 + p \\ \rho uv \\ \rho uw \\ (E+p)u \end{pmatrix}_x + \begin{pmatrix} \rho v \\ \rho uv \\ \rho v^2 + p \\ \rho vw \\ (E+p)v \end{pmatrix}_y + \begin{pmatrix} \rho w \\ \rho uw \\ \rho vw \\ \rho w^2 + p \\ (E+p)w \end{pmatrix}_z = 0$$

Solution of the Euler Equations

Formulation

The results of potential flow calculations have proved accurate enough to be used as the basis of the wing design of the latest generation of transport aircraft, such as the Boeing 767 and Airbus A 310. Nevertheless, the assumption of potential flow is not strictly correct when shock waves are present, and this inconsistency must set a limit to the accuracy that could be obtained even if the discretion errors were entirely eliminated.To provide a correct description of inviscid transonic flow we must solve the Euler equations. The widespread use of Euler codes has so far been impeded by large numerical errors (leading, for example, to generation of, spurious vorticity), and excessively slow convergence (often no convergence). Recent developments promise to correct this situation.

The emphasis here will be on the calculation of steady state solutions. While other iterative methods can be conceived, most of the methods so far developed are based on the concept of integrating the equations in time until they reach a steady state.An exterior problem can reach a steady state as a result of the propagation of disturbances away to infinity. This mechanism of convergence by expulsion of errors is effective as long as out- going disturbances are not too strongly reflected back into the interior and boundary conditions must therefore be treated with care.

Since the time dependent terms are used merely as a device for generating an iterative scheme, they may be modified to increase the rate of convergence. The time dependent formulation is similar in principle to the Jacobi method. When applied to Laplace's equation, for example, the Jacobi method is equivalent to integrating the heat equation

$$v_t = v_{xx} + v_{yy}$$

until it reaches a steady state.

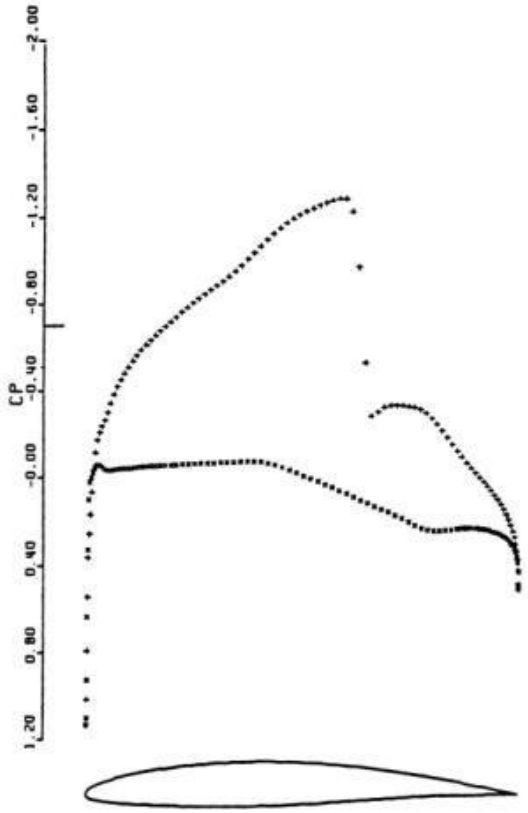

Figure 1.1: Transonic flow solution obtained with 3 multigrid cycles NACA 640410, Mach .720, $\alpha = 0\circ$, CL=.6640, CD=.0031, 192 × 32 grid Residual .58010−6

An advantage of the time dependent formulation is that it brings the problem within the frame work of the mathematical theory of difference methods for hyperbolic equations. Stemming from the early work of Courant, Von Neumann, and Lax, this theory is by now highly developed.

A stability theory for the initial boundary value problem has been formulated and refined by Kreiss, Gustaffson and Sundstrom, and the application of this theory has been worked out for a variety of discretization schemes. Procedures have also been developed for the construction of boundary conditions designed to allow outgoing waves to pass through the outer boundary. The availability of this body of theory provides a solid foundation for the development of codes to treat practical aerodynamic problems.
A special case occurs when the flow is everywhere supersonic. The steady state equations then constitute a hyperbolic system in which the stream wise coordinate plays the role of the time like variable, and the entire flow field can be calculated in a single sweep, marching downstream.

Semi-Discrete Finite Volume Schemes

A convenient way to assure a steady state solution independent of the time step is to separate completely the space and time discretization procedures. In the scheme proposed by Jameson, Schmidt and Turkel one begins by applying a semi-discretization in which only the spatial derivatives are approximated. The resulting ordinary differential equations are then solved by a multi-stage time stepping procedure.

The space discretization scheme can be developed by writing the Euler equations in the integral form. The computational domain is divided into quadrilateral cells denoted by the subscripts *i, j* as, sketched in Figure 1.1

Adaptive Dissipation

The finite volume scheme defined by equations is not dissipative, allowing undamped oscillations with alternate sign at odd and even mesh points. In order to eliminate spurious oscillations, which will be triggered by discontinuities in the solution, one can follow either of two strategies. The first is to begin with a non-dissipative scheme, and to attempt to add just enough dissipation where it is needed to control the tendency to produce spurious oscillations. The second approach is to try to construct a scheme which is guaranteed to prevent oscillations by preserving the monotonicity of an initially monotone profile, typically through the use of one-sided upwind differencing.

In this section I describe an adaptive scheme for adding dissipation which has proved effective in practice. The idea of the adaptive scheme is to add third order dissipative terms throughout the domain to provide a base level of dissipation sufficient to prevent nonlinear instability, but not sufficient to prevent oscillations in the neighborhood of shock waves. In order to capture shock waves additional first order dissipative terms are added locally by a sensor designed to detect discontinuities.

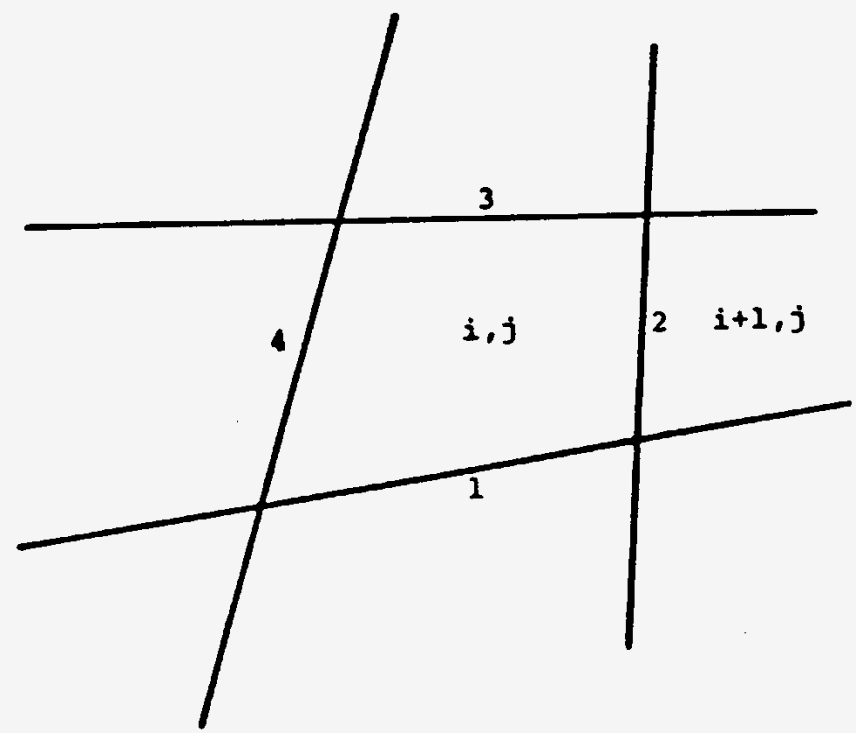

Figure 1.2: Finite Volume Scheme

The Upwind Scheme

Once again, we shall start with the inviscid Burger's equation. Regarding discretization, we can think about the following formulations

$$\frac{\zeta_i^{n+1} - \zeta_i^n}{\Delta t} + u\frac{\zeta_{i+1}^n - \zeta_i^n}{\Delta x} = 0$$

$$\frac{\zeta_i^{n+1} - \zeta_i^n}{\Delta t} + u\frac{\zeta_{i+1}^n - \zeta_{i-1}^n}{2\Delta x} = 0$$

If Von Neumann's stability analysis is applied to these schemes, we find that both are unconditionally unstable.

A well known remedy for the difficulties encountered in such formulations is the upwind scheme which is described by Gentry, Martin and Daly (1966) and Runchal and Wolfshtein (1969).

Eq. can be made stable by substituting the forward space difference by a backward space difference scheme, provided that the carrier velocity *u* is positive. If *u* is negative, a forward difference scheme must be used to assure stability. For full Burger's equation., the formulation of the diffusion term remains unchanged and only the convective term (in conservative form) is calculated in the following way:

$$\frac{\zeta_i^{n+1} - \zeta_i^n}{\Delta t} = -\frac{u\zeta_i^n - u\zeta_{i-1}^n}{\Delta x} + \text{viscous term, for } u > 0$$

$$\frac{\zeta_i^{n+1} - \zeta_i^n}{\Delta t} = -\frac{u\zeta_{i+1}^n - u\zeta_i^n}{\Delta x} + \text{viscous term, for } u < 0$$

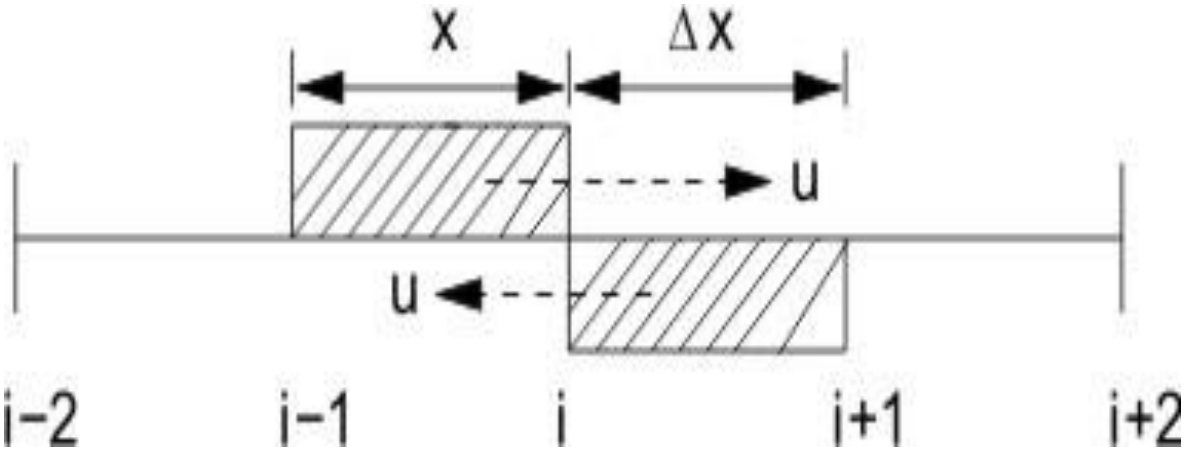

Figure 1.3: The Upwind Scheme

It is also well known that upwind method of discretization is very much necessary in convection (advection) dominated flows in order to obtain numerically stable results.

As such, upwind bias retains transportative property of flow equation. Let us have a closer look at the transportative property and related upwind bias.

On the other hand, there are more advanced spatial discretization schemes, which are constructed by considering the physical properties of the Euler equations. Because they distinguish between upstream and downstream influences (wave propagation directions), they are termed upwind schemes.

They can be roughly divided into four main groups:

- Flux-vector splitting,
- Flux-difference splitting,
- Total variation diminishing (TVD), and
- Fluctuation-splitting schemes.

Each of these is described briefly in the following.

Flux-Vector Splitting Schemes

One class of the flux-vector splitting schemes decomposes the vector of the convective fluxes into two parts according to the sign of certain characteristic variables, which are in general similar to but not identical with the eigenvalues of the convective flux Jacobian. The two parts of the flux vector are then discretized by upwind biased differences. The very first flux-vector splitting schemes of this type were developed in the beginning of the 1980's by Steger and Warming and by Van Leer, respectively.

A second class of flux-vector splitting schemes decompose the flux vector into a convective and a pressure (an acoustic) part. This idea is utilized by schemes like AUSM (Advection Upstream Splitting Method) of Liou et al. or the CUSP scheme (Convective Upwind Split Pressure) of Jameson respectively. Further similar approaches are the Low-Diffusion Flux-Splitting Scheme (LDFSS) introduced by Edwards or the Mach number-based Advection Pressure Splitting (MAPS) scheme of Rossow. The second group of flux-vector splitting schemes gained recently larger popularity particularly because of their improved resolution of shears layers, but only a moderate computational effort. An advantage of the flux-vector splitting schemes is also that they can be quite easily extended to real gas flows, as opposed to flux-difference splitting or TVD schemes. We shall return to real gas simulations further below.

The second group - flux-difference splitting schemes - is based on the solution of the locally one-dimensional Euler equations for discontinuous states at an interface. This corresponds to the Riemann (shock tube) problem. The values on either side of the interface are generally termed as the left and right state. The idea to solve the Riemann problem at the interface between two control volumes was first introduced by Godunov 1741 back in 1950. In order to reduce the numerical effort required for an exact solution of the Riemann problem, approximate Riemann solvers were developed, e.g., by Osher et al. and Roe. Roe's solver is often used today because of its excellent resolution of boundary layers and a crisp representation of shocks. It can be easily implemented on structured as well as on unstructured grids. TVD Schemes The idea of TVD schemes was first introduced by Harten in 1983. The TVD schemes are based on a concept aimed at preventing the generation of new extreme in the flow solution. The principal conditions for a TVD scheme are that maxima must be non-increasing, minima non-decreasing, and no

new local extreme may be created. Such a scheme is called monotonicity preserving. Thus, a discretization methodology with TVD properties allows it to resolve a shock wave without any spurious oscillations of the solution. The TVD schemes are in general implemented as an average of the convective fluxes combined with an additional dissipation term. The dissipation term can either depend on the sign of the characteristic speeds or not. In the first case, we speak of an upwind TVD scheme, in the second case of a symmetric TVD scheme [SO]. The experience shows that the upwind TVD scheme should be preferred since it offers a better shock and boundary layer resolution than the symmetric TVD scheme. The disadvantage of the TVD schemes is that they cannot be easily extended to higher than second-order spatial accuracy. This limitation can be overcome using the EN0 (Essentially Non-Oscillatory) discretization schemes. The last group - the fluctuation-splitting schemes - provides for true multidimensional upwinding. The aim is to resolve accurately also those flow features which are not aligned with the grid. This is a significant advantage over all above upwind schemes, which split the equations according only to the orientation of the grid cells. Within the fluctuation-splitting methodology, the flow variables are associated with the grid nodes. Intermediate residuals are computed as flux balances over the grid cells, which consists of triangles in 2D and of tetrahedral in 3D. The cell-based residuals are then distributed in an upwind-biased manner to the nodes. After that, the solution is updated using the nodal values. In the case of systems of equations (Euler or Navier-Stokes), the cell-based residuals have to be decomposed into scalar waves. Since the decomposition is not unique in 2D and in 3D, several approaches were developed in the past. The variety reaches from the wave model of Roe over the algebraic scheme of Sidilkover to the most advanced characteristic decomposition method. Despite the above mentioned advantage over the dimensionally split Riemann, TVD, etc. solvers, the fluctuation-splitting are so far used only in research codes. This can be attributed to the complexity and the high numerical effort, as well as to convergence problems.

Upwind Differencing, Total Variation Diminishing Schemes, and Flux vector Splitting

It is not easy to simulate a propagating discontinuity by a numerical method. The simplest model of convection is provided by the one dimensional wave equation

$$u_t + u_x = 0$$

This equation can be approximated by the one sided scheme

where λ is the Courant number $\Delta t/\Delta x$.

This scheme is stable for $0 < \lambda < 1$ and it is appealing for two reasons:

- It simulates the physical process of wave propagation by looking back- wards along the direction of propagation: if $\lambda = 1$, it exactly represents propagation along characteristics.

- It has the property of preserving the monoticity of an initially mono- tone profile: this excludes the possibility of generating an overshoot behind a shock wave.

These observations have motivated numerous studies of one sided schemes, dating back to the early work of Courant, Isaacson and Rees. There has recently been a revival of interest in the use of one sided differencing for compressible flow calculations, beginning with the nonconservative λ scheme of Moretti, and the conservative scheme of Steger and Warming. There is by now a rather extensive theory of difference schemes for the treatment of a scalar conservation law.

Boundary Conditions

The pressure at the wall is then estimated by extrapolation from the pressure at the adjacent cell centers, using the known value.

The rate of convergence to a steady state will be impaired if outgoing waves are reflected back into the flow from the outer boundaries. The treatment of the far field boundary condition is based on the introduction of Riemann invariants for a one dimensional flow normal to the boundary. Let subscripts and e denote free stream values and values extrapolated from the interior cells adjacent to the boundary and let qn and c be the velocity component normal to the boundary and the speed of sound. Assuming that the flow is subsonic at infinity.

Steger and Warming flux vector splitting scheme (upwind scheme)

The upwind scheme for the Euler equation developed in this section is based on a non-conservative form of the Euler equation. Numerical calculations have revealed that this scheme cannot correctly capture the discontinuities that occur in the solution. A better upwind scheme is based on the conservative form of the Euler equation. Before doing this, we consider the advection equation:

$$\frac{\partial u}{\partial t} + a\frac{\partial u}{\partial x} = 0$$

This equation may be written in the conservative form, namely

$$\frac{\partial u}{\partial t} + \frac{\partial f}{\partial x} = 0$$

Where $f=au$ and $a=df/du$. Now suppose that a is a function of u, namely a=a(u) , then f=f(u) and we construct an upwind scheme depending on the sign of a(u) as follows:

$$u_i^{n+1} = \begin{cases} u_i^n - \frac{\Delta t}{h}\left[f\left(u_i^n\right) - f\left(u_{i-1}^n\right)\right] & \text{if } a(u) > 0 \\ u_i^n - \frac{\Delta t}{h}\left[f\left(u_{i+1}^n\right) - f\left(u_i^n\right)\right] & \text{if } a(u) < 0 \end{cases}$$

Defining the function μ as follows

$$\mu = \begin{cases} 1 & \text{if } a(u) > 0 \\ 0 & \text{if } a(u) < 0 \end{cases}$$

And

$$f^+(u) = \mu f(u), \quad f^-(u) = (1-\mu) f(u), \quad f = f^+ + f^-$$

Therefore the upwind scheme takes the following form

$$u_i^{n+1} - u_i^n = -\frac{\Delta t}{h}\left(f_i^+ - f_{i-1}^+\right) - \frac{\Delta t}{h}\left(f_{i+1}^- - f_i^-\right)$$

Now we extend this scheme for the Euler equation in conservative form, see equation (2.77), namely

$$\frac{\partial U}{\partial t} + \frac{\partial F}{\partial x} = 0$$

It is important to note that for a perfect gas, U, F and the matrix A obey a very simple relationship given by

$$F = AU$$

Considering equation, we may define the following flux splitting by

$$F^+ = A^+U, \quad F^- = A^-U, \quad F = F^+ + F^-$$

Therefore, similar to equation the upwind scheme for the Euler equation has the following form

$$U_i^{n+1} - U_i^n = -\frac{\Delta t}{h}\left(F_i^+ - F_{i-1}^+\right) - \frac{\Delta t}{h}\left(F_{i+1}^- - F_i^-\right)$$

Van Leer's flux-vector splitting scheme

Van Leer's flux-vector splitting scheme is based on characteristic decomposition of the convective fluxes. An extension of the approach to body-fitted grids.
The convective flux is split into a positive and a negative part, i.e.,

$$\vec{F}_c = \vec{F}_c^+ + \vec{F}_c^-$$

according to the Mach number normal to the face of the control volume (e.g.,at (1+1/2) - see Fig)

$$(M_n)_{I+1/2} = \left(\frac{V}{c}\right)_{I+1/2}$$

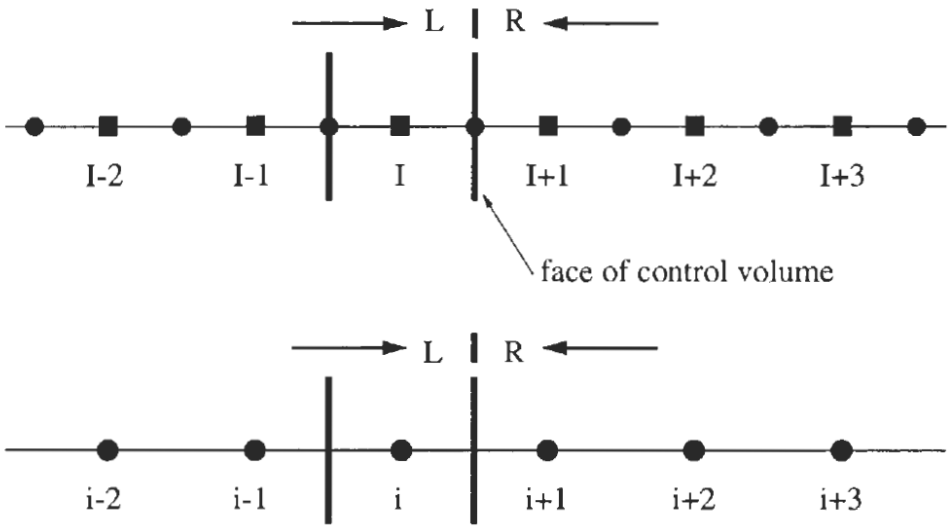

Fig1.4 Illustration of control volume

Where V represents the contravariant velocity and c the speed of sound, respectively. In the case of the cell-vertex scheme with dual control volumes, the cell indices have to be changed to node indices.

The values of the flow variables p, u, v, w, and p, respectively, have to be interpolated first to the faces of the control volume correspondingly to above equations. Then, the positive fluxes are computed with the left state and the negative fluxes with the right state.

The advection Mach number (Mn)i+1/2 is obtained from the relation.

$$(M_n)_{I+1/2} = M_L^+ + M_R^-$$

where the split Mach numbers are defined as if M_{L+1}, M_L

$$M_L^+ = \begin{cases} M_L & \text{if } M_L \geq +1 \\ \frac{1}{4}(M_L + 1)^2 & \text{if } |M_L| < 1 \\ 0 & \text{if } M_L \leq -1 \end{cases}$$

and

$$M_R^- = \begin{cases} 0 & \text{if } M_R \geq +1 \\ \frac{1}{4}(M_R - 1)^2 & \text{if } |M_R| < 1 \\ M_R & \text{if } M_R \leq -1 \end{cases}$$

The Mach numbers M_L and M_R are evaluated using the left and right state, respectively, i.e.,

$$M_L = \frac{V_L}{c_L},$$

$$M_R = \frac{V_R}{c_R}$$

In the case of |Mn| < 1 (subsonic flow), the positive and the negative flux parts are given by

$$\vec{F}_c^{\pm} = \begin{bmatrix} f_{\text{mass}}^{\pm} \\ f_{\text{mass}}^{\pm}\left[n_x(-V \pm 2c)/\gamma + u\right] \\ f_{\text{mass}}^{\pm}\left[n_y(-V \pm 2c)/\gamma + v\right] \\ f_{\text{mass}}^{\pm}\left[n_z(-V \pm 2c)/\gamma + w\right] \\ f_{\text{energy}}^{\pm} \end{bmatrix}$$

The mass and energy flux components are defined as

$$f^{+}_{\text{mass}} = +\rho_L c_L \frac{(M_L + 1)^2}{4}$$

$$f^{-}_{\text{mass}} = -\rho_R c_R \frac{(M_R - 1)^2}{4}$$

$$f^{\pm}_{\text{energy}} = f^{\pm}_{\text{mass}} \left\{ \frac{[(\gamma - 1)V \pm 2c]^2}{2(\gamma^2 - 1)} + \frac{u^2 + v^2 + w^2 - V^2}{2} \right\}_{L/R}$$

For supersonic flow, i.e., for the fluxes are evaluated from

$$\vec{F}_c^{+} = \vec{F}_c \quad \vec{F}_c^{-} = 0 \quad \text{if } M_n \geq +1$$

$$\vec{F}_c^{+} = 0 \quad \vec{F}_c^{-} = \vec{F}_c \quad \text{if } M_n \leq -1$$

The evaluation of the left and right state follows generally the MUSCL approach, which is given by the higher order schemes R = -1, R = 0 and R = 1/3, respectively, require a limiter if the flow field contains discontinuities like shocks.

The flux-vector splitting scheme of Van Leer performs very well in the case of Euler equations. But several investigations carried out with the Navier-Stokes equations revealed that splitting errors in the momentum and the energy equations smear out the boundary layers and also lead to inaccurate stagnation and wall temperatures. A modification to the momentum flux in the direction normal to the boundary layer. Both modifications together remove the splitting errors, and hence they improve the solution accuracy considerably.

Reconstruction

The basic problem is that we have to know their values at all NF faces of a control volume, but the flow variables are not directly available there. This means, we have to interpolate either the fluxes or the flow variables to the faces of the control volume. The interpolation of flow variables is known as reconstruction of the solution from values inside the control volumes.

In principle, the interpolation can be conducted in one of two ways:

- by arithmetic averaging like in centered discretization schemes;
- by some biased interpolation like in upwind discretization schemes, which take care of the characteristics of the flow equations.

Besides the description, we shall treat aspects such as accuracy, range of applicability and numerical effort of the most widely used discretization schemes for the convective fluxes

Piecewise Quadratic Reconstruction

In order to achieve higher than second-order accuracy with a polynomial reconstruction, we have to keep further terms in the truncated Taylor-series expansion around the neighboring cell-centers l nodes of the face. Based on the work of Barth and Frederickson, Barth developed the concept of k-exact reconstruction scheme, i.e., a reconstruction exact for a polynomial of degree IC.

The polynomial in Barth's method is defined in a way which guarantees the conservation of the mean, or in other words, the average of the reconstruction polynomial is equal to the mean solution in the control volume. This property assures the conservation of mass, momentum, and energy during the reconstruction. The method was implemented for k = 3 in a median-dual scheme. The coefficients of the polynomial were computed using a least-squares approach.

Similar ideas were followed for the cell-centred scheme by Mitchell and Walters, and by Mitchell 1601. However, these methods require a prohibitively high numerical effort and a complicated data structure which prevented widespread use. Delanaye and Essers and Delanaye developed a particular form of quadratic reconstruction for the cell-centered scheme which is computationally

more efficient than the method of Barth. The left and right state is approximated using Taylor series truncated after the quadratic term

$$U_L = U_I + \Psi_{I,1}\left(\nabla U_I \cdot \vec{r}_L\right) + \frac{1}{2}\Psi_{I,2}\left(\vec{r}_L^{\,T}\,\bar{H}_I\,\vec{r}_L\right)$$

$$U_R = U_J + \Psi_{J,1}\left(\nabla U_J \cdot \vec{r}_R\right) + \frac{1}{2}\Psi_{J,2}\left(\vec{r}_R^{\,T}\,\bar{H}_J\,\vec{r}_R\right)$$

In the above Eq. , HI denotes the Hessian matrix, i.e.,

$$\bar{H}_I = \begin{bmatrix} \partial^2_{xx}U & \partial^2_{xy}U & \partial^2_{xz}U \\ \partial^2_{xy}U & \partial^2_{yy}U & \partial^2_{yz}U \\ \partial^2_{xz}U & \partial^2_{yz}U & \partial^2_{zz}U \end{bmatrix}_I$$

evaluated at the cell-centroid I. The variables PI,I and QI, represent two different limiter functions for the linear and the quadratic term [61], respectively. The quadratic reconstruction method is third-order accurate on regular grids and at least second-order accurate on arbitrary grids due to cancellation of error terms [62]. Necessary conditions for achieving these properties are, however, that the gradient VU in Eq. (5.43) is evaluated at least with second-order and the Hessian with first-order accuracy.

This is accomplished by combining Green Gauss gradient evaluation with least-squares based approximation of the second derivatives [61], [62], which leads to a numerically efficient scheme. But the memory and time overheads are still quite significant in comparison to the linear reconstruction. The method utilises a fixed stencil composed of face and node neighbors.

The stencil is shown in Fig. 1.5 together with the integration path employed for the Green-Gauss gradient computation. In order to determine all coefficients of the quadratic polynomial, at least six (ten in 3D) values must be provided by the stencil. To mainta.in the accuracy provided by the quadratic reconstruction, it is necessary to consider a linear variation of the solution over the face instead of a constant value. This implies that the solution must be reconstructed at two points - so-called Gauss quadrature points (cf. Fig. 5.14) - of a 2-D face (at three points of a triangular face) and that the fluxes have to be integrated in a piecewise manner over the face of the control volume [36].

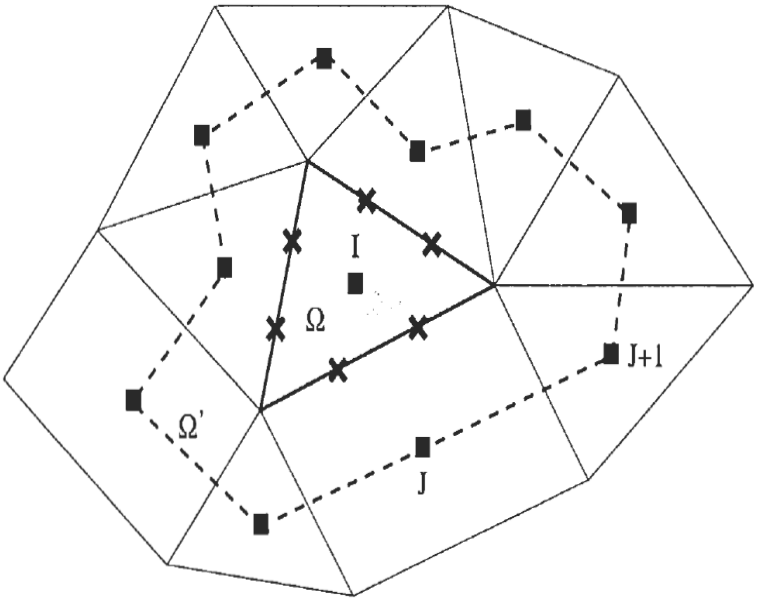

Figure 1.5: Stencil of the quadratic reconstruction method due to Delanaye [61], [62] in 2D (filled rectangles). Dashed line represents the integration path of the Green-Gauss gradient evaluation (control volume a'). Crosses denote the quadrature points for integration of the fluxes.

$$|\Delta\vec{F}_{2,3,4}| = |\tilde{V}| \left\{ \left(\Delta\rho - \frac{\Delta p}{\tilde{c}^2} \right) \begin{bmatrix} 1 \\ \tilde{u} \\ \tilde{v} \\ \tilde{w} \\ \tilde{q}^2/2 \end{bmatrix} + \tilde{\rho} \begin{bmatrix} 0 \\ \Delta u - \Delta V n_x \\ \Delta v - \Delta V n_y \\ \Delta w - \Delta V n_z \\ \tilde{u}\Delta u + \tilde{v}\Delta v + \tilde{w}\Delta w - \tilde{V}\Delta V \end{bmatrix} \right\}$$

$$|\Delta\vec{F}_5| = |\tilde{V} + \tilde{c}| \left(\frac{\Delta p + \tilde{\rho}\tilde{c}\Delta V}{2\tilde{c}^2} \right) \begin{bmatrix} 1 \\ \tilde{u} + \tilde{c}n_x \\ \tilde{v} + \tilde{c}n_y \\ \tilde{w} + \tilde{c}n_z \\ \tilde{H} + \tilde{c}\tilde{V} \end{bmatrix}.$$

Godonov Scheme

The Riemann Problem is an initial value problem with piecewise-constant initial data. For the Godunov scheme, the exact solution of the Riemann Problem is utilized. The exact solution is made up of constant states separated by transitions in the values of the 6 dependent variables across each family of waves. Each wave family is associated with an eigenvalue of the Jacobian matrix A.

The wave transitions can be of three types:

1. Continuous transition across rarefaction fans,
2. Abrupt nonlinear jumps across shock waves, and
3. Linearly degenerate jumps across contact surfaces.

Consider now the one-dimensional Euler equations (m = 3) for which

$$q = \begin{pmatrix} e \\ \rho \\ u \end{pmatrix} \quad , \quad f = \begin{pmatrix} (e+p)u \\ \rho u \\ \rho u^2 + p \end{pmatrix}$$

define the various positive and negative flux differences of Eq.

$$df^{1+}_{j+1/2} = \max[\text{sign}\{(u-c)_j\}, 0][f(q_{j+1/6}) - f(q_j)]$$
$$+ \max[\text{sign}\{(u-c)_{j+1/3}\}, 0][f(q_{j+1/3}) - f(q_{j+1/6})]$$
$$df^{1-}_{j+1/2} = \max[-\text{sign}\{(u-c)_j\}, 0][f(q_{j+1/6}) - f(q_j)]$$
$$+ \max[-\text{sign}\{(u-c)_{j+1/3}\}, 0][f(q_{j+1/3}) - f(q_{j+1/6})]$$
$$df^{2+}_{j+1/2} = \max[\text{sign}\{u_{j+1/3}\}, 0][f(q_{j+2/3}) - f(q_{j+1/3})]$$
$$df^{2-}_{j+1/2} = \max[-\text{sign}\{u_{j+1/3}\}, 0][f(q_{j+2/3}) - f(q_{j+1/3})]$$
$$df^{3+}_{j+1/2} = \max[\text{sign}\{(u+c)_{j+2/3}\}, 0][f(q_{j+5/6}) - f(q_{j+2/3})]$$
$$+ \max[\text{sign}\{(u+c)_{j+1}\}, 0][f(q_{j+1}) - f(q_{j+5/6})]$$
$$df^{3-}_{j+1/2} = \max[-\text{sign}\{(u+c)_{j+2/3}\}, 0][f(q_{j+5/6}) - f(q_{j+2/3})]$$
$$+ \max[-\text{sign}\{(u+c)_{j+1}\}, 0][f(q_{j+1}) - f(q_{j+5/6})]$$

Source from Computational Fluid Mechanics and Heat Transfer by Tannehill John C, Anderson Dale A, Pletcher Richard H

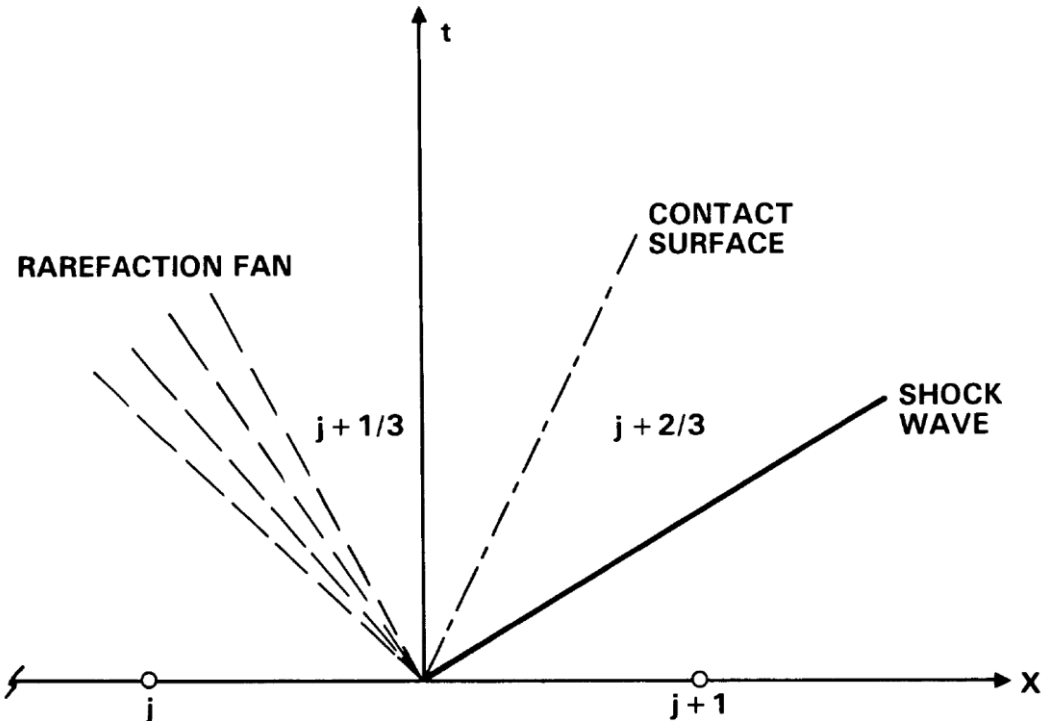

Fig. 1.6 Roe's Scheme Roe's algorithm is based on an approximate Riemann Problem2'. In Roe's approach, specially averaged cell interface values (denoted by subscript j + 1/2) are determined for density, velocity and enthalpy.

Roe Scheme

Roe's approximate Riemann solver can be implemented either in the framework of the cell-centered scheme or the dual control-volume scheme. It is based on the decomposition of the flux difference over a face of the control volume into a sum of wave contributions, while ensuring the conservation properties of the Euler equations. On the face (1+1/2) or (i+1/2), respectively, the difference is
expressed as

$$(\vec{F}_c)_R - (\vec{F}_c)_L = (\bar{A}_{Roe})_{I+1/2}\,(\vec{W}_R - \vec{W}_L)$$

In the above Eq, A_{Roe} denotes the so-called Roe matrix, and L or R the left and right state respectively.

The Roe matrix is identical to the convective flux Jacobian A, where the flow variables are replaced by the so-called Roe-averaged variables. These are computed from the left and the right state by the formulae

$$\tilde{\rho} = \sqrt{\rho_L \rho_R}$$

$$\tilde{u} = \frac{u_L\sqrt{\rho_L} + u_R\sqrt{\rho_R}}{\sqrt{\rho_L} + \sqrt{\rho_R}}$$

$$\tilde{v} = \frac{v_L\sqrt{\rho_L} + v_R\sqrt{\rho_R}}{\sqrt{\rho_L} + \sqrt{\rho_R}}$$

$$\tilde{w} = \frac{w_L\sqrt{\rho_L} + w_R\sqrt{\rho_R}}{\sqrt{\rho_L} + \sqrt{\rho_R}}$$

$$\tilde{H} = \frac{H_L\sqrt{\rho_L} + H_R\sqrt{\rho_R}}{\sqrt{\rho_L} + \sqrt{\rho_R}}$$

$$\tilde{c} = \sqrt{(\gamma - 1)\left(\tilde{H} - \tilde{q}^2/2\right)}$$

$$\tilde{V} = \tilde{u}n_x + \tilde{v}n_y + \tilde{w}n_z$$

$$\tilde{q}^2 = \tilde{u}^2 + \tilde{v}^2 + \tilde{w}^2 .$$

We can make the decomposition into waves in Roe's scheme clearer when T-l, into the

$$(\vec{F}_c)_R - (\vec{F}_c)_L = \bar{T}\bar{\Lambda}_c(\vec{C}_R - \vec{C}_L)$$

The matrix of left (F-') and right (F) eigenvectors, as well as the diagonal matrix of eigenvalues (A_c) are evaluated using Roe's averaging. In the above Eq. the characteristic variables c' represent the wave amplitudes, the eigenvalues A, are the associated wave speeds of the approximate Riemann problem, and finally the right eigenvectors are the waves themselves.

We insert the diagonalisation of the Roe matrix.

Following from the previous discussion, the convective fluxes are evaluated at the faces of a control volume faces corresponding to

$$(\vec{F}_c)_{I+1/2} = \frac{1}{2}\left[\vec{F}_c(\vec{W}_R) + \vec{F}_c(\vec{W}_L) - |\bar{A}_{Roe}|_{I+1/2}(\vec{W}_R - \vec{W}_L)\right]$$

The product of $|A_{Roe}|$ and the difference of the left and right state can be evaluated as follows

$$|\bar{A}_{Roe}|(\vec{W}_R - \vec{W}_L) = |\Delta\vec{F}_1| + |\Delta\vec{F}_{2,3,4}| + |\Delta\vec{F}_5|$$

$$|\Delta\vec{F}_1| = |\tilde{V} - \tilde{c}|\left(\frac{\Delta p - \tilde{\rho}\tilde{c}\Delta V}{2\tilde{c}^2}\right)\begin{bmatrix} 1 \\ \tilde{u} - \tilde{c}n_x \\ \tilde{v} - \tilde{c}n_y \\ \tilde{w} - \tilde{c}n_z \\ \tilde{H} - \tilde{c}\tilde{V} \end{bmatrix}$$

This section presents some typical results of multigrid calculations of the Euler equations for two-dimensional flow. The 5 stage scheme defined by equation was used in all the examples, and residual averaging was also used to allow steps corresponding to a Courant number of 7.5.

The first example is the flow past a circular cylinder at Mach .50, calculated on a grid with 128 cells in the circumferential direction and 32 cells in the radial direction. The calculation was started from an initial condition of uniform flow.

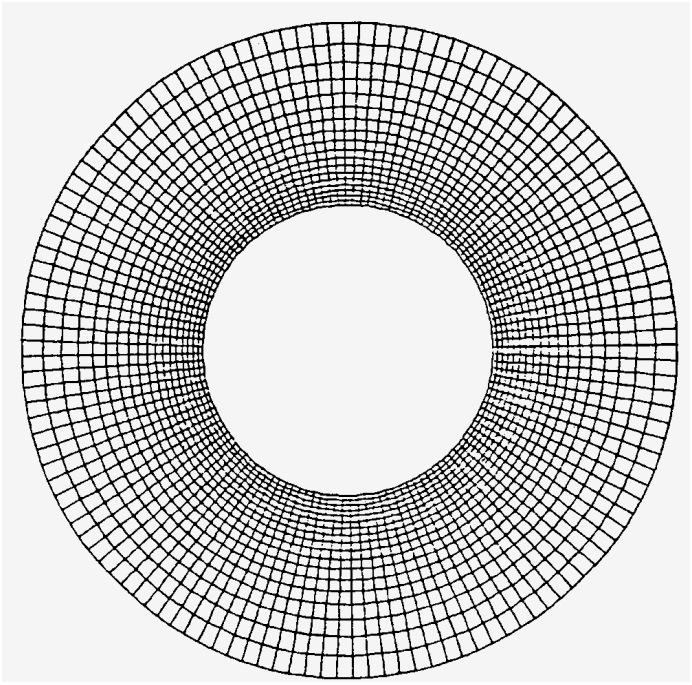

Figure 1.7 Inner part of the grid for 128 X 32 cells

There is a shockwave of moderate strength slightly beyond the crest of the cylinder. One curve shows the decay of the logarithm of the error (measured by the root mean square rate of change of density on he fine grid): the mean rate of convergence is just less than 8 per multigrid cycle. The other curve shows the buildup of the number of grid points in the supersonic zone: it can be seen that the flow field is fully developed in about 30 cycles.

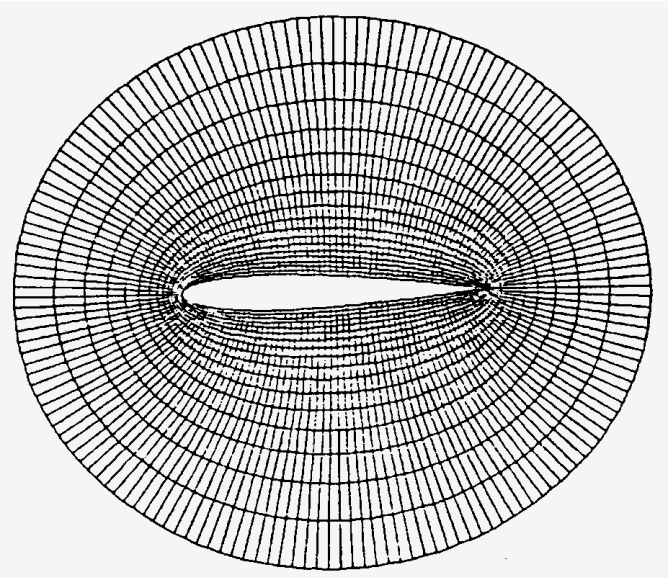

Figure 1.8 Inner part of the grid for NACA 0012 160 X 32 cells

The next examples are transonic flows past airfoils. A 0-mesh was used in these calculations with the outer boundary at a distance of about 50 chords. Each result was obtained with 50 cycles on an 80 x 16 mesh, followed by 50 cycles on a 160 x 32 mesh. This was sufficient for full development of the flow field. The flow past the NACA 0012 airfoil contains a fairly strong shock wave on the upper surface, which is resolved in about 5 mesh cells, and a weak shock wave on the lower surface, which is quite smeared. The Korn airfoil is designed to be shock free at the given Mach number and angle of attack. The result of the Euler calculation is in close agreement with the result of the design calculation.

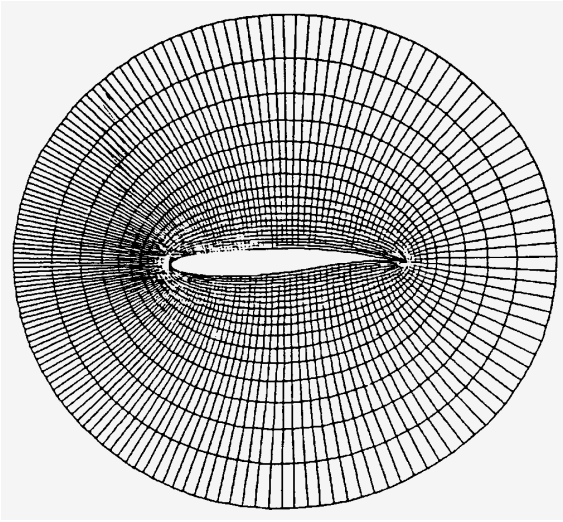

Figure 1.9 Inner part of the grid of Korn airfoil 160 X 32 cells

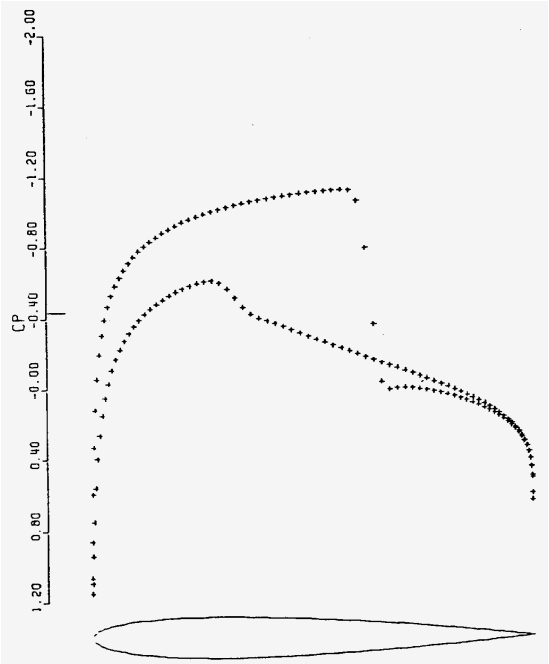

Figure 1.10 Pressure distribution for NACA 0012 Mach .800 α1.25◦ CL .3504 CD .0227 160X32 grid 50 cycles Residual .15210−3

The drag should be zero in a shock free flow, and the calculated value of the drag coefficient CD =.0005 is an indication of the level of discretization error. Another measure of error is the entropy, which should also be zero.

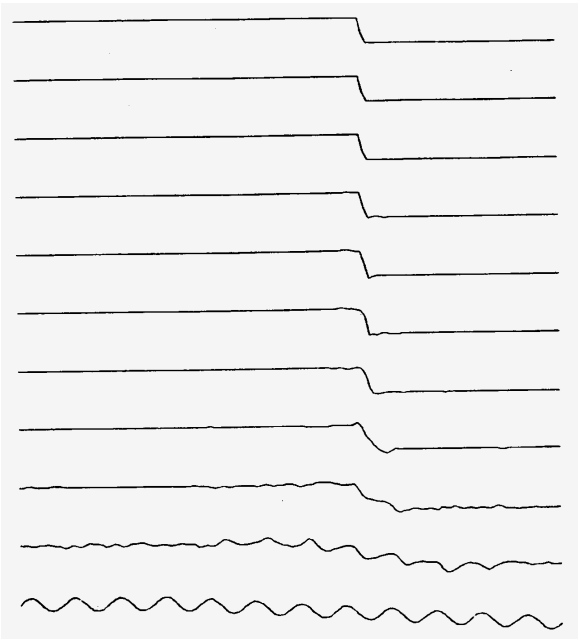

Figure 1.11 Initial state and first 10 cycles in evolution of Burger's equation (reading upwards) Adaptive dissipation (scheme 1a) 128 cells 5 grids $\lambda = 2.0$

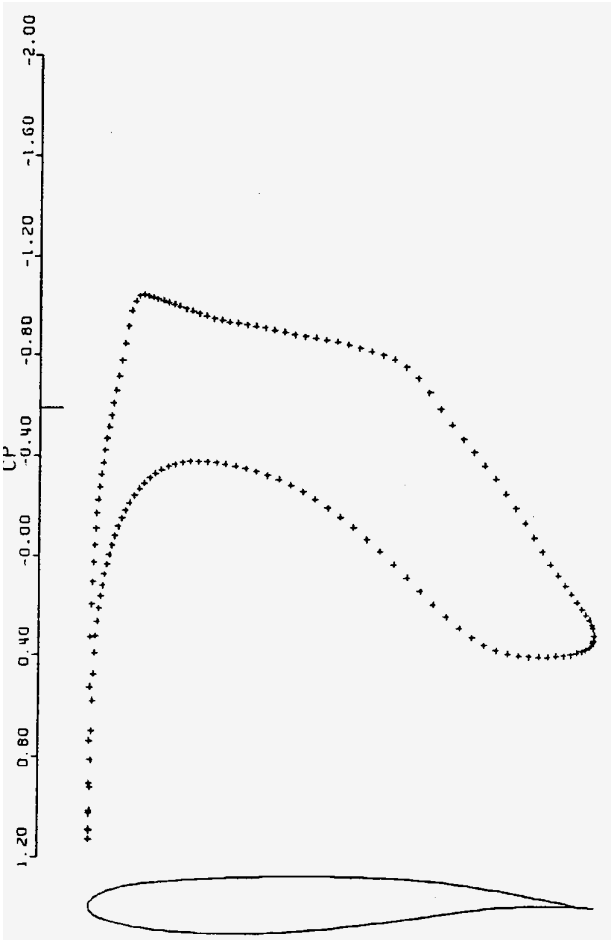

Figure 1.12 Pressure distribution for Korn airfoil Mach .750 α0◦ CL .6254 CD .005 160X32 grid 50 cycles Residual .11210−3

Source from Computational Fluid Mechanics and Heat Transfer by Tannehill John C, Anderson Dale A, Pletcher Richard H

UNIT-II
TIME DEPENDENT METHODS

Stability

Let us look at the stability requirement for the second-order wave equation given by

$$\frac{\partial^2 u}{\partial t^2} = c^2 \frac{\partial^2 u}{\partial x^2}$$

We replace both the spatial and time derivative with central difference scheme (which is second-order accurate)

$$\frac{u_i^{n+1} - 2u_i^n + u_i^{n-1}}{(\Delta t)^2} = c^2 \left[\frac{u_{i+1}^n - 2u_i^n + u_{i-1}^n}{(\Delta x)^2} \right] \tag{2.1}$$

Again assume

$$N = D + \varepsilon \tag{2.2}$$

and

$$\varepsilon_i^n = e^{at} e^{Ik_m x} \tag{2.3}$$

Substituting Eq. (2.3) and (2.2) in (2.1) and dividing both side by $e^{at} e^{Ik_m x}$, we get

$$e^{a\Delta t} - 2 + e^{-a\Delta t} = C^2 \left[e^{Ik_m \Delta x} + e^{-Ik_m \Delta x} - 2 \right] \tag{2.4}$$

where

$$\text{C, the Courant number} = c(\Delta t/\Delta x) \tag{2.5}$$

From Eq. (2.4), using trigonometric identities, we get

$$e^{a\Delta t} + e^{-a\Delta t} = 2 - 4C^2 \sin^2\left(\frac{k_m \Delta x}{2}\right) \tag{2.6}$$

and, the amplification factor

$$G = \left| \frac{\varepsilon_i^{n+1}}{\varepsilon_i^n} \right| = \left| e^{a\Delta t} \right| \tag{2.7}$$

However, from Eq. (2.6) we arrive at

$$e^{2a\Delta t} - 2\left[1 - 2C^2 \sin^2\left(\frac{k_m \Delta x}{2}\right) \right] e^{a\Delta t} + 1 = 0 \tag{2.8}$$

Which is a quadratic equation for $e^{a\Delta t}$ This equation, quite obviously, has two roots, and the product of the roots is equal to +1. Thus, it follows that the magnitude of one of the roots (value of $e^{a\Delta t}$) must exceed 1 unless both the roots are equal to unity.

But $e^{a\Delta t}$ is the magnification factor. If its value exceeds 1, the error will grow exponentially which will lead to an unstable situation. All these possibilities mean that Eq (2.8) should possess complex roots in order to both have the values of $e^{a\Delta t}$ equal to unity.

This implies that the discriminant of Eq. (2.8) should be negative.

$$\left[1-2C^2\sin^2\left(\frac{k_m\Delta x}{2}\right)\right]^2-1<0 \tag{2.9}$$

or

$$C^2<\frac{1}{\sin^2\left(\frac{k_m\Delta x}{2}\right)} \tag{2.10}$$

which is always true if C<1 .

Hence CFL condition C<1, must again be satisfied for the stability of second-order hyperbolic equations.

In light of the previous discussion, we can say that a finite-difference procedure will be unstable if for that procedure, the solution becomes unbounded, i.e the error grows exponentially as the calculation progresses in the marching direction.

In order to have a stable calculation, we pose different conditions based on stability analysis. Here we have discussed the Von Neumann stability analysis which is indeed a linear stability analysis.

However, situations may arise where the amplification factor is always less than unity. These conditions are referred to as unconditionally stable. In a similar way for some procedures, we may get an amplification factor which is always greater than unity. Such methods are unconditionally unstable. Over and above, it should be realized that such stability analysis are not really adequate for practical complex problems.

In actual fluid flow problems, the stability restrictions are applied locally. The mesh is scanned for the most restrictive value of the stability limitations and the resulting minimum Δt is used throughout the mesh. For variable coefficients, the Von Neumann condition is only necessary but not sufficient. As such, stability criterion of a procedure is not defined by its universal applicability.

For nonlinear problems we need numerical experimentation in order to obtain stable solutions wherein the routine stability analysis will provide the initial clues to practical stability. In other words, it will give tutorial guidance.

Fundamentals of Fluid Flow Modeling

We have discussed the finite-difference methods with respect to the solution of linear problems such as heat conduction. The problems of fluid mechanics are more complex in character. The governing partial differential equations form a nonlinear system which must be solved for the unknown pressures, densities, temperature and velocities.

Before entering into the domain of actual flow modeling, we shall discuss some subtle points of fluid flow equations with the help of a model equation.

The model equation should have convective, diffusive and time-dependent terms. Burgers (1948) introduced a simple nonlinear equation which meets the aforesaid requirements (Burger's equation).

$$\frac{\partial \zeta}{\partial t} + u\frac{\partial \zeta}{\partial x} = \upsilon \frac{\partial^2 \zeta}{\partial x^2}$$

Here, u is the velocity, υ is the coefficient of diffusivity and ζ is any property which can be transported and diffused.

If the viscous term (diffusive term) on the right-hand side is neglected, the remaining equation may be viewed as a simple analog of Euler's equation.

$$\frac{\partial \zeta}{\partial t} + u\frac{\partial \zeta}{\partial x} = 0$$

Now we shall see the behavior of Burger's equations for different discretization methods. In particular, we shall study their influence on conservative and transportive property, and artificial viscosity.

Explicit and Implicit Methods

The solution of Eq. takes the form of a "marching" procedure (or scheme) in steps of time.

We know the dependent variable at all x at a time level from given initial conditions.

Examining Eq. we see that it contains one unknown, namely u_i^{n+1}.

Thus, the dependent variable at time (t+Δt) is obtained directly from the known values of u_{i+1}^n, u_i^n and u_{i-1}^n

$$\frac{u_i^{n+1} - u_i^n}{\Delta t} = \alpha \left[\frac{u_{i+1}^n - 2u_i^n + u_{i-1}^n}{(\Delta x^2)} \right]$$

This is a typical example of an explicit finite difference method.

Let us now attempt a different discretization of the original partial differential equation given by Eq. Here we express the spatial difference on the right-hand side in terms of averages between n and (n+1) time level

$$\frac{u_i^{n+1} - u_i^n}{\Delta t} = \alpha \left[\frac{u_{i+1}^n - 2u_i^n + u_{i-1}^n}{(\Delta x^2)} \right]$$

The differencing shown in Eq. is known as the Crank-Nicolson implicit scheme.

The unknown u_i^{n+1} is not only expressed in terms of the known quantities at time level n but also in terms of unknown quantities at time level (n+1). Hence Eq. at a given grid point i, cannot itself result in a solution of u_i^{n+1}.

Eq. has to be written at all grid points, resulting in a system of algebraic equations from which the unknowns u_i^{n+1} for all i can be solved simultaneously. This is a typical example of an implicit finite-difference solution.

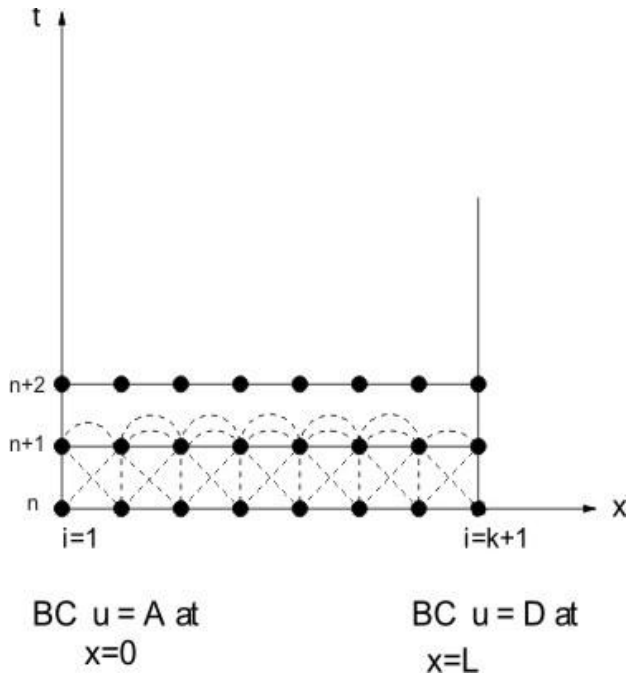

Figure 2.1: Crank Nicolson Implicit Scheme

Since they deal with the solution of large system of simultaneous linear algebraic equations, implicit methods usually require the handling of large matrices.

Generally, the following steps are followed in order to obtain a solution. Eq can be rewritten as

$$u_i^{n+1} - u_i^n = \frac{r}{2}\left[u_{i+1}^{n+1} + u_{i+1}^n - 2u_i^{n+1} - 2u_i^n + u_{i-1}^{n+1} + u_{i-1}^n\right]$$

where $r = \alpha(\Delta t)/(\Delta x)^2$ or

$$-ru_{i-1}^{n+1} + (2+2r)u_i^{n+1} - ru_{i+1}^{n+1} = ru_{i-1}^n + (2-2r)u_i^n + ru_{i+1}^n$$

Or

$$-u_{i-1}^{n+1} + \left(\frac{2+2r}{r}\right)u_i^{n+1} - u_{i+1}^{n+1} = u_{i-1}^n + \left(\frac{2-2r}{r}\right)u_i^n + ru_{i+1}^n$$

Eq. has to be applied at all grid points, i.e., from i = 1 to i = K+1. A system of algebraic equations will result.

$$\begin{aligned}
&\text{at } i=2 && -A + B(1)u_2^{n+1} - u_3^{n+1} = C(1)\\
&\text{at } i=3 && -u_2^{n+1} + B(2)u_3^{n+1} - u_4^{n+1} = C(2)\\
&\text{at } i=4 && -u_3^{n+1} + B(3)u_4^{n+1} - u_5^{n+1} = C(3)\\
&\quad\vdots && \quad\vdots\\
&\text{at } i=k && -u_{k-1}^{n+1} + B(k-1)u_k^{n+1} - D = C(k-1)
\end{aligned}$$

Source from Computational Fluid Mechanics and Heat Transfer by Tannehill John C, Anderson Dale A, Pletcher Richard H

Finally the equation will be of the form:

$$\begin{bmatrix} B & (1) & -1 & 0 & 0 & \dots & 0 \\ -1 & B(2) & -1 & 0 & & \dots & 0 \\ 0 & -1 & B(3) & -1 & & \cdots & 0 \\ \vdots & & & & & & \\ 0 & 0 & 0 & \dots & & -1 & B(k-1) \end{bmatrix} \begin{bmatrix} u_2^{n+1} \\ u_3^{n+1} \\ u_4^{n+1} \\ \vdots \\ u_k^{n+1} \end{bmatrix} = \begin{bmatrix} (C(1)+A)^n \\ C(2)^n \\ C(2)^n \\ \vdots \\ (C(k-1)D)^n \end{bmatrix}$$

Here, we express the system of equation in the form of A$x = C$,

where,

C: right-hand side column vector (known),
A: tridiagonal coefficient matrix (known) and
x: the solution vector (to be determined).

Note that the boundary values at i = 1 and i = K+1 are transferred to the known right-hand side. For such a tridiagonal system, different solution procedures are available. In order to derive advantage of the zeros in the coefficient-matrix, the well-known Thomas algorithm (1949) can be used .

Explicit and Implicit Methods for Two-Dimensional Heat Conduction Equation

The two-dimensional conduction is given by

$$\frac{\partial u}{\partial t} = \alpha\left(\frac{\partial^2 u}{\partial x^2} + \frac{\partial^2 u}{\partial x^2}\right)$$

Here, the dependent variable, u (temperature) is a function of space (x,y) and (t)and (α) is the thermal diffusivity.

If we apply the simple explicit method to heat conduction equation, the following algorithm results

$$\frac{u_{i,j}^{n+1} - u_{i,j}^n}{\Delta t} = \alpha\left[\frac{u_{i+1,j}^n - 2u_{i,j}^n + u_{i-1,j}^n}{(\Delta x^2)} + \frac{u_{i,j+1}^n - 2u_{i,j}^n + u_{i,j-1}^n}{(\Delta y^2)}\right]$$

When we apply the crank-Nicolson to the two-dimensional heat conduction equation, we obtain

$$\frac{u_{i,j}^{n+1} - u_{i,j}^n}{\Delta t} = \frac{\alpha}{2}\left[\left(\delta_x^2 + \delta_y^2\right)\left(u_{i,j}^{n+1} + u_{i,j}^n\right)\right]$$

where the central difference operators δ_x^2 and δ_y^2 in two different spatial directions are defined by

$$\delta_x^2\left[u_{i,j}^n\right] = \frac{u_{i+1,j}^n - 2u_{i,j}^n + u_{i-1,j}^n}{\left(\Delta x^2\right)}$$

$$\delta_y^2\left[u_{i,j}^n\right] = \frac{u_{j+1}^n - 2u_{i,j}^n + u_{i,j-1}^n}{\left(\Delta y^2\right)}$$

The resulting system of linear algebraic equations is not tridiagonal because of the five unknowns $u_{i,j}^{n+1}, u_{i+1,j}^{n+1}, u_{i-1,j}^{n+1}, u_{i,j+1}^{n+1}$ and $u_{i,j-1}^{n+1}$. In order to examine this further, let us rewrite Eq. as

$$au_{i,j-1}^{n+1} + bu_{i-1,j}^{n+1} + du_{i,j}^{n+1} + bu_{i+1,j}^{n+1} + au_{i,j+1}^{n+1} + c_{i,j}^{n+1}$$

where

$$a = -\frac{\alpha\Delta t}{2\left(\Delta y\right)^2} = -\frac{1}{2}P_y$$

$$b = -\frac{\alpha\Delta t}{2\left(\Delta x\right)^2} = -\frac{1}{2}P_x$$

$$d = 1 + P_x + P_y$$

$$c_{i,j}^n = u_{i,j}^n + \frac{\alpha\Delta t}{2}\left(\delta_x^2 + \delta_y^2\right)u_{i,j}^n$$

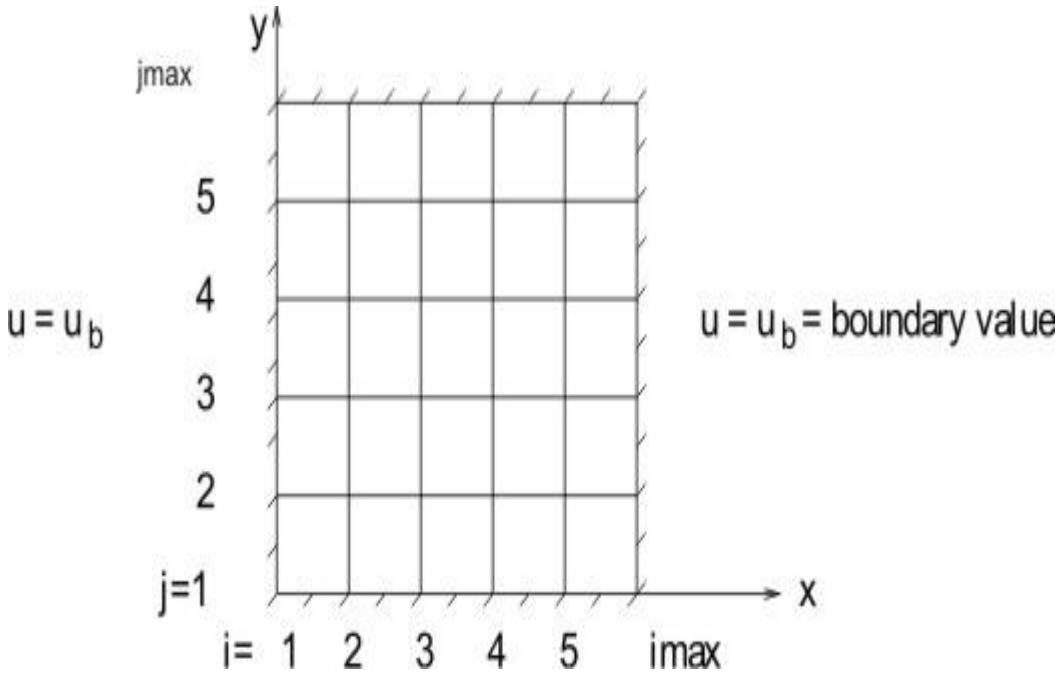

Figure 2.2: Two-dimensional grid on the ($x-y$) plane.

Equation can be applied to the two-dimensional (6×6) computational grid shown in Fig. 2.2.

A system of 16 linear algebraic equations has to be solved at (n+1) time level, in order to get the

Source from Computational Fluid Mechanics and Heat Transfer by Tannehill John C, Anderson Dale A, Pletcher Richard H

temperature distribution inside the domain.

The matrix equation will be as the following:

$$\begin{bmatrix}
d & b & 0 & 0 & a & 0 & & & & & & & & & 0 \\
b & d & b & & & a & & & & & & & & & \\
0 & b & d & b & & & a & & & & & & & & \\
0 & & b & d & b & & & a & & & & & & & \\
a & & & b & d & b & & & a & & & & & & \\
0 & a & & & b & d & b & & & a & & & & & \\
 & & a & 0 & & b & d & b & & & a & & & & \\
 & & & a & & & b & d & 0 & & & a & & & \\
 & & & & a & & & 0 & d & b & & & a & & \\
 & & & & & a & & & b & d & b & & & a & \\
 & & & & & & a & & & b & d & b & & a & 0 \\
 & & & & & & & a & & & b & d & 0 & & a \\
 & & & & & & & & a & & & 0 & d & b & 0 \\
 & & & & & & & & & a & & & b & d & b & 0 \\
 & & & & & & & & & & a & & & b & d & b \\
 & & & & & & & & & & & a & & & b & d
\end{bmatrix}
\begin{bmatrix} u_{2,2} \\ u_{3,2} \\ u_{4,2} \\ u_{5,2} \\ u_{2,3} \\ u_{3,3} \\ u_{4,3} \\ u_{5,3} \\ u_{2,4} \\ u_{3,4} \\ u_{4,4} \\ u_{5,4} \\ u_{2,5} \\ u_{3,5} \\ u_{4,5} \\ u_{5,5} \end{bmatrix}
=
\begin{bmatrix} c''_{2,2} \\ c'_{3,2} \\ c'_{4,2} \\ c''_{5,2} \\ c''_{2,3} \\ c_{3,3} \\ c_{4,3} \\ c''_{5,3} \\ c''_{2,4} \\ c_{3,4} \\ c_{4,4} \\ c''_{5,4} \\ c''_{2,5} \\ c'_{3,5} \\ c'_{4,5} \\ c''_{5,5} \end{bmatrix}$$

where

$$c' = c - au_b$$
$$c'' = c - bu_b$$
$$c''' = c - (a+b)u_b$$

The system of equations, described by Eq. requires substantially more computer time as compared to a tridiagonal system. The equations of this type are usually solved by iterative methods.. The quantity u_b is the boundary value.

FTCS, Forward Time Central Space method of discretization Basic Aspects of Finite-Difference Equations

Consider the following one dimensional unsteady state heat conduction equation. The dependent variable u (temperature) is a function of x and t (time) and α is a constant known as thermal diffusivity.

$$\frac{\partial u}{\partial t} = \alpha \frac{\partial^2 u}{\partial x^2}$$

It is to be noted that Equation is classified as a parabolic partial differential equation.
If we substitute the time derivative in Equation with a forward difference, and a spatial derivative with a central difference (usually called FTCS, Forward Time Central Space method of discretization), we obtain

$$\frac{u_i^{n+1} - u_i^n}{\Delta t} = \alpha \left[\frac{u_{i+1}^n - 2u_i^n + u_{i-1}^n}{(\Delta x^2)} \right]$$

In Eq. the index for time appears as a superscript, where n denotes conditions at time t, (n+1) denotes conditions at time (t+Δt) and so on. The subscript denotes the grid point in the spatial dimension.
However, there must be a truncation error for the equation because each one of the finite difference quotient has been taken from a truncated series.

Considering Eqns. and looking at the truncation error associated with the difference quotients we can write

$$\frac{\partial u}{\partial t} - \alpha \frac{\partial^2 u}{\partial x^2} = \frac{u_i^{n+1} - u_i^n}{\Delta t} - \alpha \frac{u_{i+1}^n - 2u_i^n + u_{i-1}^n}{(\Delta x^2)}$$

$$+ \left[-\left(\frac{\partial^2 u}{\partial t^2}\right)_i^n \frac{(\Delta t)}{2} + \alpha \left(\frac{\partial^4 u}{\partial x^4}\right)_i^n \frac{(\Delta x)^2}{12} + \ldots \right]$$

In Equation the terms in the square brackets represent truncation error for the complete equation. It is evident that truncation error (TE) for this representation is $o[\Delta t,(\Delta x)^2]$

Consistency

A finite difference representation of a partial differential equation (PDE) is said to be consistent if we can show that the difference between the PDE and its finite difference (FDE) representation vanishes as the mesh is refined, i.e,

$$\lim_{mesh \to 0} (\text{PDE-FDE}) = \lim_{mesh \to 0} (\text{TE}) = 0$$

A questionable scheme would be one for which the truncation error is $o(\Delta t/\Delta x)$ and not explicitly $o(\Delta t)$ or $o(\Delta x)$ or higher orders.

In such cases the scheme would not be formally consistent unless the mesh were refined in a manner such that $(\Delta t/\Delta x) \to 0$. Let us take Eq. and use the Dufort-Frankel (1953) differencing scheme. The FDE is

$$\frac{u_i^{n+1} - u_i^{n-1}}{2\Delta t} = \alpha \left[\frac{u_{i+1}^n - u_i^{n+1} - u_i^{n-1} + u_{i-1}^n}{(\Delta x^2)} \right]$$

Now the leading terms of truncated series form the truncation error for the complete equation:

$$\frac{\alpha}{12}\left(\frac{\partial^4 u}{\partial x^4}\right)_i^n (\Delta x)^2 - \alpha \left(\frac{\partial^2 u}{\partial t^2}\right)_i^n \left(\frac{\Delta t}{\Delta x}\right)^2 - \frac{1}{6}\left(\frac{\partial^3 u}{\partial t^3}\right)_i^n (\Delta t)^2$$

The above expression for truncation for error is meaningful if $(\Delta t/\Delta x) \to 0$ together with $\Delta t \to 0$ and $\Delta x \to 0$ .However, (Δt) and (Δx) may individually approach zero in such a way that $(\Delta t/\Delta x) = \beta$. Then if we reconstitute the PDE from FDE and TE, we shall obtain

$\lim_{(\Delta t/\Delta x)\to 0}(\text{PDE-FDE}) = \lim_{\text{mesh}\to 0}(\text{TE}) = -\alpha\beta^2\left(\frac{\partial^2 u}{\partial t^2}\right)$

And finally PDE becomes

$$\frac{\partial u}{\partial t} + \alpha\beta^2\frac{\partial^2 u}{\partial t^2} = \alpha\frac{\partial^2 u}{\partial x^2}$$

We started with a parabolic one and ended with a hyperbolic one!

So, DuFort-Frankel scheme is not consistent for the 1D unsteady state heat conduction equation unless$(\Delta t/\Delta x) \to 0$ together with $\Delta t \to 0$ and $\Delta x \to 0$.

Convergence

A solution of the algebraic equation that approximates a partial differential equation (PDE) is convergent if the approximate solution approaches the exact solution of the PDE for each value of the independent variable as the grid spacing tend to zero.
The requirement is

$$u_i^n = \bar{u}(x_i, t_n) \text{ as } \Delta x, \Delta t \to 0$$

Where, $\bar{u}(x_i, t_n)$ is the solution of the system of algebraic equations.

TIME-DEPENDENT METHODS

The time-dependent scalar-transport equation

- One-step methods for single variables
- One-step methods for CFD
- Multi-step methods
- Uses of time-marching in CFD

The Time-Dependent Scalar-Transport Equation

The time-dependent scalar-transport equation for an arbitrary control volume is

$$\frac{\mathrm{d}}{\mathrm{d}t}(amount) + net\ \ flux = source$$

$$\frac{\mathrm{d}}{\mathrm{d}t}(\rho V\phi_P) + a_P\phi_P - \sum_F a_F\phi_F = b_P$$

As a preliminary we examine numerical methods for the first-order differential equation

$$\frac{d\Phi}{dt} = F(t, \Phi), \qquad \Phi(0) = \Phi_0$$

Initial-value problems of the form are solved by time-marching.

There are two main types of method:

- One-step methods: use the value from the previous time level only;
- Multi-step methods: use values from several previous times.

CFL conditions

In mathematics, the Courant–Friedrichs–Lewy (CFL) condition is a necessary condition for convergence while solving certain partial differential equations (usually hyperbolic PDEs) numerically by the method of finite differences. It arises in the numerical analysis of explicit time integration schemes, when these are used for the numerical solution. As a consequence, the time step must be less than a certain time in many explicit time-marching computer simulations; otherwise the simulation produces incorrect results.

$$\frac{\partial u}{\partial t} + a\frac{\partial u}{\partial x} = 0$$

FTCS scheme

In numerical analysis, the FTCS (Forward-Time Central-Space) method is a finite difference method used for numerically solving the heat equation and similar parabolic partial differential equations.

It is a first-order method in time, explicit in time, and is conditionally stable when applied to the heat equation. When used as a method for advection equations, or more generally hyperbolic partial differential equation, it is unstable unless artificial viscosity is included.

By definition, is explicit because u_i at time step $n + 1$ can be solved explicitly in terms of the known quantities at the previous time step n, thus called an explicit scheme.

Order of accuracy of the scheme is $O(\Delta t, \Delta x^2)$. The method is conditionally stable, and the stability condition is given by $d \leq 0.5$.

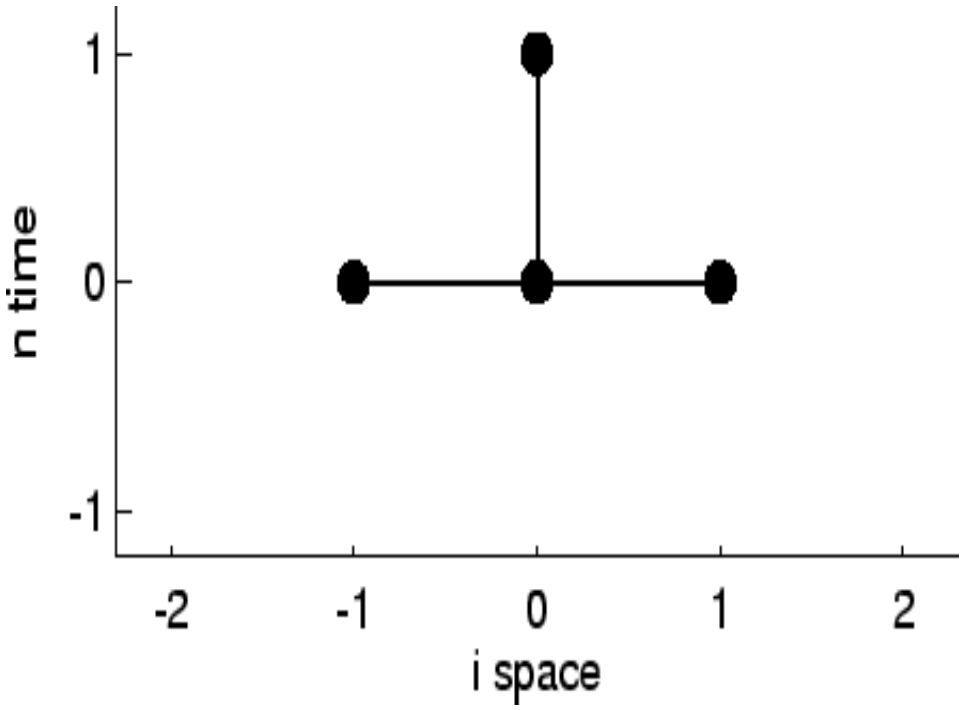

Figure 2.2: Explicit FTCS scheme.

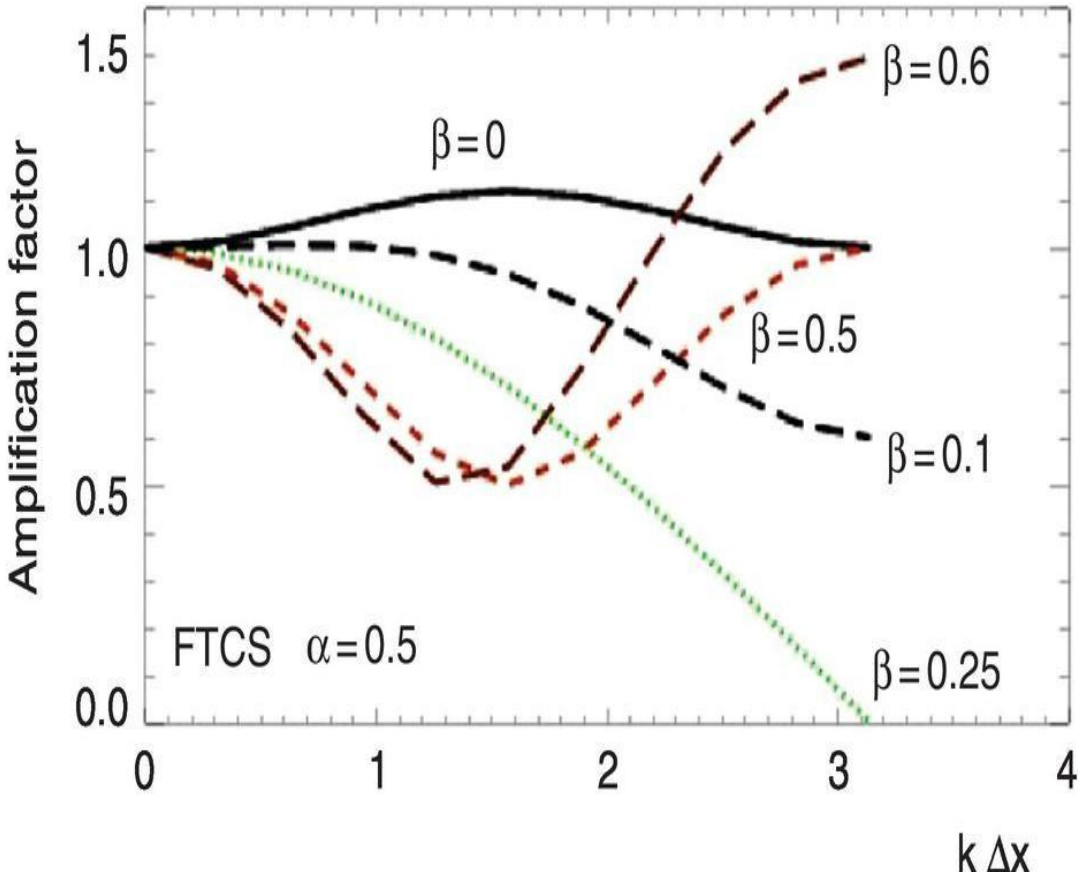

Figure 2.3: Explicit FTCS

Source from Computational Fluid Mechanics and Heat Transfer by Tannehill John C, Anderson Dale A, Pletcher Richard H

BTCS scheme

Writing this equation for all grid points at n +1 time level, leads to a tridiagonal system and can be solved using TDMA algorithm. The BTCS scheme is also known as the Laasone method. This is unconditionally stable. Order of accuracy of the scheme is $O(\Delta t, \Delta x^2)$.

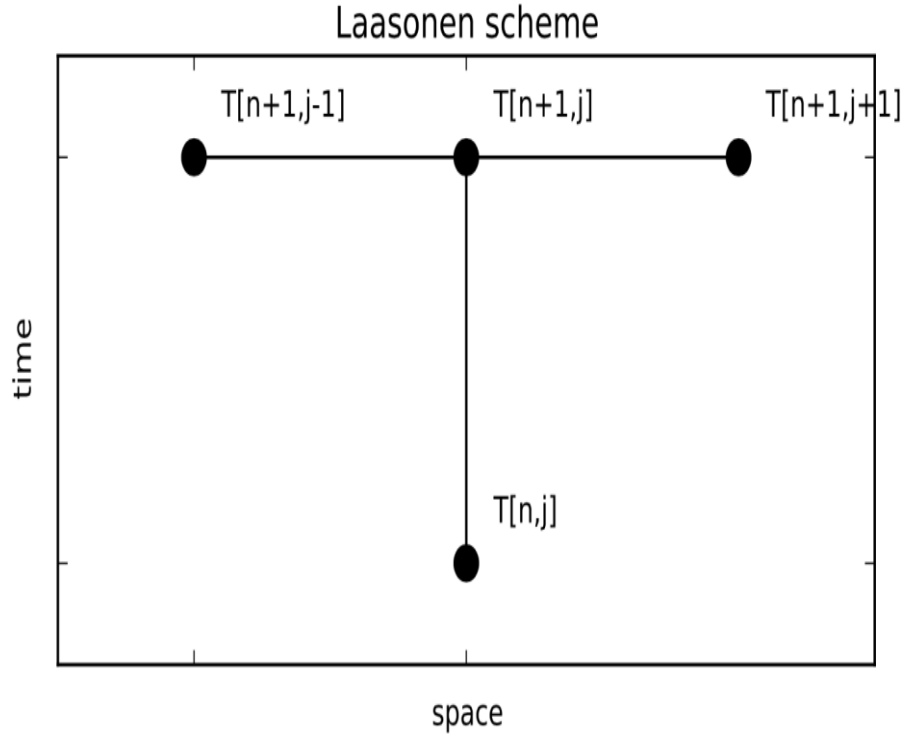

Figure 2.4: Computational molecule for the implicit BTCS scheme.

Richardson method

Richardson method is a Central Time Central Space (CTCS) scheme for parabolic type diffusion equations. This is known as the Richardson method. Order of accuracy of the scheme is O(Δt^2 , Δx^2). A stability analysis would show that it is unconditionally unstable, no matter how small t is. Thus, it is of no practical use. It may be noted that the unstable behavior refers to the equation as a whole. It is a stable method for convection equation.

Dufort–Frankel scheme

The Richardson method can be modified to produce a stable algorithm. This is achieved n by replacing ui on the right-hand side with the time-average of previous and current time values at n − 1 and n + 1. This new formulation is called Dufort–Frankel scheme.

This scheme is explicit and can be shown to be unconditionally stable by the von Neumann stability analysis. Since Dufort–Frankel stencil is constructed on the basis of an ad-hoc modification of the Richardson scheme, its consistency must be examined by computing the modified equation.

Note that the Dufort–Frankel method is a two-level method since the stencil contains values of *u* at two time levels other than the current level *n*.

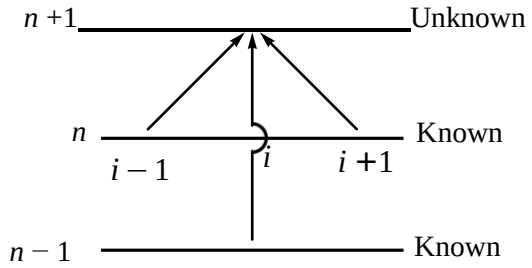

Figure 2.5: Computational molecule for the Dufort–Frankel scheme.

Consequently, to start the computation, values of *u* at *n* and *n* − 1 are required. Therefore, either two sets of initial data must be available or from a practical point of view, a one-step method may be used as a starter to generate additional data.

Order of accuracy of the scheme is $O(\Delta t^2, \Delta x^2, (\Delta t/\Delta x)^2)$. Even though the method is unconditionally stable, accurate solution will be obtained only if Δt, Δx.

Crank–Nicolson scheme

Both FTCS and BTCS schemes are first-order in time and second-order in space. Since they are first-order accurate in time, the time step Δt must be kept small to ensure acceptable accuracy. A scheme having a second-order accuracy in time for parabolic PDE can be obtained by taking the average of the FTCS and BTCS schemes.

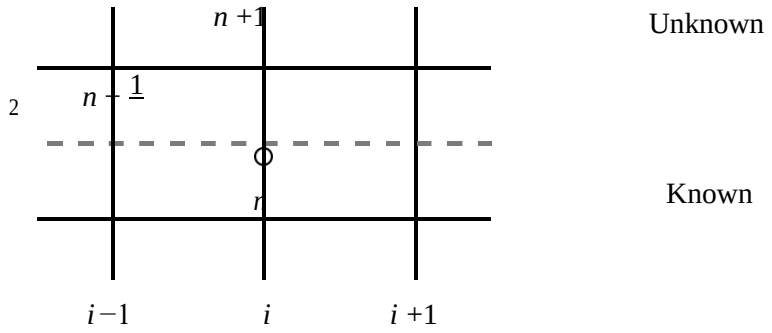

Figure 2.6: Grid points for the Crank–Nicolson scheme.

The new scheme known as the *Crank–Nicolson scheme* or *trapezoidal differencing scheme* named after their inventors John Crank and Phyllis Nicolson.

Where we have expressed u_{xx} at $n + 1/2$ time level by the average of the previous and current time values at *n* and *n* + 1 respectively. Crank–Nicolson method can also be written as an algorithm. A stability analysis would indicate that this implicit method is unconditionally stable.

Generalized implicit method

A general form of the finite difference approximation for diffusion equation may be obtained from Crank–Nicolson method by expressing space derivative by a weighted average of previous and current time values at n and $n + 1$. Where in practice $0 < \beta < 1$. This is known as the β-method. $\beta = 0$ gives the explicit FTCS scheme, $\beta = 1$ gives the fully implicit BTCS scheme, and $\beta = 1/2$ gives the Crank–Nicolson method. For $1/2 \leq \beta \leq 1$, the method is unconditionally stable, but for $0 \leq \beta < 1/2$

Alternating Direction Implicit (ADI) method

It is clear that, when implicit schemes are applied to multidimensional problems, the resulting implicit matrix system is not tridiagonal anymore as for three point discretizations on one- dimensional equations. Since each discretized equation consists of five unknowns, we obtain a pentadiagonal matrix system. Unfortunately, we do not have an efficient direct solver, such as Thomas algorithm, for the solution of a pentadiagonal matrix system.

However, a multidimensional problem can be split into a series of pseudo-one-dimensional problems and each of which can be solved using Thomas algorithm. More specifically, in a two-dimensional problem, each time step is split into two sub step of equal duration $\Delta t/2$ and approximating the spatial derivative in a partially implicit manner while alternating between x and y directions. This method is called Alternating Direction Implicit (ADI) method. The following are the two steps of ADI method by Peaceman and Rachford.

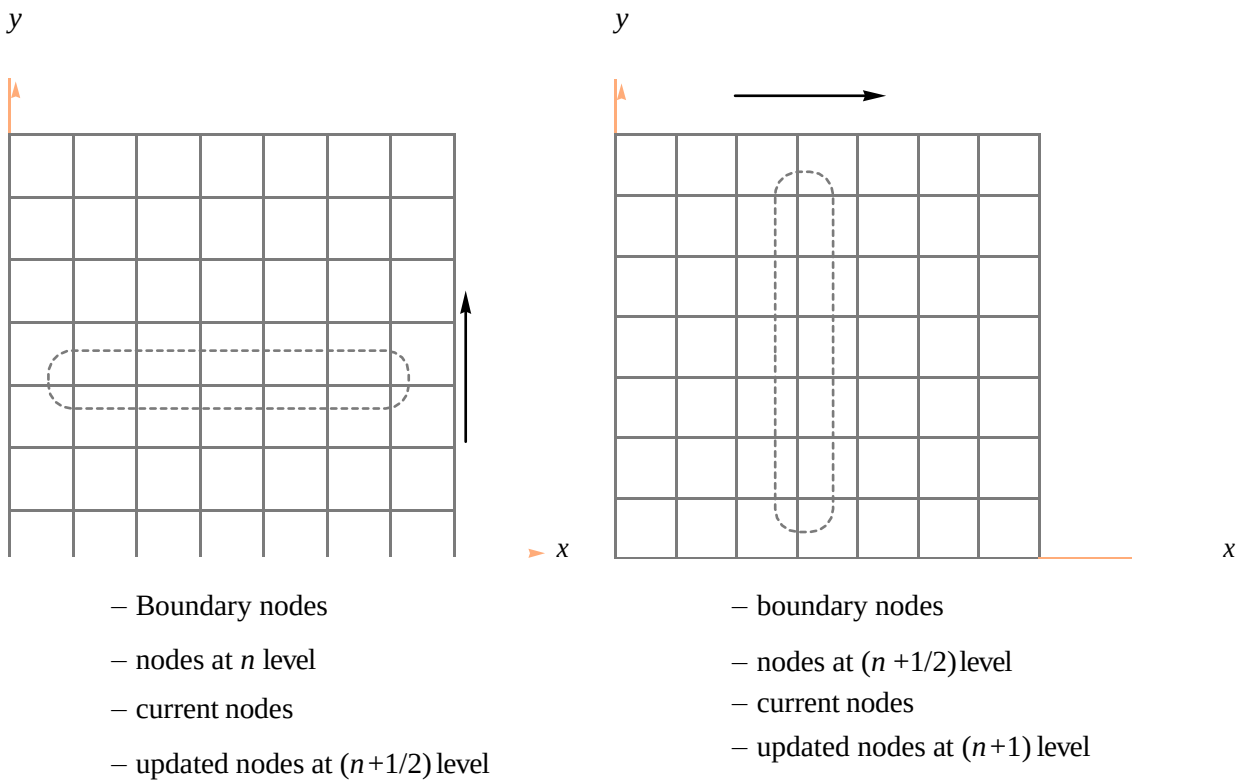

Figure 2.7: Grid system for ADI method.

The ADI formulation can be shown to be an approximate factorization method based on the Crank–Nicolson scheme.

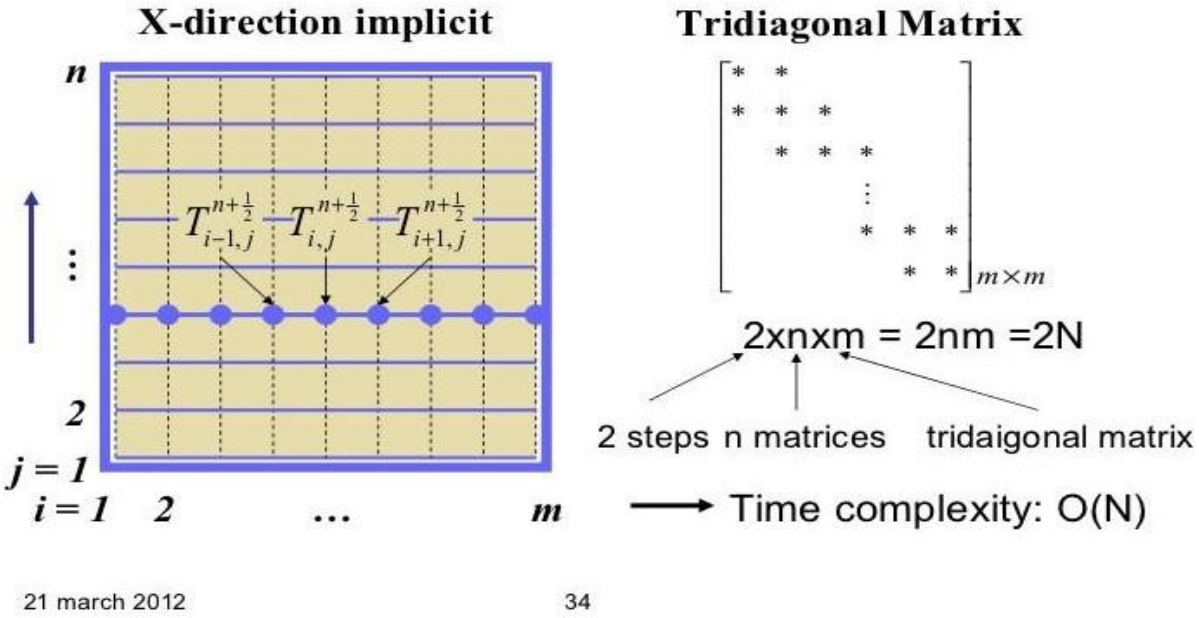

Figure 2.9 Analysis of ADI Method

Splitting or fractional step method

In the fractional step method, introduced by Yanenko, the original multidimensional equation is split into a series of one-dimensional equations and then solve them sequentially TDMA. This formulation can also be considered as a approximate factorization method. The method provides the following discretized equations for two-dimensional diffusion equation. This scheme is of the order of O Δt, Δx2, Δy2 and is unconditionally stable. The temporal accuracy can be made second-order by using a Crank–Nicolson scheme within each fractional step.

This scheme is of the order of O.Δt2, Δx2, Δy2. and is unconditionally stable.

Source from Computational Fluid Mechanics and Heat Transfer by Tannehill John C, Anderson Dale A, Pletcher Richard H

UNIT – III
BOUNDARY CONDITIONS

Steady State Laminar Boundary Layer on a Flat Plate

We consider a flat plate at $y = 0$ with a stream with constant speed U parallel to the plate. We are interested in the steady state solution. We are not interested in how the flow outside the boundary layer reached the speed U.

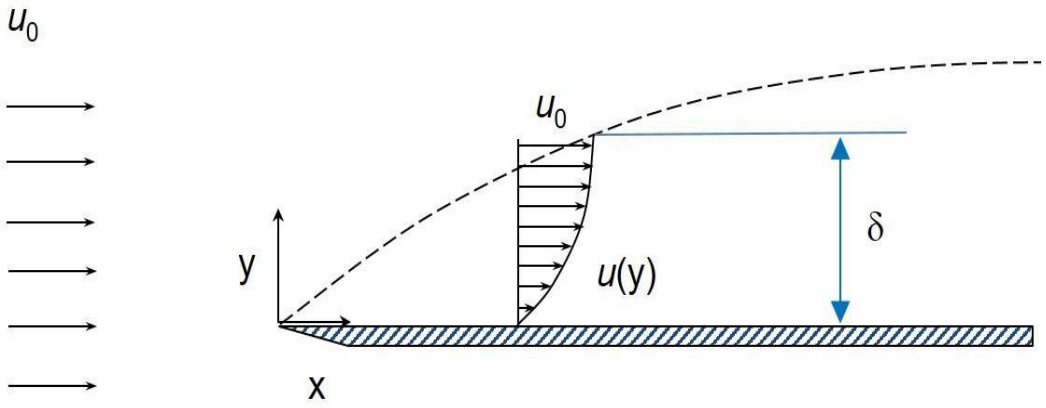

Figure 3.1: Laminar Boundary Layer on a Flat Plate

In this case, we need only to consider boundary conditions and the equation simplifies since $\partial u / \partial t = 0$. At the plate surface there is no flow across it, which implies that
$v = 0$ at $y = 0$.

Boundary Layer on a Flat Plate

Consider a flat plate of length L, infinite width, and negligible thickness, that lies in the x - z plane, and whose two edges correspond to x=0 and x=L . Suppose that the plate is immersed in a low viscosity fluid whose unperturbed velocity field is V= U0ex. In the inviscid limit, the appropriate boundary condition at the surface of the plate, $v_y = 0$ corresponding to the requirement of zero normal velocity is already satisfied by the unperturbed flow. Hence, the original flow is not modified by the presence of the plate.

However, when we take the finite viscosity of the fluid into account, an additional boundary condition, $v_x = 0$ corresponding to the no slip condition--must be satisfied at the plate. The imposition of this additional constraint causes thin boundary layers, of thickness $\delta(x) << L$, to form above and below the plate. The fluid flow outside the boundary layers remains effectively inviscid, whereas that inside the layers is modified by viscosity. It follows that the flow external to the layers is unaffected by the presence of the plate. Hence, the tangential velocity at the outer edge of the boundary layers is $U(x) = U_0$.

This corresponds to the case m=0 discussed in the previous section. (Here, we are assuming that the flow upstream of the trailing edge of the plate, x=L, is unaffected by the edge's presence, and, is, therefore, the same as if the plate were of infinite length. Of course, the flow downstream of the edge is modified as a consequence of the finite length of the plate.)

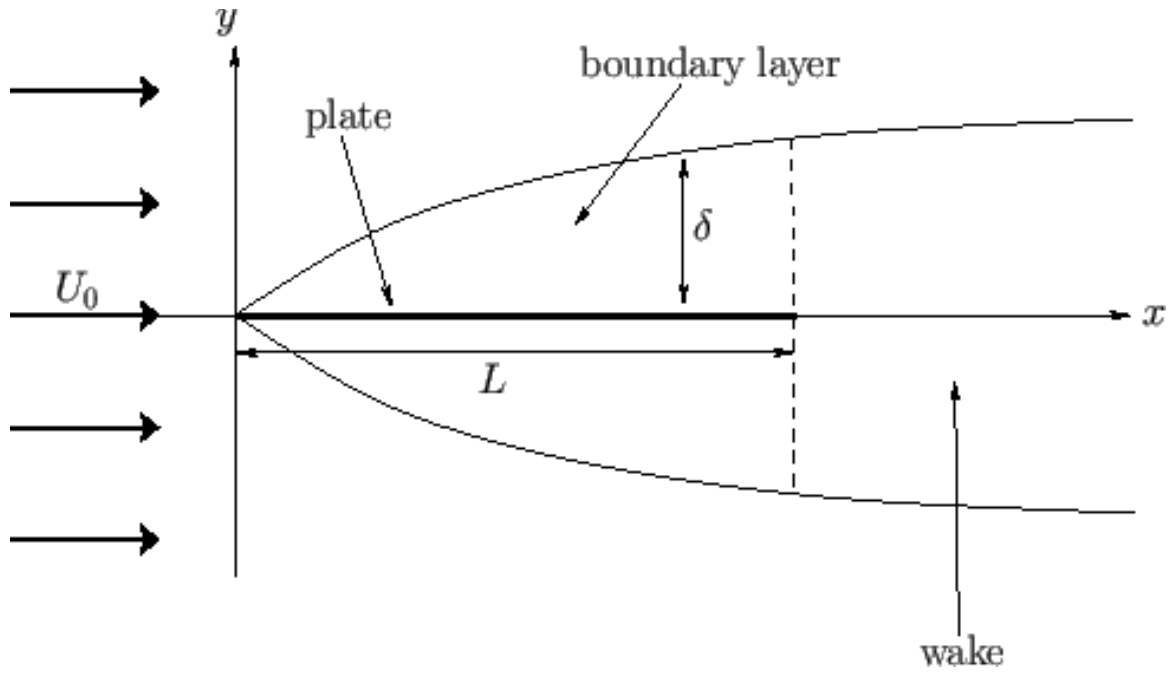

Figure 3.2**:** Flow over a flat plate.

Making use of the analysis contained in the previous section (with m=0), as well as the fact that, by symmetry, the lower boundary layer is the mirror image of the upper one, the tangential velocity profile across the both layers is written

$$v_x(x,y) = U_0\, f'(\eta),$$

where

$$\eta = \left(\frac{U_0}{2\,\nu\,x}\right)^{1/2} |y|.$$

Here,f(η) is the solution of

$$f''' + f\, f'' = 0$$

that satisfies the boundary conditions

$$f(0) = f'(0) = 0,$$

and

$$f'(\infty) = 1,$$

$$f''(\infty) = 0.$$

Equation is known as the *Blasius equation.*

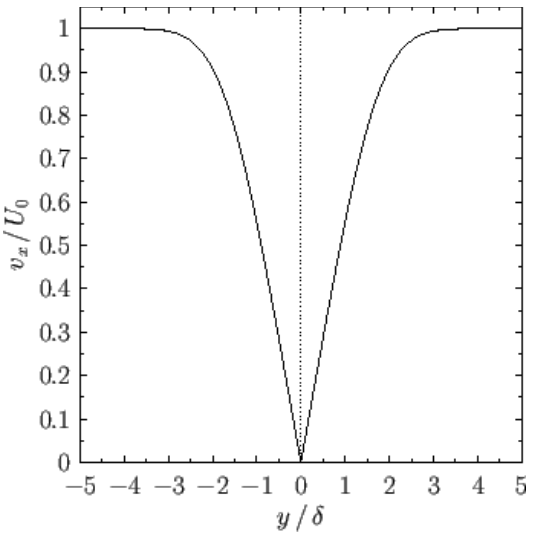

Figure: 3.3 Tangential velocity profile across the boundary layers located above and below a flat plate of negligible thickness located at y=0.

It is convenient to define the so-called *displacement thickness* of the upper boundary layer,

$$\delta(x) = \int_0^\infty \left[1 - \frac{v_x(x,y)}{U_0}\right] dy,$$

which can be interpreted as the distance through which streamlines just outside the layer are displaced laterally due to the retardation of the flow within the layer. (Of course, the thickness of the lower boundary layer is the same as that of the upper layer.) It follows that

$$\delta(x) = \left(\frac{\nu\, x}{U_0}\right)^{1/2} \sqrt{2} \int_0^\infty [1 - f'(\eta)]\, d\eta.$$

In fact, the numerical solution of Equation, subject to the boundary conditions, yields

$$\delta(x) = 1.72 \left(\frac{\nu\, x}{U_0}\right)^{1/2}.$$

Hence, the thickness of the boundary layer increases as the square root of the distance from the leading edge of the plate. In particular, the thickness at the trailing edge of the plate is

$$\frac{\delta(L)}{L} = \frac{1.72}{\mathrm{Re}^{1/2}},$$

where

$$\mathrm{Re} = \frac{U_0\, L}{\nu}$$

Re>>1is the appropriate Reynolds number for the interaction of the flow with the plate. Note that if then the thickness of the boundary layer is much less than its length, as was previously assumed.

The tangential velocity profile across the both boundary layers, which takes the form

$$v_x(x,y) = U_0\, f'\left[1.22\,\frac{|y|}{\delta(x)}\right],$$

is plotted in Figure . In addition, the vorticity profile across the layers, this is written

$$\omega(x,y) = -\mathrm{sgn}(y)\,1.22\,\frac{U_0}{\delta(x)}\,f''\left[1.22\,\frac{|y|}{\delta(x)}\right],$$

is shown in Figure . The vorticity is negative in the upper boundary layer (i.e.,y > 0), positive in the lower boundary layer (i.e., y < 0), and discontinuous across the plate (which is located at y = 0). Finally, the net viscous drag force per unit width (along the z -axis) acting on the plate in the x -direction is

$$D = 2\int_0^L \sigma_{xy}|_{y=0}\,dx,$$

where the factor of 2 is needed to take into account the presence of boundary layers both above and below the plate. It follows from Equation (with $m = 0$) that

$$D = \rho\,U_0^2\left(\frac{\nu}{U_0}\right)^{1/2}\sqrt{2}\,f''(0)\int_0^L x^{-1/2}\,dx = \rho\,U_0^2\left(\frac{\nu\,L}{U_0}\right)^{1/2}2\sqrt{2}\,f''(0).$$

In fact, the numerical solution of equation yields

$$D = 1.33\,\frac{\rho U_0^2\,L}{\mathrm{Re}^{1/2}} = 1.33\,\rho\,U_0\,(\nu\,U_0\,L)^{1/2}.$$

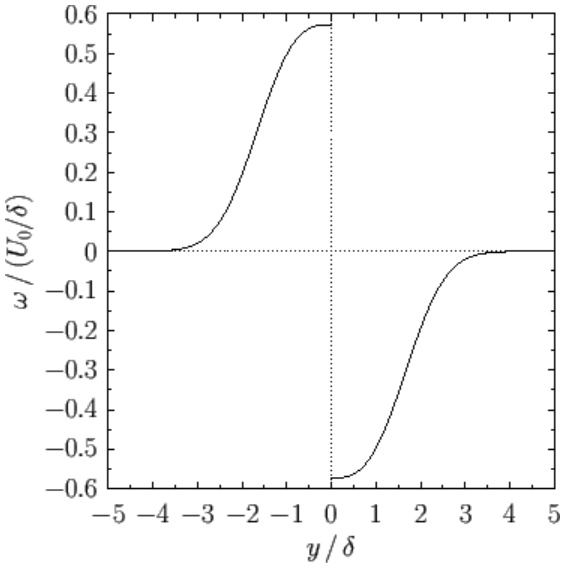

Figure: 3.4 Vorticity profile across the boundary layers located above and below a flat plate of negligible thickness located at y=0.

Source from Computational Fluid Mechanics and Heat Transfer by Tannehill John C, Anderson Dale A, Pletcher Richard H

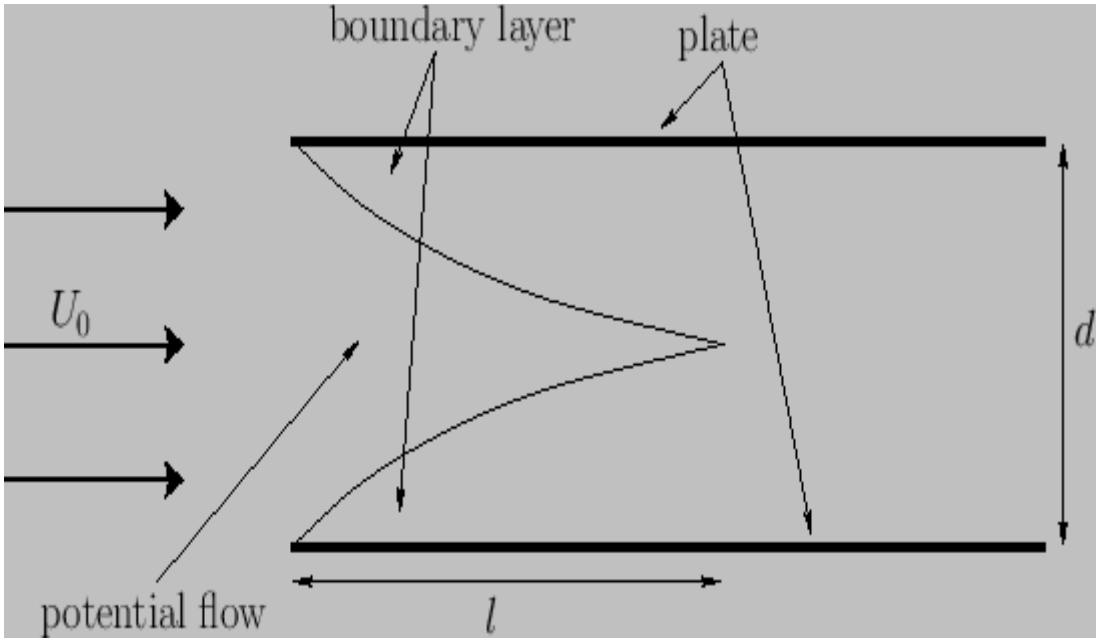

Figure 3.5: Flow between two flat parallel plates.

Consider, finally, the situation illustrated in Figure in which an initially irrotational fluid passes between two flat parallel plates. Let d be the perpendicular distance between the plates. As we have seen, the finite viscosity of the fluid causes boundary layers to form on the inner surfaces of the upper and lower plates. The flow within these layers possesses non-zero vorticity, and is significantly affected by viscosity. On the other hand, the flow outside the layers is irrotational and essentially inviscid--this type of flow is usually termed potential flow (because it can be derived from a velocity potential satisfying Laplace's equation). The thickness of the two boundary layers increases like $x^{1/2}$, where x represents distance, parallel to the flow, measured from the leading edges of the plates. It follows that, as x increases, the region of potential flow shrinks in size, and eventually disappears. Assuming that, prior to merging, the two boundary layers do not significantly affect one another, their thickness, $\delta(x)$, is given by formula, where U_o is the speed of the incident fluid. The region of potential flow thus extends from $x = 0$ (which corresponds to the leading edge of the plates) to $x = l$, where

$$\delta(l) = \frac{d}{2}. \tag{8.80}$$

It follows that

$$\frac{l}{d} = 11.8\,\mathrm{Re}, \tag{8.81}$$

where

$$\mathrm{Re} = \frac{U_0\, d}{\nu}. \tag{8.82}$$

Thus, when an irrotational high Reynolds number fluid passes between two parallel plates then the region of potential flow extends a comparatively long distance between the plates, relative to their spacing (i.e.,l/d>>1). By analogy, if an irrotational high Reynolds number fluid passes into a pipe then the fluid remains essentially irrotational until it has travelled a considerable distance along the pipe, compared to its diameter. Obviously, these conclusions are modified if the flow becomes turbulent.

Due to the viscosity we have the no slip condition at the plate. In other words,
$u = 0$ at $y = 0$.
At infinity (outside the boundary layer), away from the plate, we have that
$u \rightarrow U$ as $y \rightarrow \infty$.
For the flow along a flat plate parallel to the stream velocity U, we assume no pressure gradient, soothe momentum equation in the x direction for steady motion in the boundary layer is
$u\partial u + v\ \partial u$
These conditions demand an infinite gradient in speed at the leading edge $x = y = 0$, which implies a singularity in the mathematical solution there. However, the assumptions implicit in the boundary layer approximation break down for the region of slow flow around the leading edge. The solution given by the boundary layer approximation is not valid at the leading edge. It is valid downstream of the point $x = 0$.
At $y \rightarrow \infty$, all x; $\partial y = U$.
The boundary value problem admits a similarity solution. We would like to reduce the partial differential equation to an ordinary differential equation. We would like to find a change of variables which allows us to perform the reduction mentioned above.

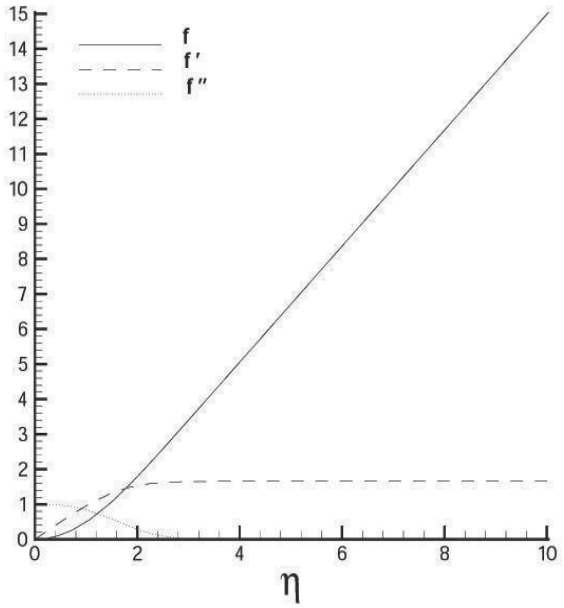

Figure 3.6: Functions f (η), ft(η) and ftt(η). The horizontal axis represents the range of values of η considered, and in the vertical axis we have the values of the functions f (η), ft(η) and ftt(η).

Once we have computed numerically f (η) and its derivatives up to second order, we can obtain the velocity components (u, v) at any point (x, y) of the flow domain, according to the equations.

Boundary-layer Thickness, Skin friction, and Energy dissipation

According to equation, the pressure across the boundary layer is constant in the boundary-layer approximation, and its value at any point is therefore determined by the corresponding main-stream conditions. If U(x,t) now denotes the main stream velocity.

Elimination of the pressure from equation gives in terms of dimensional variables the boundary layer momentum equation.
In most physical problems the solutions of the boundary layer equations are such that the velocity component u attains its main-stream value U only asymptotically as R1/2y/L $\rightarrow \infty$. The thickness of the layer is therefore indefinite, as there is always some departure from the asymptotic value at any finite distance y from the surface. In practice the approach to the limit is rapid and a point is soon reached beyond which the influence of viscosity is imperceptible. It would therefore be possible to regard the boundary layer thickness as a distance δ from the surface beyond which u/Y > 0.99, for example, but this is not sufficiently precise (since $\partial u/\partial y$ is small there) for experimental work, and is not of theoretical significance.

The scale of the boundary layer thickness can, however, is specified adequately by certain lengths capable of precise definition, both for experimental measurement and for theoretical study. These measures of boundary layer thickness are defined as follows:
Displacement thickness $\delta 1$
Momentum thickness $\delta 2$
Energy thickness $\delta 3$

The upper limit of integration is taken as infinity owing to the asymptotic approach of u/U to 1, but in practice the upper limit is the point beyond which the integrand is negligible.
$U\delta 1$ is the diminution, due to the boundary layer, of the volume flux across a normal to the surface; the streamlines of the outer flow are thus displaced away from the surface
Two other quantities related to these boundary layer thickness are the skin friction $\tau\omega$ and the dissipation integral D.

Turbulent Flat Plate Boundary Layer

A laminar boundary layer over a flat plate eventually becomes turbulent over certain range of Reynolds number. There is no unique value pf Reynolds number, for this change to happen. It mainly depends on the free stream turbulence and surface roughness parameters. With a very fine polished wall and with a quiet free stream, one can delay the transition. A controlling parameter such as the critical Reynolds number of transition Rex, CR may be defined.

On a flat plate with a sharp leading edge in a typical free stream air flow, the transition occurs between the Reynolds number ranges of 2×10^5 to 3×10^5.
So the transitional Reynolds number is normally taken as Rex, CR =3×10^5.

The complex process of transition from laminar to turbulent flow involves the instability in the flow field. The small disturbances imposed on the boundary layer flow will either grow (i.e. instability) or decay (stability) depending on the location where the disturbance is introduced. If the disturbance occurs at a location where $Re_x < Re_x$, C_R, then the boundary layer will return to laminar flow at that location.

Disturbances imposed on locations $Re_x > Re_x$, C_R will grow and the boundary layer flow becomes turbulent from this location. The transition to turbulence involves noticeable change in the shape of boundary layer velocity profile as shown in Fig. As compared to laminar profiles, the turbulent velocity profiles are flatter and thicker at the same Reynolds number. Also, they have larger velocity gradient at the wall.

There is no exact theory for turbulent flat plate flow rather many empirical models are available. To begin with the analysis of turbulent boundary layer, let us recall the momentum-integral relation which is valid for both laminar as well as turbulent flows.

$$\tau_w(x) = \rho U^2 \frac{d\theta^*}{dx}$$

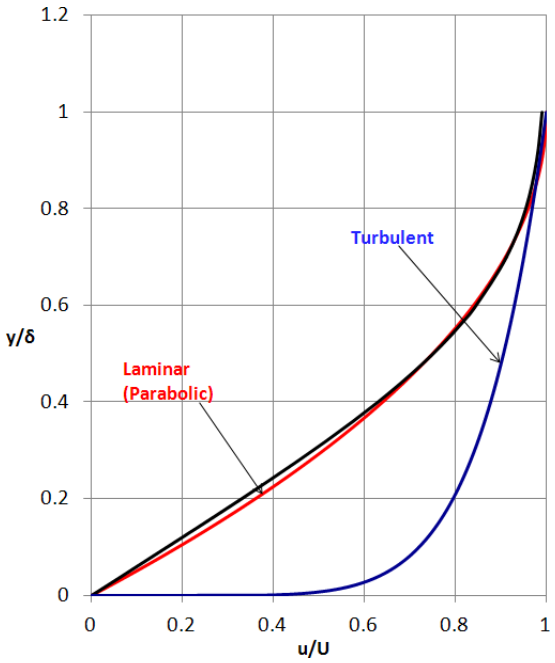

Fig. 3.7: Comparison of laminar and turbulent boundary layer profiles for flat plate.

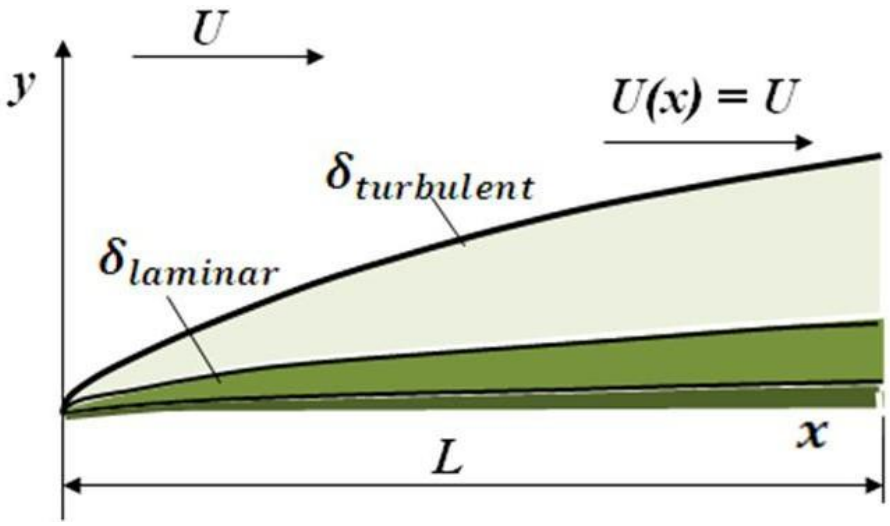

Fig. 3.8: Comparison of laminar and turbulent boundary layer profiles for flat plate.

Parameters	*Laminar (Blasius solution)*	*Turbulent (Prandtl approximation)*
Boundary layer thickness	$\frac{\delta}{x}=\frac{5}{\sqrt{\mathrm{Re}_x}}$	$\frac{\delta}{x}=\frac{0.16}{(\mathrm{Re}_x)^{1/7}}$
Displacement thickness	$\frac{\delta^*}{x}=\frac{1.72}{\sqrt{\mathrm{Re}_x}}$	$\frac{\delta^*}{x}=\frac{0.02}{(\mathrm{Re}_x)^{1/7}}$
Momentum thickness	$\frac{\theta^*}{x}=\frac{0.664}{\sqrt{\mathrm{Re}_x}}$	$\frac{\theta^*}{x}=\frac{0.016}{(\mathrm{Re}_x)^{1/7}}$
Shape factor	$H=\frac{\delta^*}{\theta^*}=2.59$	$H=\frac{\delta^*}{\theta^*}=1.25$
Local skin friction coefficient	$c_f=\frac{0.664}{\sqrt{\mathrm{Re}_x}}$	$c_f=\frac{0.027}{(\mathrm{Re}_x)^{1/7}}$
Wall shear stress	$\tau_w=\frac{0.332\mu^{1/2}\rho^{1/2}U^{3/2}}{x^{1/2}}$	$\tau_w=\frac{0.0135\mu^{1/7}\rho^{6/7}U^{13/7}}{x^{1/7}}$
Drag coefficient	$c_d=\frac{1.328}{\sqrt{\mathrm{Re}_L}}$	$c_d=\frac{0.031}{(\mathrm{Re}_L)^{1/7}}$

Two-dimensional Laminar Jet

We consider a two-dimensional jet as illustrated in the figure below. x is the horizontal coordinate and y is the vertical coordinate. u and v are, respectively, the horizontal and vertical fluid velocities. The jet in the direction of the x axis generates a flow where the fluid velocity along the y axis tends to zero.

We assume that the boundary layer approximation is valid and the governing equation for the fluid motion are equations but with ∂u/∂t.

The pressure does not vary in the y direction according to equation, soothe pressure is constant across the boundary layer and its gradient is given by the pressure gradient outside the boundary layer.

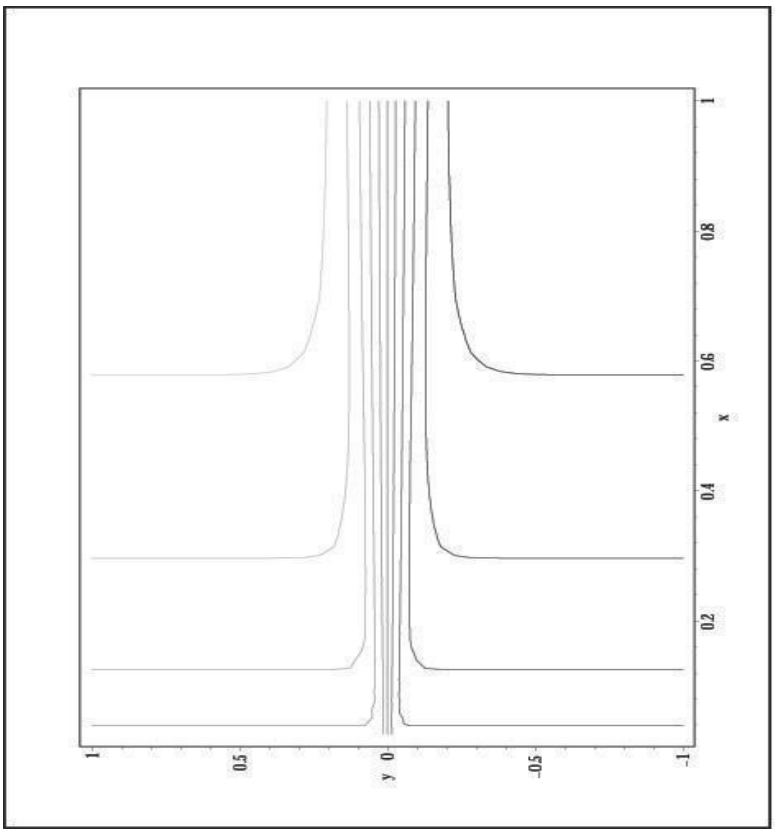

Figure 3.9: Streamlines obtained from equation with M = 1000kg/sec2, ν = 0.01m2/sec and ρ = 1000kg/m3.

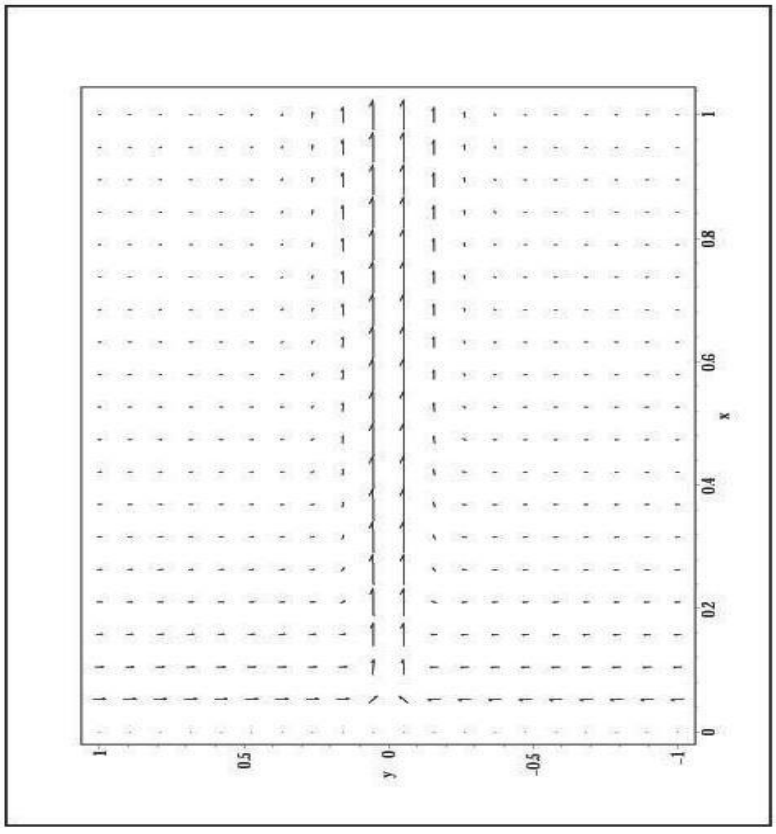

Figure 3.10: Velocity field obtained from equations (8.177) and (8.178) with M = 1000kg/sec2, ν = 0.01m2/sec and ρ = 1000kg/m3.

Source from Computational Fluid Mechanics and Heat Transfer by Tannehill John C, Anderson Dale A, Pletcher Richard H

Boundary Condition

Now let us discuss about the boundary conditions.

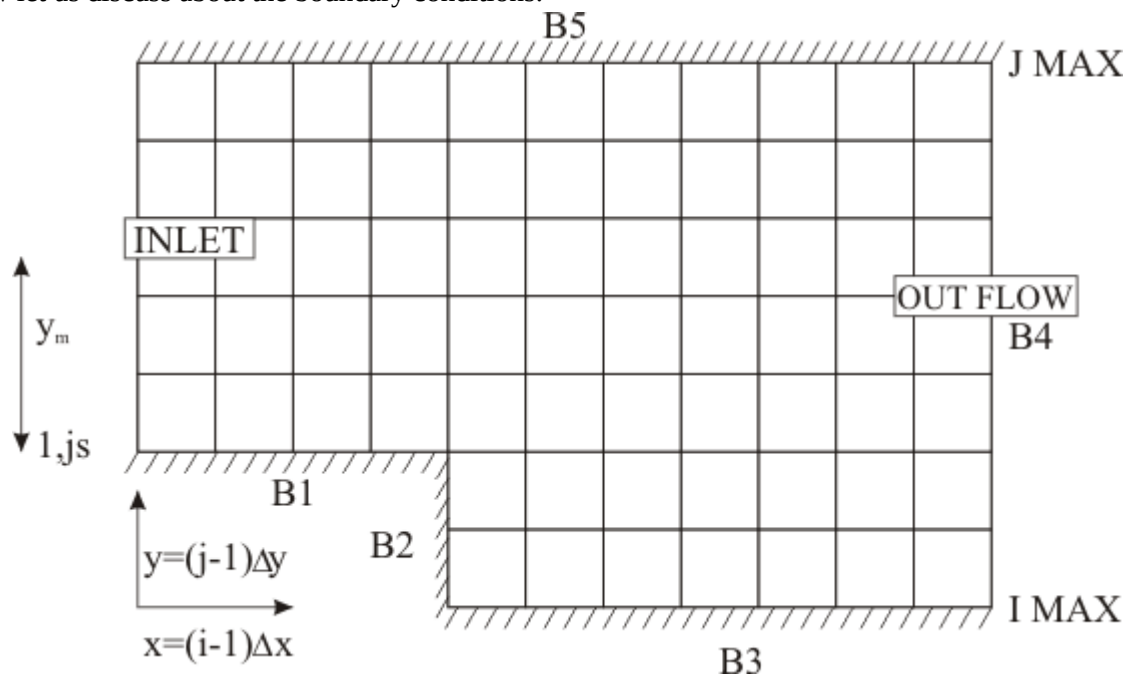

Figure 3.11 Illustration of boundary condition

Consider Fig. 3.11, we shall call B1 and B3 as bottom wall. Similar kind of boundary conditions is applicable on B1 and B3. At the nodal points which are coinciding with the solid wall we can directly put $u_{i,j}=0$ and $V_{i,j}=0$ Since the line B1-B2-B3 is a streamline, any constant value of ψ on it is acceptable. The usual choice is $\psi_{i,j}=0$. The wall vorticity is an extremely important evaluation. At no-slip boundaries $\omega_{i,j}$ is produced. It is the diffusion and subsequent advection of the wall produced vorticity which governs the physics. Using boundary B1 as an example, we expend $\psi_{i,j+1}$ by a Taylor series as

$$\psi_{i,js+1} = \psi_{i,js} + \left.\frac{\partial \psi}{\partial y}\right|_{i,js} \Delta y + \frac{1}{2}\left.\frac{\partial^2 \psi}{\partial y^2}\right|_{i,js} (\Delta y)^2 + \frac{1}{6}\left.\frac{\partial^3 \psi}{\partial y^3}\right|_{i,js} (\Delta y)^3 + \ldots.$$

But $\left.\frac{\partial \psi}{\partial y}\right|_{i,js} = u_{i,js} = 0$ by no-slip condition and $\left.\frac{\partial^2 \psi}{\partial y^2}\right|_{i,js} = \left.\frac{\partial u}{\partial y}\right|_{i,js}$

Again, $\omega = \frac{\partial v}{\partial x} - \frac{\partial u}{\partial y}$

Along the wall, $\left.\frac{\partial v}{\partial x}\right|_{i,js} = 0$ [because υ constant = 0].

Thus, $\omega_{i,js} = -\left.\frac{\partial u}{\partial y}\right|_{i,js}$

Substituting this into (25.1) and solving for $\omega_{i,js}$ with $\psi_{i,js}=0$ gives

$$\omega_{i,js} = \frac{-2\psi_{i,js+1}}{(\Delta y)^2}$$

More general from regardless of the wall orientation or value of ψ at the boundary, it can be written as

$$\omega\Big|_{at\ W} = \frac{-2(\psi_{W+1} - \psi_W)}{(\Delta n)^2}$$

where Δη is the distance from(w+1) to (w) in the normal direction [w denotes at the wall].

Upper Boundary

The upper boundary B5 in Fig 3.11 is having the usual no-slip and impervious conditions for velocity components. i.e., $u_{i,j}$ =0 $V_{i,j}$=0 For vorticity (ψi,j) will apply.
But how to evaluate $\psi_{i,j}$ at the upper wall?
The value of $\psi_{i,j}$ at the upper wall is constant and may be evaluated by integrating the u velocity profile at the inlet. Integration may be performed through Simpson's rule to get

$$\psi_{i,j|w} = \int_{y\ at\ j=js}^{y\ at\ j=JMAX} u(y)_{inlet}\ \ dy$$

If we want to model the condition of no boundary at B5, or, in other words, in y-direction, fluid at infinite extent is assumed, the problem is little more difficult.

However, Thoman and Szewczyk (1966) used a treatment which specifies this far-field condition

of $\psi_{i,j}$ =0 with $\frac{\partial \psi}{\partial y} = u = U_\infty$ and $\frac{\partial \psi}{\partial x} = v = 0.$

Thus u=U∞ was applied through a Neumann condition at the boundary along B5 as

$$\psi_{i,ju} = \psi_{i,ju-1} + U_\infty \Delta y$$

where B5 is considered at j=ju

Inlet Boundary

Inlet boundary in Fig. 3.11 cannot have any unique prescription. It will depend on the physical situation. For the axial velocity (u) uniform or parabolic or any possible profile can be taken.

Most widely used conditions are:

$u_{1,j}$=U_∞ for $j = js$ to JMAX

or,

$$u_{1,j} = 1.5U_{av}\left[1 - \left(\frac{y_m - y}{y_m}\right)^2\right]_{j=js\ to\ JMAX}$$

For normal velocity(v), Formm and Harlow (1963) set

$u_{1,j} = 0$ for $j = js$ to JMAX

The stream function $\psi_{i,j}$ can be obtained from the axial velocity profile at the inlet as

$$\psi_{1,j} = \int_{y\ at\ js}^{y\ at\ j} u(y)\Big|_{inlet}\ dy$$

Vorticity ($\psi_{i,j}$) also depends on inlet velocity profile. Pao and Daugherty (1969) used uniform axial velocity profile, v=0, and then specified $\omega_{i,j}$=0 Greenspan (1969) fixed up ($\omega_{i,j}$) from axial velocity

profile and assumed $\partial v/\partial x = 0,$ which result in

$$\omega_{1,j} = -\frac{\partial^2 \psi}{\partial y^2} = -\frac{\partial u}{\partial y}$$

Outflow Boundary

B4 is the outflow boundary (Fig. 3.11). If the outflow boundary conditions are known beforehand, then why are we computing? They are not known explicitly, but we can prescribe or set some gradients at the out let which are physically meaningful. We can imagine about continuative outflow conditions which will ensure smooth transition through the outlet boundary. For axial and normal velocities, we can impose less restrictive type condition, which are

$$\frac{\partial u}{\partial x} = \frac{\partial v}{\partial x} = 0$$

Thoman and Szewczyk (1966) developed outflow boundary conditions through setting

$$\frac{\partial \omega}{\partial x} = 0$$

Boundary Conditions

Any numerical simulation can consider only a part of the real physical domain or system. The truncation of the domain leads to artificial boundaries, where we have to prescribe values of certain physical quantities. Furthermore, walls which are exposed to the flow represent natural boundaries of the physical domain.The numerical treatment of the boundary conditions requires a particular care.

An improper implementation can result in inaccurate simulation of the real system. Additionally, the stability and the convergence speed of the solution scheme can be negatively influenced.

The following types of boundary conditions are in general encountered in the numerical solution of the Euler and the Navier-Stokes equations:

- Solid wall,
- Far field in external and inflow/outflow in internal flows,
- Symmetry,
- Coordinate cut and periodic boundary,
- Boundary between blocks.

Concept of Dummy Cells

Before we proceed with the discussion of the boundary conditions, we should mention the concept of dummy cells (also known as dummy points). This approach is very popular on structured grids. However, dummy cells offer some advantages also on unstructured grids. The dummy cells are additional layers of grid points outside the physical domain. This is sketched in Fig. 3.12 for the case of a 2-D structured grid. As we can see, the whole computational domain is surrounded by two layers of dummy cells (denoted by dashed line). The dummy cells (points) are usually not generated as the grid inside the domain (except on multiblock grids). Rather, the cells are only virtual, although there are also geometrical quantities like volume or face vector associated with them.

The purpose of the dummy cells is to simplify the computation of the fluxes, gradients, dissipation, etc. along the boundaries. This is achieved by the possibility to extend the stencil of the spatial discretization scheme beyond the boundaries. As we can see in Fig. 8.1, the same discretization scheme can be employed at the boundaries like inside the physical domain. Thus, we can solve the governing equations in the same way in all “physical” grid points. This makes the discretization scheme much easier to

implement. Furthermore, all grid points of a structured grid can be accessed in a single loop, which is of significant advantage particularly on vector computers. The condition is of course that the dummy cells (points) contain appropriate values of the conservative variables as well as of geometrical quantities. Clearly, the number of dummy cell layers must be such that the part of the stencil outside the physical domain is completely covered. The conservative variables in the dummy cells (points) are obtained from boundary conditions.

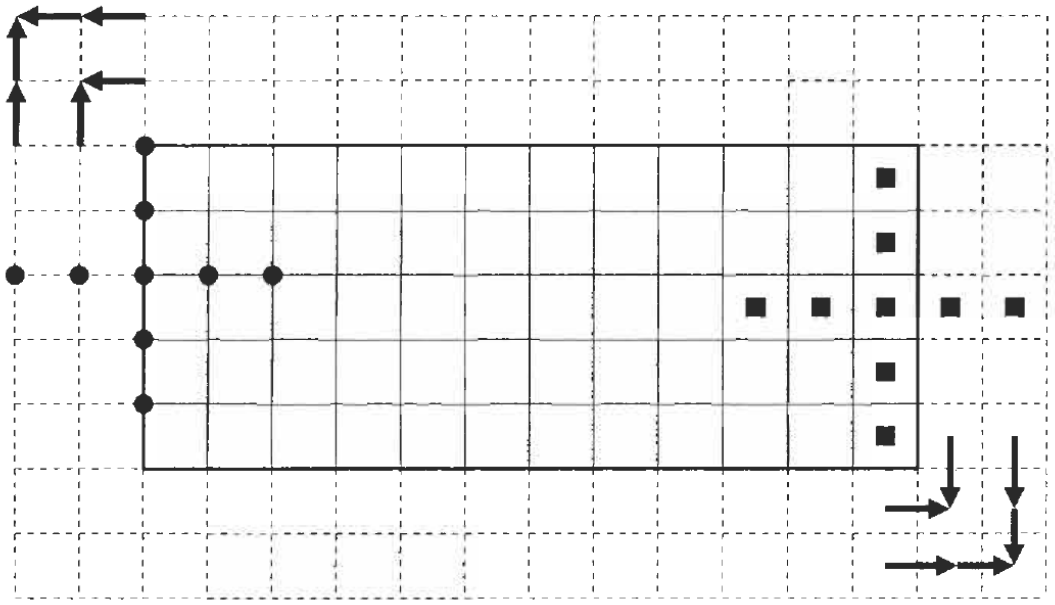

Figure 3.12: Two layers of dummy cells (dashed line) around the computational domain (thick line) in 2D. Filled circles represent the standard stencil of a 2ndorder cell-vertex (dual) scheme, filled rectangles outline the stencil of a 2nd-order cell-centered scheme

The geometrical quantities are usually taken from the Corresponding control volume at the boundary. In the case of boundaries between multiple grid blocks (Section 3.1), all flow variables and the geometry are transferred from the neighboring block. The grey-shaded dummy cells in Fig. 3.12 represent a certain problem, since it is not quite clear how to set their values (if there is no adjacent grid block).
The values are not required by the standard cross-type discretization stencil. However, they may become necessary for the computation of gradients. Usually, an averaging of the values from the adjacent "regular" dummy cells, as indicated in Fig. 3.12 by arrows, is sufficient.

Solid Wall

Inviscid Flow

In the case of an inviscid flow, the fluid slips over the surface. Since there is no friction force, the velocity vector must be tangent to the surface. This is equivalent to the condition that there is no flow normal to the surface, i.e.,v. n' = 0 at the surface, where fi denotes the unit normal vector at the surface. Hence, the contravariant velocity V is zero at the wall. Consequently, the vector of convective fluxes Eq. reduces to the pressure term alone, i.e, with p, being the wall pressure.

$$\vec{v} \cdot \vec{n} = 0 \qquad \text{at the surface}$$

$$(\vec{F}_c)_w = \begin{bmatrix} 0 \\ n_x\, p_w \\ n_y\, p_w \\ n_z\, p_w \\ 0 \end{bmatrix}$$

Structured Cell-Centered Scheme

Within the cell-centered scheme, the pressure is evaluated at the centroid of the cell. However, pw in Equation is required at the face of the boundary cell. We can obtain the wall pressure easily by extrapolation from the interior of the domain. Considering Fig. 8.2, we could simply set p, = pz. Higher accuracy is achieved by using either a two-point

$$p_w = \frac{1}{2}(3p_2 - p_3)$$

or a three-point extrapolation formula

$$p_w = \frac{1}{8}(15p_2 - 10p_3 + 3p_4)$$

In order to account for grid stretching, distances to the wall could be employed instead of the constant coefficients.

The above extrapolation formulae do not account for the grid and the surface geometry. An alternative approach - the so-called nominal momentum relation -was developed by Ftizzi. It is based on the fact that the wall represents a streamline in inviscid flow. Differentiation of the zero normal flow condition in Eq. along the surface streamline, and the substitution of the result into the momentum equation yields

$$\rho\vec{v} \cdot (\vec{v} \cdot \vec{\nabla})\, \vec{n} = \vec{n} \cdot \vec{\nabla} p$$

Equation relates the density, the velocity and the wall geometry to the normal derivative of the pressure. It was demonstrated that the normal-momentum relation gives very accurate results. However, in the case of complex geometries there can be problems with the numerical solution of the normal momentum relation.

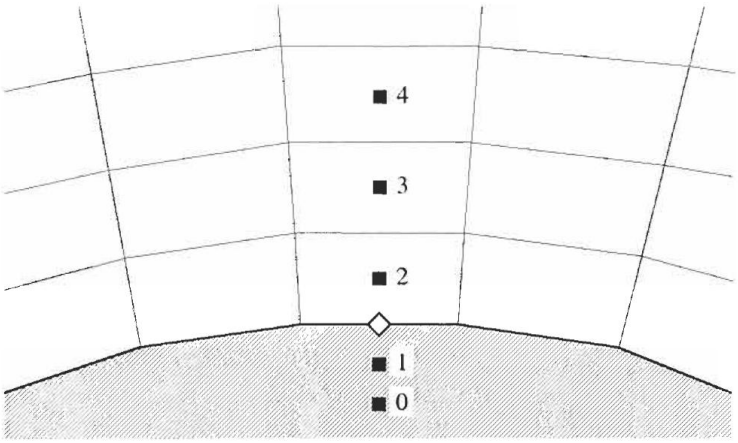

Figure 3.13: Solid wall boundary condition for the cell-centered scheme. Dummy cells are denoted as 0 and 1. Location, where the convective fluxes Equation are evaluated, is marked by a diamond.

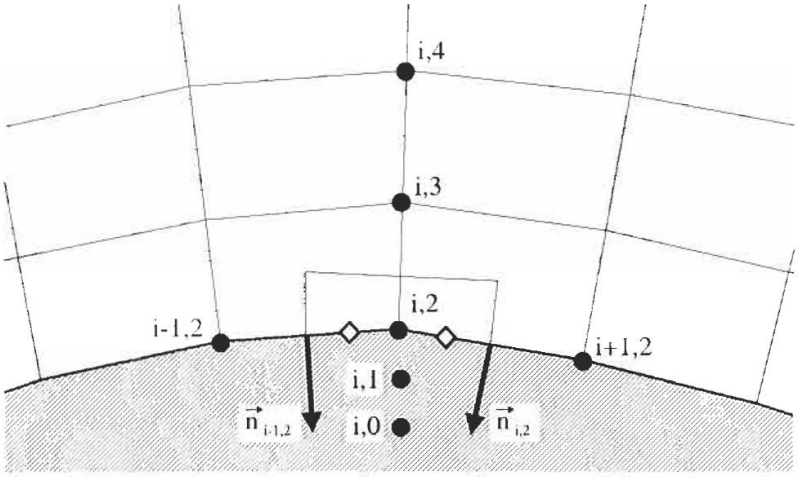

Figure 3.14: Solid wall boundary condition for the structured, cell-vertex dual control-volume scheme. Dummy points are denoted as (i, 0) and (i, 1). Locations, where the convective fluxes Equations are evaluated, are marked by diamonds.

The values of the conservative variables in the dummy cells can be obtained by linear extrapolation from the interior, i.e.,

$$\vec{W}_1 = 2\vec{W}_2 - \vec{W}_3$$

$$\vec{W}_0 = 3\vec{W}_2 - 2\vec{W}_3$$

Structured Cell-Vertex Scheme

The implementation of the boundary condition is straightforward for the cell-vertex discretization scheme with overlapping control volumes. The convective fluxes at the wall faces are computed according to Equation. The wall pressure p, is obtained by averaging the nodal values as indicated in Equation for a 2-D, or in Equation for a 3-D case. The distribution formula accounts now for only two cells.

Several different ways can be followed in the case of the cell-vertex scheme with dual control volumes. One approach is to apply the condition in Equation separately for each face of the control volume which is on the wall. Thus, according to Fig.3.14, we can write

$$(\vec{F}_{c,w})_{i,2} = \begin{bmatrix} 0 \\ (n_x)_{i-1,2}\,(p_w)_{i-1/4,2} \\ (n_y)_{i-1,2}\,(p_w)_{i-1/4,2} \\ (n_z)_{i-1,2}\,(p_w)_{i-1/4,2} \\ 0 \end{bmatrix} + \begin{bmatrix} 0 \\ (n_x)_{i,2}\,(p_w)_{i+1/4,2} \\ (n_y)_{i,2}\,(p_w)_{i+1/4,2} \\ (n_z)_{i,2}\,(p_w)_{i+1/4,2} \\ 0 \end{bmatrix}.$$

The pressures (Pw)i-1/4,2 and (p,)i+1/4,2 in Equation can be obtained by linear interpolation, e.g.,

$$(p_w)_{i+1/4,2} = \frac{1}{4}\left[3(p_w)_{i,2} + (p_w)_{i+1,2}\right]$$

The corresponding 3-D formula will be presented further below in the subsection on unstructured grids.

Another possible implementation employs the condition in Equation directly in the respective wall node (i.e., node 2 in Fig. 8.3). The wall pressure p, is simply set equal to p2. The unit normal vector is computed as the average of the normal vectors of all wall facets which share the node 2.
This approach requires a correction of the velocity vector. After the solution update by the time-stepping scheme, the velocity vector at the wall is projected onto the tangential plane with day being the averaged unit normal vector. In this way, the Row will become tangential to the wall.

$$(\vec{v}_{i,2})_{corr} = \vec{v}_{i,2} - \left[\vec{v}_{i,2} \cdot (\vec{n}_{av})_{i,2}\right] \cdot (\vec{n}_{av})_{i,2}$$

Unstructured Cell-Centred Scheme

The wall boundary condition in Equation can be implemented for a cell-centered unstructured scheme in a way similar to that on structured grids. If the boundary cell is a quadrilateral, hexahedron or a prism (with triangular face on the wall), the pressure can be extrapolated to the wall by using equation. The neighboring cell is known from the face-based data structure. For the case of a triangular or tetrahedral cell, it was suggested to employ one layer of dummy cells. The velocity components in the dummy cells were obtained by reflecting the velocity vectors in the boundary cells at the wall. For example, in the dummy cell 1, the velocity would become

$$\vec{v}_1 = \vec{v}_2 - 2\,V_2\vec{n}$$

Where

$$V_2 = u_2 n_x + v_2 n_y + w_2 n_z$$

is the contravariant velocity and

$$\vec{n} = \left[n_x, n_y, n_z\right]^T$$

stands for the wall unit-normal vector. The pressure and density in the dummy cells were set equal to the values in the corresponding boundary cell (this implies Pw = P2).

Unstructured Median-Dual Scheme

The boundary condition Equation requires more attention in the case of the median-dual unstructured discretization scheme. The situation is shown in Fig. 3.15 for the 2-D and in Fig. 3.16 for the 3-D case. The convective fluxes in equation are computed separately at each face of the control volume which is located on the wall. This is identical to the first approach discussed above for the structured cell-vertex scheme with dual control volumes. For quadrilateral elements, the pressure is interpolated correspondingly to equation. In the case of hexahedra, prisms or pyramids, where the face of the control volume is quadrilateral, the interpolation formula reads

$$p_{int} = \frac{1}{16}(9p_1 + 3p_4 + 3p_6 + p_5)$$

If the boundary elements are tetrahedral (or triangles in 2-D), the pressure at the wall face should be evaluated like in the finite element method. At the wall segment 1-2 in Fig. 3.15 for example, the pressure at the face 1-2* would be computed as

$$p_{int} = \frac{1}{6}(5p_1 + p_2)$$

In the case of a tetrahedral with, e.g., the wall face 1-2-3 in Fig. 3.16, the pressure is given by

$$p_{int} = \frac{1}{8}(6p_1 + p_2 + p_3)$$

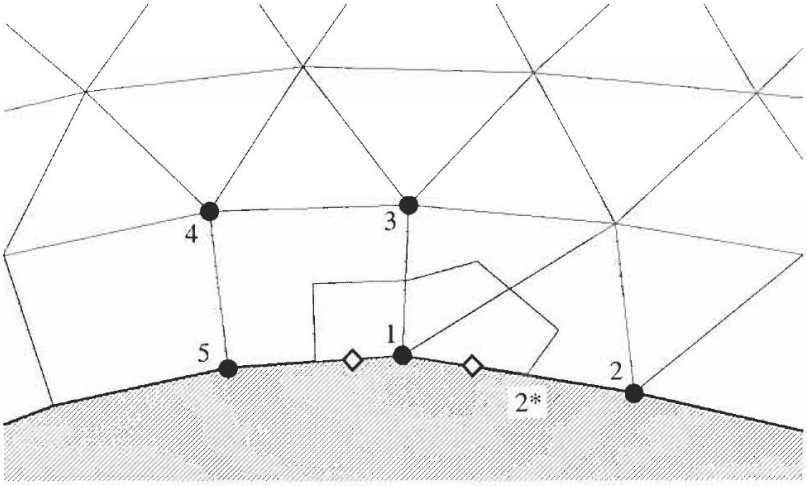

Figure 3.15: Solid wall boundary condition for the 2-D unstructured, dual control volume mixed-grid scheme. Locations, where the convective fluxes Equation are evaluated, are marked by diamonds.

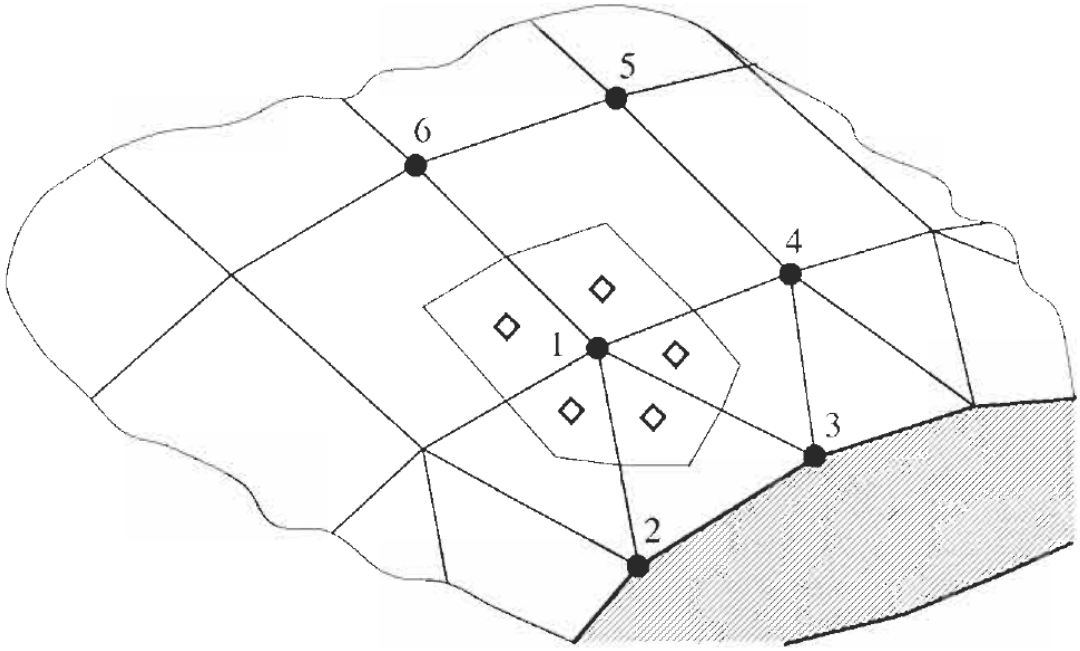

Figure 3.16: Solid wall boundary condition for the 3-D unstructured, mixed grid scheme. Locations, where the convective fluxes Equation are evaluated, are marked by diamonds.

Viscous Flow

For a viscous fluid which passes a solid wall, the relative velocity between the surface and the fluid directly at the surface is assumed to be zero. Therefore, we speak of noslip boundary condition. In the case of a stationary wall surface, the Cartesian velocity components become u = v = w = 0 at the surface.

There are two basic consequences of the noslip condition. First, we do not need to solve the momentum

equations on the wall. This fact is utilized in the cell vertex scheme. Second, the convective fluxes through the noslip+wall are given again by Equation and the terms in equation simplify to 0 = kVT. Hence, the wall pressure in the convective fluxes is obtained in the same way as described above for the inviscid flow. However, the dummy cells (points) are treated in a different way.

Cell- Centered Scheme

The implementation of the noslip boundary condition in equation can be simplified by the utilization of dummy cells. In the case of an adiabatic wall (no heat flux through the wall), we can set

$$\rho_1 = \rho_2 , \quad E_1 = E_2$$

$$u_1 = -u_2 , \quad v_1 = -v_2 , \quad w_1 = -w_2$$

and likewise for the cells 0 and 3. The approach is applicable to both, structured and unstructured schemes. If the wall temperature is given, the velocity components are still reversed as in equation. The temperature is linearly extrapolated from the interior field by using the specified wall temperature. Since the pressure gradient normal to the wall is zero, the pressure in the boundary element is prescribed also in the dummy cells (i.e., PO = pl = p2). The density and the total energy in the dummy cells are evaluated from the interpolated values.

Cell-Vertex Scheme

Since the momentum equations need not to be solved, there is no contribution from the convective fluxes at the wall. The viscous fluxes in equation contribute only the temperature gradient normal to the wall to the energy equation. For an adiabatic wall, Tw . n' is zero. Hence, we do not have to compute any convective or viscous fluxes at the wall. The residuals of the momentum equations should be set to zero, in order to prevent the generation of nonzero velocity components at the wall nodes.
In the case of prescribed wall temperature, we can directly set the total energy at the wall using (perfect gas assumed)

$$(\rho E)_{i,2} = \frac{c_p}{\gamma} \rho_{i,2} T_w$$

where T, denotes the given wall temperature. The residuals of the momentum and the energy equation have to be zeroed out. The same strategy is applicable also to unstructured schemes.

Another approach, which seems to be more robust for some applications, does not solve the governing equations at the wall at all. Both, the density and the energy are directly specified

$$\rho_{i,2} = \frac{p_{i,3}}{T_w R} \quad \text{and} \quad (\rho E)_{i,2} = \frac{p_{i,3}}{\gamma}$$

The relations in equation assume that there is no pressure gradient normal to the wall (therefore p2 = p3). Since all conservative variables are prescribed, the residuals of all equations should be set to zero. This technique can be utilized on unstructured grids as well. However, the extrapolation of the pressure requires additional operations on triangular or tetrahedral grids.

If the wall is adiabatic, the values in the dummy points are obtained as follows

$$\rho_{i,1} = \rho_{i,3}\,, \quad E_{i,1} = E_{i,3}$$

$$u_{i,1} = -u_{i,3}\,, \quad v_{i,1} = -v_{i,3}\,, \quad w_{i,1} = -w_{i,3}$$

The same applies to the nodes 0 and 4. If the wall temperature is given, the temperature in the dummy points is extrapolated from the interior, i.e.,

$$T_{i,1} = 2T_w - T_{i,3} \quad \text{and} \quad T_{i,0} = 3T_w - 2T_{i,3}$$

The velocity components are again reversed as in Eq. (8.18). The density and energy are computed with the interpolated temperature value and with the pressure.

Farfield

The numerical simulation of external flows past airfoils, wings, cars and other configurations has to be conducted within a bounded domain. For this reason, artificial farfield boundary conditions become necessary. The numerical implementation of the farfield boundary conditions has to fulfil two basic requirements. First, the truncation of the domain should have no notable effects on the flow solution as compared to the infinite domain. Second, any outgoing disturbances must not be reflected back into the flow field. Due to their elliptic nature, sub- and transonic flow problems are particularly sensitive to the farfield boundary conditions. An inadequate implementation can lead to a significant slowdown of convergence to the steady state. Furthermore, the accuracy of the solution is likely to be negatively influenced. Various methodologies were developed which are capable of absorbing the outgoing waves at the artificial boundaries.

In the following two subsections, we shall discuss the concept of characteristic variables as it was described by Whitfield and Jams. We shall also present an extension of the farfield boundary conditions for lifting bodies.

Concept of Characteristic Variables

Depending on the sign of the eigenvalues of the convective flux Jacobians, the information is transported out of or into the computational domain along the characteristics. For example, in the case of subsonic inflow there are four incoming characteristics (in 3D) and one outgoing. The situation reverses for subsonic outflow. According to the one-dimensional theory of Kreiss, the number of conditions to be imposed from outside at the boundary should be equal to the number of incoming characteristics. The remaining conditions should be determined from the solution inside the domain.
The approach of Whitfield and Janus is based on the characteristic form of the one-dimensional Euler equations normal to the boundary. The methodology was found to perform very well on structured and unstructured grids in a variety of flow cases. It can be applied not only to far field boundaries but also to inviscid solid walls.

The two basic flow situations at the far field boundary are sketched in Fig.3.17 . The flow can either enter or it can leave the domain. Therefore, depending on the local Mach number, four different types of far field boundary conditions have to be treated:

- Supersonic inflow,
- Supersonic outflow,
- Subsonic inflow, and
- Subsonic outflow.

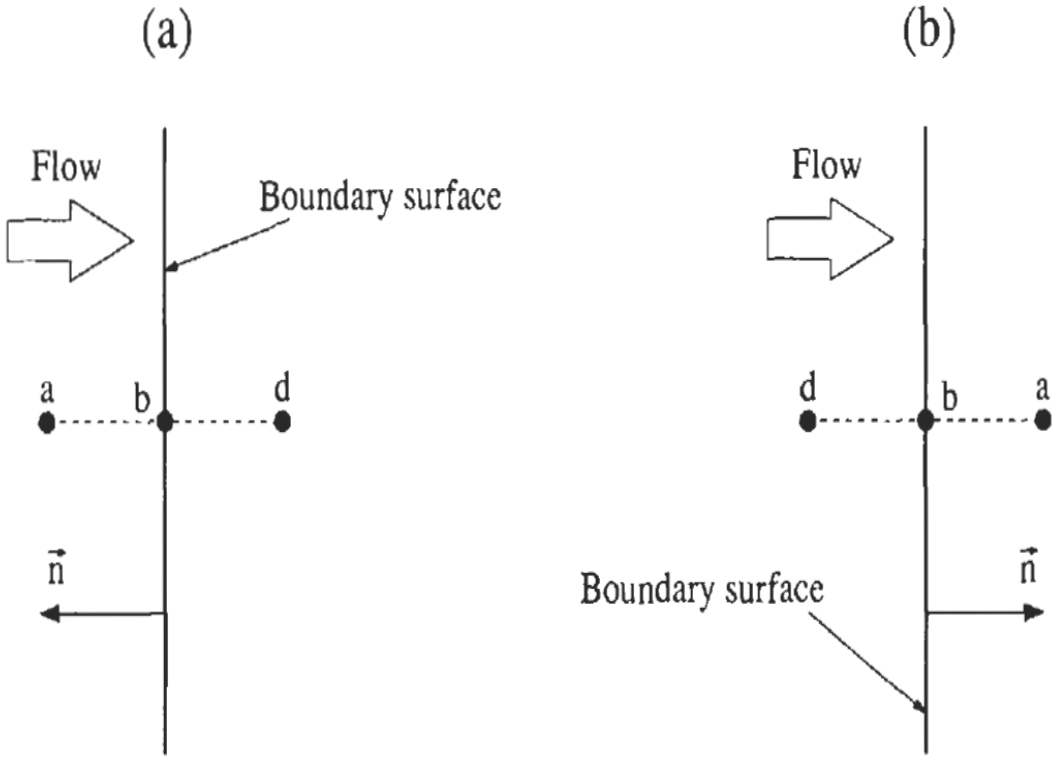

Figure 3.17: Farfield boundary: inflow (a) and outflow (b) situation. Position a is outside, b on the boundary, and position d is inside the physical domain.

Supersonic Inflow

For supersonic inflow, all eigenvalues have the same sign. Since the flow is entering the physical domain, the conservative variables on the boundary are determined by freestream values only. Thus,

$$\vec{W}_b = \vec{W}_a$$

The values are specified based on the given Mach number M, and on twoflow angles (angle of attack, side-slip angle).

Supersonic Outflow

In this case, all eigenvalues have also the same sign. However, the flow leaves now the physical domain and all conservative variables at the boundary must be determined from the solution inside the domain. This can be accomplished simply by setting

$$\vec{W}_b = \vec{W}_d$$

Subsonic Inflow

Here, four characteristics enter and one leaves the physical domain. Therefore, four characteristic variables are prescribed based on the freestream values. One characteristic variable is extrapolated from the interior of the physical domain.

This leads to the following set of boundary conditions

$$p_b = \frac{1}{2}\left\{p_a + p_d - \rho_0 c_0\left[n_x(u_a - u_d) + n_y(v_a - v_d) + n_z(w_a - w_d)\right]\right\}$$

$$\rho_b = \rho_a + (p_b - p_a)/c_0^2$$

$$u_b = u_a - n_x(p_a - p_b)/(\rho_0 c_0)$$

$$v_b = v_a - n_y(p_a - p_b)/(\rho_0 c_0)$$

$$w_b = w_a - n_z(p_a - p_b)/(\rho_0 c_0)\,,$$

The reference state is normally set equal to the state at the interior point. The values in point a are determined from the free stream state.

Subsonic Outflow

In the case of subsonic outflow, four flow variables (density and the three velocity components) have to be extrapolated from the interior of the physical domain. The remaining fifth variable (pressure) must be specified externally.

The primitive variables at the farfield boundary are obtained from

$$p_b = p_a$$

$$\rho_b = \rho_d + (p_b - p_d)/c_0^2$$

$$u_b = u_d + n_x(p_d - p_b)/(\rho_0 c_0)$$

$$v_b = v_d + n_y(p_d - p_b)/(\rho_0 c_0)$$

$$w_b = w_d + n_z(p_d - p_b)/(\rho_0 c_0)$$

Modifications for Lifting Bodies

The above characteristic far field boundary conditions assume zero circulation, which is not correct for a lifting body in sub- or transonic flow. For this reason, the far field boundary has to be located very far away from the body. Otherwise, the flow solution will be inaccurate. The distance to the far field can be significantly shortened (one order of magnitude), if the freestream flow includes the effect of a single vortex (horse-shoe vortex in 3D). The vortex is assumed to be centered at the lifting body. The strength of the vortex is proportional to the lift produced by the body. In the following, we shall present implementations of the vortex correction in 2D and in 3D.

Vortex Correction in 2D

The approach, which we want to describe here, was suggested by Usab and Murman [lS]. The components of the corrected freestream velocity are given by the expressions (compressible flow assumed)

$$u_\infty^* = u_\infty + \left(\frac{\Gamma \sqrt{1 - M_\infty^2}}{2\pi d} \right) \frac{1}{1 - M_\infty^2 \sin^2(\theta - \alpha)} \sin\theta$$

$$v_\infty^* = v_\infty - \left(\frac{\Gamma \sqrt{1 - M_\infty^2}}{2\pi d} \right) \frac{1}{1 - M_\infty^2 \sin^2(\theta - \alpha)} \cos\theta$$

Cosθ with r being the circulation, (d, 8) the polar coordinates of the farfield point, CY the angle of attack, and M, denoting the freestream Mach number, respectively.
The circulation is obtained from

$$\Gamma = \frac{1}{2} \|\vec{v}_\infty\|_2 \, a \, C_L$$

by using the theorem of Kutta-Joukowsky. In Equation, a represents the chord length of the airfoil and CL is the lift coefficient evaluated by the integration of the surface pressure. The polar coordinates in Equation are calculated as

$$d = \sqrt{(x - x_{ref})^2 + (y - y_{ref})^2}$$

$$\theta = \tan \left(\frac{y - y_{ref}}{x - x_{ref}} \right) ,$$

where x_{ref} and y_{ref} are the coordinates of the reference point (location of the vortex - e.g., at 1/4 chord).
The modified freestream pressure p_Z, is given by from the equation of the state. The corrected freestream density is obtained

$$p_\infty^* = \left[p_\infty^{(\gamma-1)/\gamma} + \left(\frac{\gamma - 1}{\gamma} \right) \frac{\rho_\infty \left(\|\vec{v}_\infty\|_2^2 - \|\vec{v}_\infty^*\|_2^2 \right)}{2 p_\infty^{1/\gamma}} \right]^{\gamma/(\gamma-1)}$$

$$\rho_\infty^* = \rho_\infty \left(\frac{p_\infty^*}{p_\infty} \right)^{1/\gamma}$$

The above vortex correction Equation is strictly valid in subsonic flow only. However, the modification of the freestream conditions proved to be helpful in transonic flow as well.

Boundary Conditions

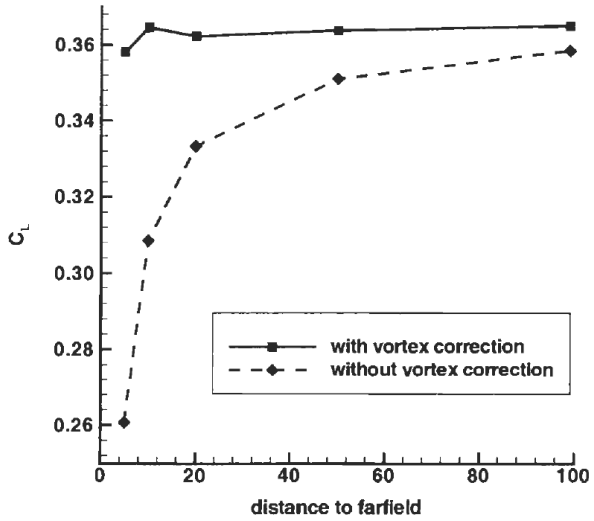

Figure 3.18: Effects of distance to the farfield boundary and of single vortex on the lift coefficient. NACA 0012 airfoil, Mm = 0.8, a = 1.25'.

We can see, the simulation without the vortex correction experiences a strong dependence on the farfield distance. On contrary, the calculations with the vortex remain sufficiently accurate up to a distance of about 20 chords. This leads to a significant reduction of the number of grid cells/points. It was demonstrated that by using higher-order terms in the vortex correction, the farfield boundary can be placed only about 5 chords away without loss of accuracy.

Vortex Correction in 3D

The effect of a wing on the farfield boundary can be approximated by a horseshoe vortex. In the case of compressible flow, the modified freestream velocity components can be obtained

$$u_\infty^* = u_\infty + \frac{\Gamma\beta^2}{2\pi}\mathcal{A}$$

$$v_\infty^* = v_\infty - \frac{\Gamma}{2\pi}\left[\frac{z+l}{(z+l)^2+y^2}\mathcal{B} - \frac{z-l}{(z-l)^2+y^2}\mathcal{C} + \frac{x\beta^2}{x^2+y^2\beta^2}\mathcal{A}\right]$$

$$w_\infty^* = w_\infty + \frac{\Gamma}{2\pi}\left[\frac{y}{(z+l)^2+y^2}\mathcal{B} - \frac{y}{(z-l)^2+y^2}\mathcal{C}\right],$$

where r denotes the circulation, (x, y, z) the Cartesian coordinates of the farfield point, and 1 stands for the half span, respectively. Furthermore, in Equation it was assumed that the flow is in the positive x-direction with the wing being oriented along the z-axis. The terms A, B and C in Equation read

$$\mathcal{A} = \frac{z+l}{\sqrt{\psi_+}} - \frac{z-l}{\sqrt{\psi_-}}$$

$$\mathcal{B} = 1 + \frac{x}{\sqrt{\psi_+}}$$

$$\mathcal{C} = 1 + \frac{x}{\sqrt{\psi_-}}.$$

The abbreviations are given by

$$\psi_+ = x^2 + \beta^2(z+l)^2 + y^2\beta^2$$

$$\psi_- = x^2 + \beta^2(z-l)^2 + y^2\beta^2$$

$$\beta = \sqrt{1 - M_\infty^2}$$

These are the points

Z=+l, y=0,
Z=-1, y=0,

and $x = x_{farf}$.

In order to avoid the numerical singularity, it was suggested to constrain the values of

$(Z + 1)^2 + y^2$ and
$(Z - 1)^2 + y^2$

in Equation to the 1/4 wingspan, i.e., 1/2. This measure reduces the corrections to the velocities v, and woo within the distance 112 around the vortex lines Z = 1 and Z = -1.
The numerical results indicate a reduced sensitivity of the lift and drag coefficient with respect to the farfield distance, if the vortex correction in Equation is applied. It was found that a distance of 7 to the farfield boundary is sufficient for accurate results.

Inlet/Outlet Boundary

Various approaches were devised for the implementation of numerical inlet, and in particular, of outlet (also named open) boundary conditions for the Navier-Stokes equations. Here, we will concentrate on methodologies, which were developed for turbomachinery applications. Suitable non-reflecting inlet and outlet boundary conditions were described. Giles and Hirsch and Verhoff suggested non-reflecting boundary conditions for the Euler equations, which are intended for domains with a short distance between the body and the inlet or the outlet plane.

In certain cases, the inlet, and outlet boundary are additionally periodic with respect to the velocity as well as the pressure and temperature gradient. This type of flow is encountered, for example, in the simulation of heat exchangers. The implementation of periodic inlet and outlet boundary conditions was presented in for LES in channels.

Subsonic Inlet

A common procedure consists of the specification of the total pressure, total temperature, and of two flow angles. One characteristic variable has to be interpolated from the interior of the flow domain. One possibility is to employ the outgoing Riemann invariant, which is defined as

$$\mathcal{R}^- = \vec{v}_d \cdot \vec{n} - \frac{2\,c_d}{\gamma - 1}$$

where the index d denotes the state inside the domain. The Riemann invariant is used to determine either the absolute velocity or the speed of sound at the boundary. In practice, it was found that selecting the speed of sound leads to a more stable scheme, particularly for low Mach-number flows.

Therefore, we set

$$c_b = \frac{-\mathcal{R}^-(\gamma-1)}{(\gamma-1)\cos^2\theta+2}\left\{1+\cos\theta\sqrt{\frac{[(\gamma-1)\cos^2\theta+2]c_0^2}{(\gamma-1)(\mathcal{R}^-)^2}-\frac{\gamma-1}{2}}\right\}$$

with 6' being the flow angle relative to the boundary, and co denoting the stagnation speed of sound. Hence,

$$\cos\theta = -\frac{\vec{v}_d\cdot\vec{n}}{||\vec{v}_d||_2}$$

and

$$c_0^2 = c_d^2 + \frac{\gamma-1}{2}||\vec{v}_d||_2^2$$

Where $||v_d||^2$ denotes the total velocity at the interior point d. The unit normal vector n' in Equation was assumed to point outwards of the domain.

Quantities like static temperature, pressure, density, or the absolute velocity at the boundary are evaluated as follows

$$T_b = T_0\left(\frac{c_b^2}{c_0^2}\right)$$

$$p_b = p_0\left(\frac{T_b}{T_0}\right)^{\gamma/(\gamma-1)}$$

$$\rho_b = \frac{p_b}{RT_b}$$

$$||\vec{v}_b||_2 = \sqrt{2\,c_p(T_0-T_b)}\,,$$

where T_o and p_o are the given values of total temperature and pressure, R and c_p represent the specific gas constant and the heat coefficient at constant pressure, respectively. The velocity components at the inlet are obtained by decomposing $||v_d||^2$ according to the two (one in 2D) prescribed flow angles.

Subsonic Outlet

In turbormachinery, the static pressure is usually prescribed at the outlet. The subsonic outlet boundary can be treated in a way quite similar to the outflow condition in equation. Only the ambient pressure pa is replaced here by the given static exit pressure.
Flow variables in the dummy cells can be obtained by linearly extrapolating the states at the boundary and at the interior point d.

Symmetry Plane

If the flow is to be symmetrical with respect to a line or a plane, the first condition which must be met is that there is no flux across the boundary. This is equivalent to the requirement that the velocity normal to the symmetry boundary is zero.

Furthermore, the following gradients have to vanish:

- Gradient normal to boundary of a scalar quantity,
- Gradient normal to boundary of a tangential velocity,
- Gradient along the boundary of the normal velocity (since v'. n' = 0).

We can write these conditions as

$$\vec{n} \cdot \vec{\nabla} U = 0$$

$$\vec{n} \cdot \vec{\nabla} (\vec{v} \cdot \vec{t}) = 0$$

$$\vec{t} \cdot \vec{\nabla} (\vec{v} \cdot \vec{n}) = 0 \,,$$

where U stands for a scalar variable and z denotes a vector tangential to the symmetry boundary.

Cell-Centered Scheme

The implementation of the symmetry boundary condition can be largely simplified by employing dummy cells. The flow variables in the dummy cells are obtained using the concept of reflected cells. This means that scalar quantities like density or pressure in the dummy cells are set equal to the values in the opposite interior cells, i.e.,

$$U_1 = U_2, \text{ and } U_O = U_3$$

The velocity components are reflected with respect to the boundary. The normal gradient of the normal velocity in the dummy cell equals to that in the opposite interior cell, but it has reversed sign.

Cell-Vertex Scheme (Dual Control Volume)

Two different approaches can be followed. One possibility is to construct the missing half of the control volume by mirroring the grid on the boundary. The fluxes and the gradients are then evaluated like in the interior using reflected flow variables. The second methodology computes the fluxes for the half control volume. The components normal to the symmetry plane of the residual are then zeroed out. It is also necessary to correct normal vectors of those faces of the control volume, which touch the boundary. The modification consists of removing all components of the face vector, which are normal to the symmetry plane.

Coordinate Cut

This type of boundary condition is encountered only in the case of structured grids. The coordinate cut represents an artificial, not a physical, boundary. It is a line (plane in 3D) composed of grid points with different computational coordinate(s) but the same physical location. This means that the grid is folded such that it touches itself. The coordinate cut appears for the so-called C- or 0-grid topology. The flow variables and their gradients have to stay continuous across the cut.

The best way to implement the cut boundary condition is to employ dummy cells (points). The situation is sketched in Fig. 3.19. As we can see, the dummy layers here are not virtual, but they coincide with the grid on the opposite side of the cut. Hence, the values of physical quantities in the dummy cells (cell centered scheme), or in the dummy points (cell-vertex scheme), are obtained directly from the opposite cells (points). In the case of the cell-centered scheme, the fluxes across the faces of the boundary cell (shaded in Fig. 8.8a) are evaluated exactly like in the interior field.

The cut boundary can be treated in two different ways for the cell-vertex scheme. One possibility is to generate a complete control volume at the cut (the second part is denoted by a dashed line in Fig. 3.19 b). Using the dummy points, the fluxes can be calculated in the same way as inside the domain. If the implementation is done correctly, the flow quantities at the points 2 (upper grid part) and 5 (lower part) will be equal. The second approach is to integrate the fluxes separately for each half of the control volume. The residuals at the points 2 and 5 in Fig. 3.19 b are then added. It is important that the partial control volumes at the points 2 and 5 are summed as well.

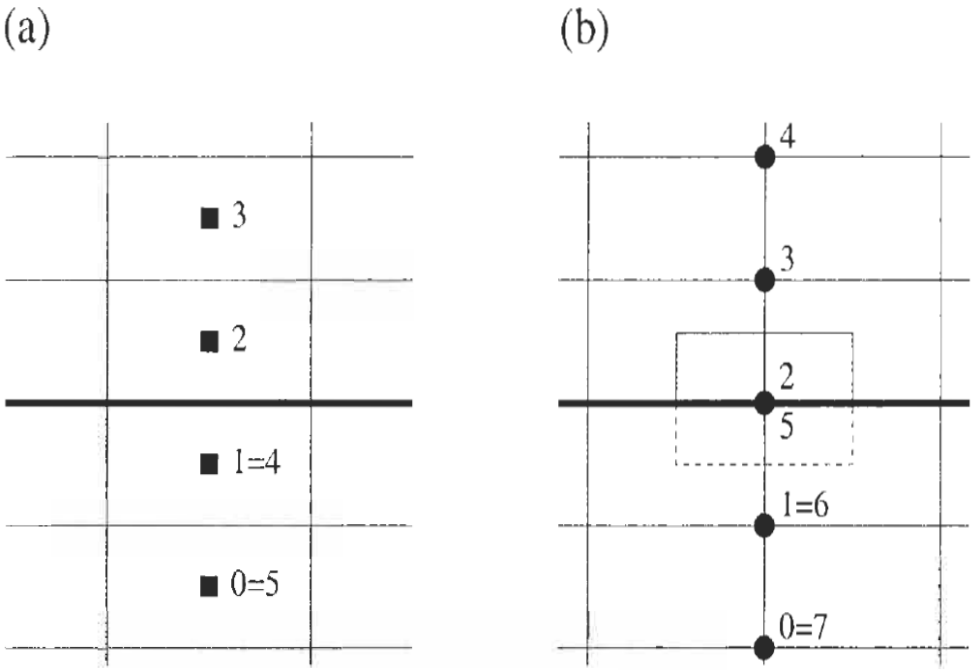

Figure 3.19: Coordinate cut (thick line): cell-centered scheme (a), dual control volume scheme (b). Dummy cells (points) are numbered as 0 and 1.

Periodic Boundaries

There are certain practical applications where the flow field is periodic with respect to one or multiple coordinate directions. In such a case, it is sufficient to simulate the flow only within one of the repeating regions. The correct interaction with the remaining physical domain is enforced via periodic boundary conditions.

We can distinguish between two basic types of periodic boundaries. The first one covers translational periodicity. This means that one periodic boundary can be transformed into the other boundary by pure coordinate translation. The second type represents periodic boundaries, which were generated by coordinate rotation. Thus, we speak of rotational periodicity.

In the following, we shall describe the implementation of the periodic boundary conditions for the cell-centered and the cell-vertex scheme. We shall also consider the case of rotational periodicity.

Cell-Centered Scheme

The utilization of the dummy-cells concept enables a simple implementation of the periodic boundary condition. Let us consider the example from turbo machinery in Fig.3.20. The configuration is periodic in the vertical direction. The shaded cells 1 and 2 are located on the lower and the upper periodic boundary, respectively. Due to the periodicity condition, the first dummy-cell layer corresponds to the boundary cells at the opposite periodic boundary.

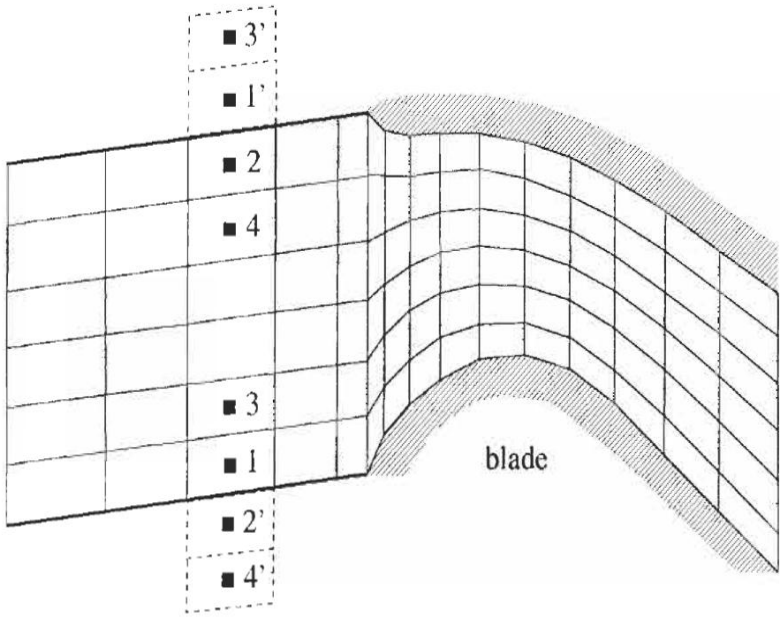

Figure 3.20: Periodic boundaries (thick lines) in the case of 2-D un-/structured, cell-centered scheme. Dummy cells (dashed line) are denoted by the (primed) numbers of the corresponding physical cells.

The second dummy-cell layer communicates with the second layer of the physical cells and so on.

Hence, all scalar quantities (density, pressure, etc.) in the dummy cells are obtained directly from the corresponding physical cells, i.e,

$$U_{1'} = U_1 \quad \text{and} \quad U_{2'} = U_2$$

The same relations hold also for the vector quantities (velocity, gradients) in the case of translational periodicity. Rotational-periodic boundaries require a correction of the vector variables.

Cell-Vertex Scheme (Dual Control Volume)

This situation is sketched in Fig. 3.21. One approach for the treatment of periodic boundaries consists of the integration of the fluxes around the faces of the shaded control volumes. The residuals at the points 1 and 2 in Fig. 3.21 are then summed in order to obtain the complete net flux. Thus,

$$\vec{R}_{1,\,sum} = \vec{R}_1 + \vec{R}_{2'} \quad \text{and} \quad \vec{R}_{2,\,sum} = \vec{R}_2 + \vec{R}_{1'}$$

The partial control volumes at the points 1 and 2 (shaded in Fig. 8.10) have to be added up as well. Rotationally periodic boundaries require a transformation of the momentum equations before Equation can be applied.

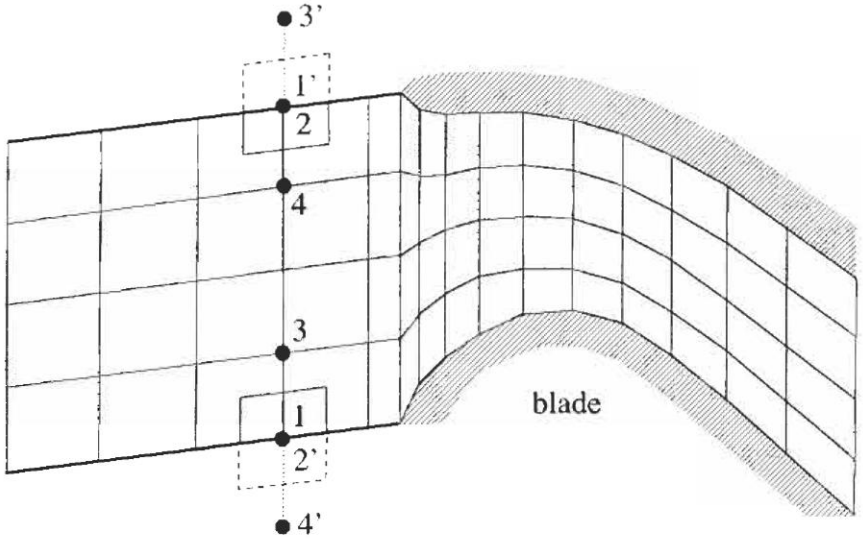

Figure 3.21: Periodic boundaries (thick lines) in the case of 2-D un-/structured, cell-vertex scheme with dual control volumes. The "dummy" parts of the control volumes (dashed line) are denoted by the (primed) numbers of the corresponding control volumes at the opposite boundary. The same holds also for the dummy points 3' and 4'.

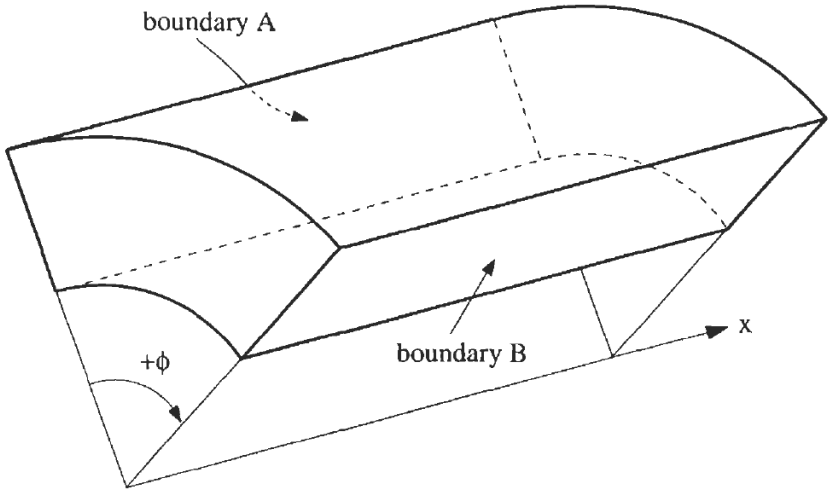

Figure 3.22: Rotationally periodic boundaries (A and B). The rotational axis is assumed to coincide with the x-axis.

Rotational Periodicity

The rotational periodicity condition is based on a rotation of the coordinate system. Therefore, all vector quantities like velocity or gradients of scalars have to be transformed accordingly. Scalar quantities like pressure or density, which are invariant with respect to coordinate rotation, remain unchanged. If we assume the rotational axis is parallel to the x-axis, the rotation matrix becomes

$$\bar{\mathcal{R}} = \begin{bmatrix} 1 & 0 & 0 \\ 0 & \cos\phi & -\sin\phi \\ 0 & \sin\phi & \cos\phi \end{bmatrix}$$

where the angle ϕ between the periodic boundaries A and B is positive in the clockwise direction. Hence, for example, the velocity vector transformed from boundary A to B reads

$$\vec{v}_B = \bar{\mathcal{R}}\,\vec{v}_A$$

It is easy to show that the z-component of GA (i.e., UA) is not changed by the rotation. Thus, UB = UA. The gradients of all flow quantities are transformed in similar way.
As stated above, in the case of the cell-vertex scheme the residuals of the momentum equations must be corrected before the summation in Equation can take place. The application of the rotation matrix Equation leads to

$$\vec{R}^{u,v,w}_{B,\,sum} = \vec{R}^{u,v,w}_{B} + \bar{\mathcal{R}}\,\vec{R}^{u,v,w}_{A}$$

Interface between Grid Blocks

During the discussion of the spatial discretization with structured grids is usually not possible to generate a single grid inside a geometrically complex domain. We mentioned two possible methodologies how to solve the problem. The first one was the multiblock approach and the second one was the Chimera technique. In the following, we shall describe the basic implementation issues of the multiblock approach.

Details of the Chimera technique, which is not treated here, can be found in Refs. Within the multiblock technique, the physical domain is split into a certain number of virtual parts. Consequently, the computational domain becomes also divided into the same number of blocks. In a general case, the physical solution in a particular block will depend on the flow in one or multiple neighboring blocks. Therefore, we have to provide a data structure which allows for an efficient exchange of information between the blocks. The structure is also required for communication, if different processors are used to solve the governing equations in the blocks.

The first part of the data structure consists of the numbering of the block boundaries. One particular numbering scheme is displayed in Fig. 8.12. The numbering strategy in Fig. 8.12 can be summarized as follows:

boundary 1 : i = IBEG
boundary 2 : i = IEND
boundary 3 : j = JBEG
boundary 4 : j = JEND
boundary 5 : k = KBEG
boundary 6 : k = KEND.

It is important that all blocks employ the same numbering scheme. The indices i, j, k of the grid points in the computational space are defined in the ranges

$$IBEG \le i \le IEND$$
$$JBEG \le j \le JEND$$
$$KBEG \le k \le KEND$$

The cell indices I, J, K, which are required by the cell-centered scheme are defined in a similar way. Since the multiblock approach is usually implemented using dummy cells/points, the physical cells/points will have a certain offset from the start or the end of each range.

The boundary of each block is divided into a number of non-overlapping patches. This allows the specification of different boundary conditions on the same block boundary. For a unique identification of each patch it is necessary to store the number of the corresponding block and the number of the block boundary. Furthermore, the origin, the height and the width of the patch must be stored.

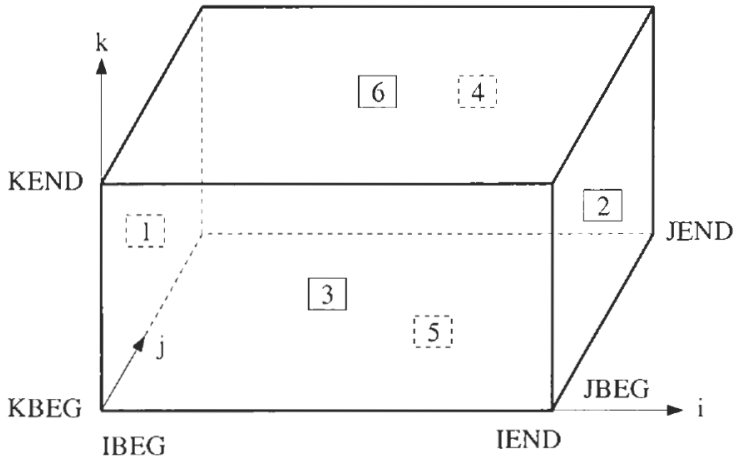

Figure 3.23: Numbering of the sides of the computational space and of the block boundaries.

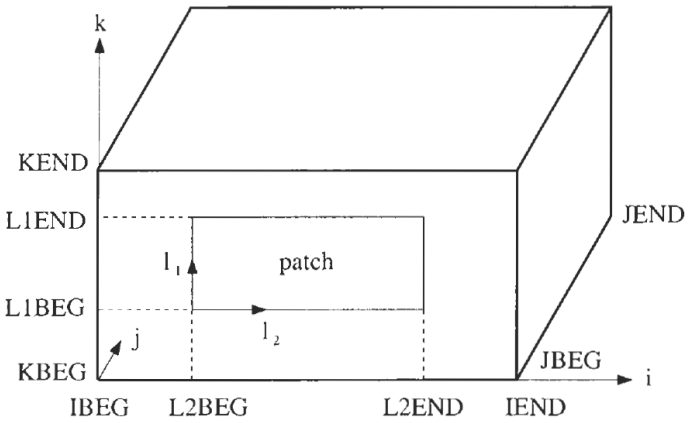

Figure 3.24: Coordinates of a boundary patch in computational space. The patch has its own local coordinate system 11, 12.

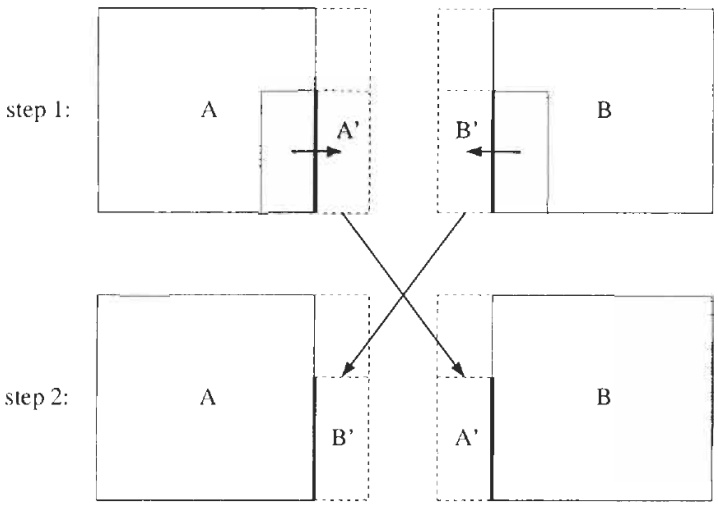

Figure 3.25: Exchange of flow variables (in shaded regions A', B') between two blocks A and B. Dummy layers are denoted by a dashed line.

It is suggested to orient the coordinate system of the patch according to the cyclic directions. This means, that if we consider the i-coordinate, j and k will be the first and the second cyclic direction. In the case of the j-coordinate, the cyclic directions will become k and i, respectively. Therefore, since the patch in figure is on the j = JBEG boundary, the 11-coordinate is oriented in the k-direction and 12 in the i-direction. The application of the cyclic directions allows for a unique definition of the patch orientation.

The remaining part of the data structure makes sure that data can be exchanged between those patches, which represent interfaces between the blocks (we assume that the blocks communicate only across their faces). For this purpose, it is required to extend the above patch data structure by the numbers of the adjacent block and patch.

The exchange of flow quantities between two blocks is sketched in Figure. The procedure consists of two steps. In the first step, variables from the part of the domain, which is overlapped by the dummy layers of the adjacent patch are written to the own dummy cells/points or to a temporary storage. This is done for all blocks. In the second step, the data in A' and B' is exchanged between both blocks. This means that A' is written to the dummy layers of block B and B' to the dummy layers of block A. If the two patches have a different orientation, the data must be transformed accordingly.

Flow Gradients at Boundaries of Unstructured Grids

We already stated in Subsection 5.3.4 that the evaluation of the flow gradients requires some care in the case of the median-dual scheme. If the gradients are calculated on triangular or tetrahedral grids using the Green-Gauss approach in Eq. (5.46), the contributions from the boundaries of the domain (except at symmetry or periodic boundaries) must be evaluated similar to Eq. (8.12) or Eq. (8.13) instead of the arithmetic average. Otherwise, the gradient will not be accurate. Considering the notation in Fig. 8.4, the contribution to the boundary node 1 reads

$$\frac{1}{6}(5U_1 + U_2)\,\vec{n}_{12}\frac{\Delta S_{12}}{2}$$

Where it is the length of the boundary face between node 1 and 2 (therefore halved). Corresponding to Equation, the contribution of the triangular face 1-2-3 to node 1 in Figure becomes

$$\frac{1}{8}(6U_1 + U_2 + U_3)\,\vec{n}_{123}\frac{\Delta S_{123}}{3}$$

being the grey area in the triangle 1-2-3. On mixed grids, it is more appropriate to employ the least squares approach with virtual edges.

The cell-centered scheme requires no special provisions at symmetry or periodic boundaries. The implementation is identical to that discussed for the fluxes. This holds also for the median-dual scheme, if the gradients are evaluated using the least-squares approach. The only additional work
required is to set certain gradients to zero.

If the Green-Gauss approach is employed within the median-dual scheme is applied), it is necessary to correct normal vectors of those faces of the control volume, which touch the boundary This is done by setting dl components of the face vector to zero, which are normal to the symmetry plane.

UNIT-IV
METHOD OF CHARACTERISTICS

Introduction

The method of characteristics has been used for many years to compute supersonic irrotational flows. Although the method has a strong analytical basis, its practical implementation is, essentially, always numerical and it is then used to compute the values of the flow variables at a series of distinct points in the flow rather than continuously throughout the flow field. Let's consider a general steady two-dimensional irrotational flowfield. We have already derived the velocity potential (φ) equation for such flowfield.

$$\left(1-\frac{u^2}{a^2}\right)\frac{\partial^2\phi}{\partial x^2}+\left(1-\frac{v^2}{a^2}\right)\frac{\partial^2\phi}{\partial y^2}-\frac{2uv}{a^2}\frac{\partial^2\phi}{\partial x\partial y}=0$$

Consider the change in any flow variable,f, df which can be determined by small changes in the coordinates dx and dy as illustrated in Fig. The change in the variable, df,

$$df=\frac{\partial f}{\partial x}dx+\frac{\partial f}{\partial y}dy$$

If f = $\partial\phi/\partial x$ then this will give:

$$d\left(\frac{\partial\phi}{\partial x}\right)=\frac{\partial^2\phi}{\partial x^2}dx+\frac{\partial^2\phi}{\partial x\partial y}dy$$

But u = $\partial\phi/\partial y$ so this equation gives:

$$du=\frac{\partial^2\phi}{\partial x^2}dx+\frac{\partial^2\phi}{\partial x\partial y}dy$$

Simillarly if f = $\partial\phi/\partial y$ then this will give:

$$d\left(\frac{\partial\phi}{\partial y}\right)=\frac{\partial^2\phi}{\partial x\partial y}dx+\frac{\partial^2\phi}{\partial y^2}dy$$

But v = $\partial\phi/\partial y$ so this equation gives:

$$dv=\frac{\partial^2\phi}{\partial x\partial y}dx+\frac{\partial^2\phi}{\partial y^2}dy$$

Now consider eqs. Which involve second derivatives of φ and can be solved using Cramer's Rule. For example

$$\frac{\partial^2\phi}{\partial x\partial y}=\frac{(1-u^2/a^2)du dy+(1-v^2/a^2)dv dx}{(1-u^2/a^2)(dy)^2+(2uv/a^2)dx dy+(1-v^2/a^2)(dx)^2}$$

In general, this equation can be solved for any chosen values of dx and dy, i.e., for any chosen direction, to give $\partial^2\phi/\partial x\partial y$ at a selected point in the flow. However, it is possible to have $\partial^2\phi/\partial x\partial y$ indeterminate in certain directions. More over this differential is expected to be finite at that point. Hence in these directions, eq. 4.4 must give an indeterminate value.

$$\frac{\partial^2 \phi}{\partial x \partial y} = \frac{0}{0}$$

Lets consider the denominator of equation since along a particular direction $\partial^2\phi / \partial x \partial y$ is indeterminate. Hence the denominator should be zero, as:

$$\left(1 - \frac{u^2}{a^2}\right)(dy)^2 + \frac{2uv}{a^2} dx dy + \left(1 - \frac{v^2}{a^2}\right)(dx)^2 = 0$$

Dividing by$(dx)^2$ gives:

$$\left(1 - \frac{u^2}{a^2}\right)\left(\frac{dy}{dx}\right)^2 + \frac{2uv}{a^2}\frac{dy}{dx} + \left(1 - \frac{v^2}{a^2}\right) = 0$$

The subscript 'ch' on dy/dx indicates that the slope of the characteristic line or a specific direction is being considered along which differentials are indeterminate. Solving above equation we get:

$$\left(\frac{dy}{dx}\right)_{ch} = \frac{-\left(\frac{uv}{a^2}\right) \pm \sqrt{\frac{(u^2+v^2)}{a^2} - 1}}{\left(1 - \frac{u^2}{a^2}\right)}$$

Lets represent the component of velocities in terms of velocity vector and angle made by the streamline with co-ordinate axes as,

$$V^2 = u^2 + v^2$$

$$u = V \cos\theta$$

$$v = V \sin\theta$$

Hence, we get the same equation for slope as,

$$\left(\frac{dy}{dx}\right)_{ch} = \frac{-M^2 \cos\theta \sin\theta \pm \sqrt{M^2 - 1}}{(1 - M^2 \cos^2\theta)}$$

where, M=V/a.

We can introduce the local Mach angle, a, where ($M = 1/\sin\alpha,\ \sqrt{M^2 - 1} = 1/\tan\alpha$) by replacing Mach number as,

$$\left(\frac{dy}{dx}\right)_{ch} = \frac{\cos\theta \sin\theta \pm \cos\alpha \sin\alpha}{\sin^2\alpha - \cos^2\alpha}$$

After much manipulation and rearrangement, it can be shown that this equation gives:

$$\left(\frac{dy}{dx}\right)_{ch} = \tan(\theta \pm \alpha)$$

There are two characteristic lines. This clearly means that the characteristic lines or lines along which derivatives are indeterminate makes Mach angle with the streamline. Hence the net angle made by the characteristic line with the x-axis is the summation of the angle made by the streamline with x-axis and angle made by the Mach wave with streamline. Hence Mach waves are the character lines.

Governing Equation

We know about the direction of the characteristic line obtained from the indeterminacy of the equation for zero denominators. However finiteness of the differential compels the zero value of the numerator. This condition evolves the equation to be solved along the characteristic lines.
Hence for the numerator equation we have,

$$(1 - u^2/a^2)dudy+(1 - v^2/a^2)dvdx = 0$$

i.e.:

$$\frac{dv}{du} = \frac{(1-u^2/v^2)}{(1-v^2/a^2)(dy/dx)}$$

Substituting for slope (dy/dx) of the characteristic lines from equation that gives:

$$\frac{dv}{du} = \frac{uv/a^2 \pm \sqrt{(u^2+v^2)/a^2 - 1}}{(1-v^2/a^2)}$$

Using the velocity relation we have,

$$\frac{dv}{du} = \frac{M^2 \sin\theta\cos\theta \pm \sqrt{M^2-1}}{1-M^2\sin^2\theta}$$

However,

$$\frac{dv}{du} = \frac{d(V\sin\theta)}{d(V\cos\theta)} = \frac{\sin\theta dV + V\cos\theta d\theta}{\cos\theta dV - V\sin\theta d\theta}$$
$$\Rightarrow \frac{dv}{du} = \frac{d(V\sin\theta)}{d(V\cos\theta)} = \frac{\sin\theta(dV/V)+\cos\theta d\theta}{\cos\theta(dV/V)-\sin\theta d\theta}$$

Substituting this expression we get,

$$\frac{\sin\theta(dV/V)+\cos\theta d\theta}{\cos\theta(dV/V)-\sin\theta d\theta} = \frac{M^2\sin\theta\cos\theta \pm \sqrt{M^2-1}}{1-M^2\sin^2\theta}$$

$$i.e. \quad \sin\theta\left(\frac{dV}{V}\right)+\cos\theta d\theta - M^2\sin^3\theta\left(\frac{dV}{V}\right) - M^2\sin^2\theta\cos\theta d\theta$$
$$= M^2\sin\theta\cos^2\theta\left(\frac{dV}{V}\right) \pm \sqrt{M^2-1}\cos\theta\left(\frac{dV}{V}\right)$$
$$- M^2\sin^2\theta\cos\theta d\theta \pm \sqrt{M^2-1}\sin\theta d\theta$$

$$i.e. \quad [\cos\theta \pm \sqrt{M^2-1}\sin\theta]$$
$$= [-\sin\theta + M^2\sin\theta(\sin^2\theta+\cos^2\theta) \pm \sqrt{M^2-1}\cos\theta]\left(\frac{dV}{V}\right.$$

$$i.e. \quad d\theta = -\left[\frac{\sin\theta(M^2-1) \pm \sqrt{M^2-1}\cos\theta}{\pm\sqrt{M^2-1}\sin\theta - \cos\theta}\right]\left(\frac{dV}{V}\right)$$

$$i.e. \quad d\theta = -\left[\frac{\sqrt{M^2-1}\sin\theta \pm \cos\theta}{\pm\sqrt{M^2-1}\sin\theta - \cos\theta}\right]\sqrt{M^2-1}\left(\frac{dV}{V}\right)$$

$$d\theta = \pm\sqrt{M^2-1}\frac{dV}{V}$$

This is the equation governing the changes in the variables along the characteristic lines. It can be noted that it is an ordinary differential equation whereas the original equation, velocity potential equation, was a partial differential equation

We have already seen the solution for equation during consideration of expansion fan (2.4). On the similar line, the integration equation of leads to,

$$\int d\theta \pm \int \sqrt{M^2-1}\frac{dV}{V} = \text{constant}$$

and the $\int \sqrt{M^2-1}\frac{dV}{V}$ is the Prandtl Mayer function,

$$\nu(M) = \int_0^M \frac{\sqrt{M^2-1}}{[1+(\gamma-1)M^2/2]}\frac{dM}{M}$$

Hence,

$$\theta \pm \nu = constant$$

This is the simple algebraic equation which we will have to solve along the characteristic line. Following figure represents the details of the characteristic lines.

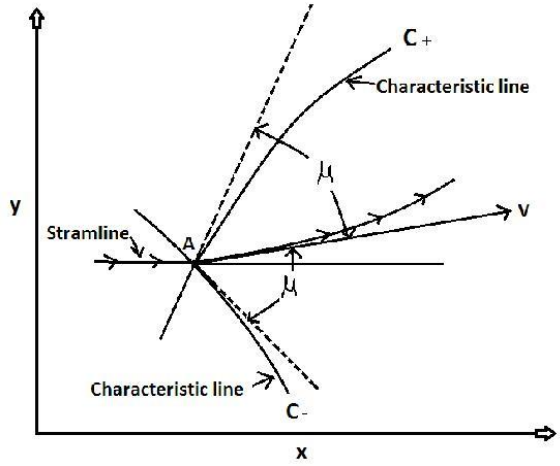

Fig. 4.1. Schematic representation of the details of the characteristic line

We know that there are two characteristic lines from equation.

For C+ characteristics line of Fig.4.1:

$$\left(\frac{dy}{dx}\right)_{ch} = \tan(\theta + \alpha)$$

$$\theta - \vartheta = K^+$$

For C- characteristics line of Fig.33.1:

$$\left(\frac{dy}{dx}\right)_{ch} = \tan(\theta - \alpha)$$

$$\theta + \vartheta = K^-$$

K+ and K - are constants along the + and - characteristic lines.

Strategy to solve numerically along the characteristic line

Consider any point 3 in the flowfield at which properties are to be evaluated. Point 1 and 2 supposed to the points of known properties. Consider C+ characteristic line passing through point 2 and C- passing through 1 intersecting at point 3. Hence point 3 lies on both the characteristic lines. Therefore for point 1 and 3 we have,

$$\theta_1 + \vartheta_1 = (K^-)_1 = \theta_3 + \vartheta_3 = (K^-)_3$$

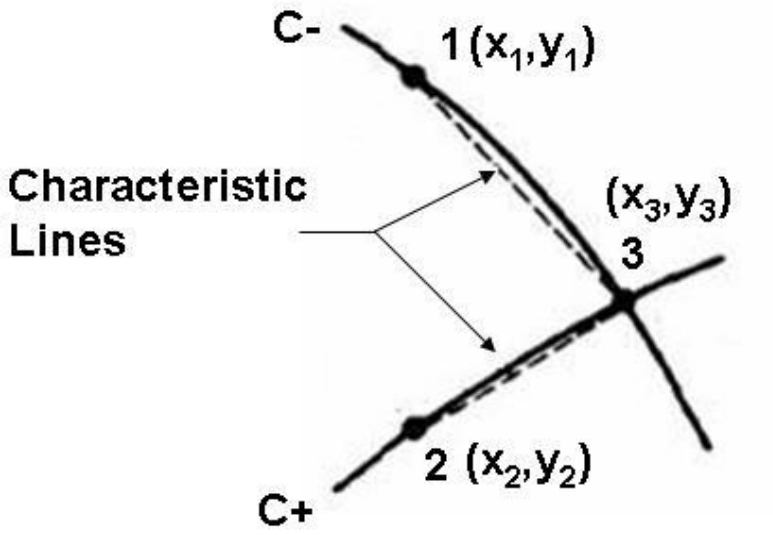

Fig. 4.2. Solution strategy at a point in the flow field.

Similarly for the point 2 and 3

$$\theta_2 - \vartheta_2 = (K^+)_2 = \theta_3 + \vartheta_3 = (K^+)_3$$

Hence,

$$\theta_3 + \vartheta_3 = (K^-)_1$$

$$\theta_3 - \vartheta_3 = (K^+)_2$$

First adding these two equations and then subtracting them gives:

$$\theta_3 = [(K^-)_1 + (K^+)_2]/2$$

$$\vartheta_3 = [(K^-)_1 - (K^+)_2]/2$$

which can be also written as:

$$\theta_3 = ((\theta_1 + \theta_2)/2) + ((\vartheta_1 - \vartheta_2)/2)$$

$$\vartheta_3 = ((\theta_1 - \theta_2)/2) + ((\vartheta_1 + \vartheta_2)/2)$$

This helps in finding θ3 and v3 from known properties. Since v3 depends only on M, this allows M3and hence a3 can be evaluated. Since the stagnation pressure and temperature are constant throughout the flow field therefore using M3 we can calculate P3, T3, a3, and ρ3 and then V3. The characteristic lines are, in general, curved. Their local slope depends on the local values of v and θ. However, if points 1 and 3 and 2 and 3 are close together, the characteristic lines can be assumed to be straight with a slope equal to the average of the values at the end points.

$$[(\theta_1 - \alpha_1) + (\theta_3 - \alpha_3)]/2 = \tan^{-1}\left[\frac{y_3 - y_1}{x_3 - x_1}\right]$$

$$[(\theta_2 + \alpha_2) + (\theta_3 + \alpha_3)]/2 = \tan^{-1}\left[\frac{y_3 - y_2}{x_3 - x_2}\right]$$

Since θ3 and a3 are determined by solving above two equations we can determine x3 and y3.
The procedure discussed above was for an "internal" point, i.e., a point 3 in the flow field that did not lie on a boundary. If a point lies on the boundary, the flow direction at this point will be determined by the slope of the boundary, e.g., consider the point 5 shown in Fig. 4.3 which lies on a solid wall. The flow direction at this point θ5 is equal to the slope of the wall as indicated. Consider the characteristic line between points 4 and 5 as shown in the same figure. Since (K-)4 = (K-)5 it follows that:

$$\theta_4 + \nu_4 = \theta_5 + \nu_5$$

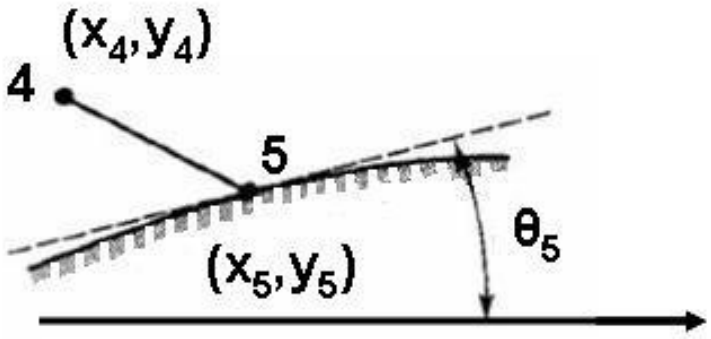

Fig. 4.3. Demonstration of wall boundary condition.

However, θ5 is known, hence v5 is given by:

$$\nu_5 = \theta_4 - \theta_5 + \nu_4$$

With v5 determined, the values of all the flow properties at 5 can be determined as discussed before. The characteristic line between 4 and 5 is, of course, assumed to be straight which determines the position of the point 5.

Irrotational Euler Equation

Irrotationality of the flow can be evident in the compressible flowfield for weak or zero entropy gradients as per the Croco's theorem. Supersonic flows shocked in the presence of weakly curved oblique shocks can be treated as irrotational flows. Let's consider such irrotational flow. We know that the curl of velocity vector being zero is the irrotationality condition. Hence,

$$\nabla \times \mathrm{V} = \begin{vmatrix} i & j & k \\ \frac{\partial}{\partial x} & \frac{\partial}{\partial y} & \frac{\partial}{\partial z} \\ u & v & w \end{vmatrix}$$

$$\mathrm{i}\left(\frac{\partial w}{\partial y} - \frac{\partial v}{\partial z}\right) - j\left(\frac{\partial w}{\partial x} - \frac{\partial u}{\partial z}\right) + \mathrm{k}\left(\frac{\partial v}{\partial x} - \frac{\partial u}{\partial y}\right) = 0$$

Component wise equality gives,

$$\frac{\partial w}{\partial y} = \frac{\partial v}{\partial z} \qquad \frac{\partial w}{\partial x} = \frac{\partial u}{\partial z} \qquad \frac{\partial v}{\partial x} = \frac{\partial u}{\partial y}$$

This gradient equality will be used for simplifying the momentum equation. The momentum equation for the in viscid compressible can be written as,

$$\rho \frac{DV}{Dt} = -\nabla P$$

The u-momentum or x-directional momentum equation is,

$$\rho u \frac{\partial u}{\partial x} + \rho v \frac{\partial u}{\partial y} + \rho w \frac{\partial u}{\partial z} = -\frac{\partial \mathrm{p}}{\partial x}$$

Multiplication of dx on either side gives,

$$-\frac{\partial \mathrm{p}}{\partial x} dx = \rho u \frac{\partial u}{\partial x} dx + \rho v \frac{\partial u}{\partial y} dx + \rho w \frac{\partial u}{\partial z} dx$$

However, from the irrotationality condition, we know that,

$$\frac{\partial u}{\partial y}=\frac{\partial v}{\partial x} \quad and \quad \frac{\partial u}{\partial z}=\frac{\partial w}{\partial x}$$

Using this, u-momentum equation gets modified as,

$$-\frac{\partial \mathrm{p}}{\partial x}dx=\rho u\frac{\partial u}{\partial x}dx+\rho v\frac{\partial v}{\partial x}dx+\rho w\frac{\partial w}{\partial x}dx$$

Further simplification of this equation leads to,

$$-\frac{\partial \mathrm{p}}{\partial x}dx=\frac{1}{2}\rho\frac{\partial u^2}{\partial x}dx+\frac{1}{2}\rho\frac{\partial v^2}{\partial x}dx+\frac{1}{2}\rho\frac{\partial w^2}{\partial x}dx$$

Similarly, v and w momentum equations can be obtained,

$$-\frac{\partial \mathrm{p}}{\partial y}dy=\frac{1}{2}\rho\frac{\partial u^2}{\partial y}dy+\frac{1}{2}\rho\frac{\partial v^2}{\partial y}dy+\frac{1}{2}\rho\frac{\partial w^2}{\partial y}dy$$

$$-\frac{\partial \mathrm{p}}{\partial z}dz=\frac{1}{2}\rho\frac{\partial u^2}{\partial z}dz+\frac{1}{2}\rho\frac{\partial v^2}{\partial z}dz+\frac{1}{2}\rho\frac{\partial w^2}{\partial z}dz$$

Adding all the momentum equations, we get,

$$-\left(\frac{\partial \mathrm{p}}{\partial x}dx+\frac{\partial \mathrm{p}}{\partial y}dy+\frac{\partial \mathrm{p}}{\partial z}dz\right)=\frac{1}{2}\rho\frac{\partial \mathrm{V}^2}{\partial z}dz+\frac{1}{2}\rho\frac{\partial \mathrm{V}^2}{\partial z}dz+\frac{1}{2}\rho\frac{\partial \mathrm{V}^2}{\partial z}dz$$

Where $\mathrm{V}^2=u^2+v^2+w^2$

This leads to the irrotational form of the Euler equation as,

$$-d\mathrm{p}=\frac{1}{2}\rho d(\mathrm{V}^2)$$

$$d\mathrm{p}=-\rho\mathrm{V}\,d\mathrm{V}$$

Velocity Potential Equation

We know that, if curl of any vector field is zero then the corresponding vector field can be represented by gradient of scalar as,

$$\nabla\times A=0$$

$$\nabla\times\nabla\zeta=0$$

In view of the same, velocity field can be represented by gradient of potential for the irrotationalitty condition.

$$\mathrm{V}\equiv\nabla\Phi$$

However we know that,

$$\mathrm{V}=ui+vj+wk$$

and

$$\nabla\Phi=\frac{\partial\Phi}{\partial x}i+\frac{\partial\Phi}{\partial y}j+\frac{\partial\Phi}{\partial z}k$$

Therefore the components of velocities can be represented by corresponding potential gradients as,

$$u=\frac{\partial\Phi}{\partial x} \qquad v=\frac{\partial\Phi}{\partial y} \qquad w=\frac{\partial\Phi}{\partial z}$$

The mass conservation equation for the steady state condition is,

$$\nabla.(\rho\mathrm{V})=0$$

$$\frac{\partial(\rho u)}{\partial x}+\frac{\partial(\rho v)}{\partial y}+\frac{\partial(\rho w)}{\partial z}=0$$

Replacing the components of velocities we get,

$$\frac{\partial}{\partial x}\rho\Phi_x+\frac{\partial}{\partial y}\rho\Phi_y+\frac{\partial}{\partial z}\rho\Phi_z=0$$

$$\rho\left(\Phi_{xx}+\Phi_{yy}+\Phi_{zz}\right)+\Phi_x\frac{\partial\rho}{\partial x}+\Phi_y\frac{\partial\rho}{\partial y}+\Phi_z\frac{\partial\rho}{\partial z}=0$$

However we have already derived the irrotational form of the Euler equation which can be used to

Source from Computational Fluid Mechanics and Heat Transfer by Tannehill John C, Anderson Dale A, Pletcher Richard H

replace the density gradients of above equations,

$$dp = -\rho V\, dV = \frac{1}{2}\rho d(V^2) = \frac{1}{2}\rho d(u^2 + v^2 + w^2)$$

$$dp = -\rho d\left(\frac{\Phi_x{}^2 + \Phi_y{}^2 + \Phi_z{}^2}{2}\right)$$

The definition of sound speed leads to,

$$\frac{dp}{d\rho} = \left(\frac{\partial p}{\partial \rho}\right)_s = a$$

$$d\rho = \frac{dp}{a^2}$$

Replacing dp of above equation using Equation we get,

$$d\rho = -\frac{\rho}{a^2} d\left(\frac{\Phi_x{}^2 + \Phi_y{}^2 + \Phi_z{}^2}{2}\right)$$

Hence, partial differentials of density are,

$$\frac{\partial \rho}{\partial x} = -\frac{\rho}{a^2}\frac{\partial}{\partial x}\left(\frac{\Phi_x{}^2 + \Phi_y{}^2 + \Phi_z{}^2}{2}\right)$$

$$\frac{\partial \rho}{\partial x} = -\frac{\rho}{a^2}\left(\Phi_x \Phi_{xx} + \Phi_y \Phi_{yx} + \Phi_z \Phi_{zx}\right)$$

$$\frac{\partial \rho}{\partial y} = -\frac{\rho}{a^2}\left(\Phi_x \Phi_{xy} + \Phi_y \Phi_{yy} + \Phi_z \Phi_{zy}\right)$$

$$\frac{\partial \rho}{\partial z} = -\frac{\rho}{a^2}\left(\Phi_x \Phi_{xz} + \Phi_y \Phi_{yz} + \Phi_z \Phi_{zz}\right)$$

The partial derivatives of density can be used to simplify the Equation as,

$$\left(1 - \frac{\Phi_x{}^2}{a^2}\Phi_{xx}\right) + \left(1 - \frac{\Phi_y{}^2}{a^2}\Phi_{yy}\right) + \left(1 - \frac{\Phi_z{}^2}{a^2}\Phi_{zz}\right) - \frac{2\Phi_x \Phi_y}{a^2}\Phi_{xy} - \frac{2\Phi_x \Phi_z}{a^2}\Phi_{xz} - \frac{2\Phi_y \Phi_z}{a^2}\Phi_{yz} = 0$$

This equation is called as velocity potential equation. This equation is derived for steady irrotational flows from mass and momentum equations. This equation has two unknowns via velocity potential and acoustic speed or speed of sound. However the speed of sound seen in above equation can also be represented by velocity potential using energy equation. Let's consider that the total enthalpy is constant in the flowfield.

$$h_\circ = constt.$$

$$C_p T + \frac{V^2}{2} = C_p T_0$$

$$\frac{\gamma RT}{\gamma - 1} + \frac{V^2}{2} = \frac{\gamma RT_0}{\gamma - 1}$$

$$\frac{a^2}{\gamma - 1} + \frac{V^2}{2} = \frac{a_0^2}{\gamma - 1}$$

$$a_0^2 = a^2 - \frac{\gamma - 1}{2}V^2 = a^2 - \frac{\gamma - 1}{2}(u^2 + v^2 + w^2)$$

$$a_0^2 = a^2 - \frac{\gamma - 1}{2}\left(\Phi_x{}^2 + \Phi_y{}^2 + \Phi_z{}^2\right)$$

Simultaneous solution of Equations gives the velocity potential. Using this we can get the velocity field using the potential gradients. However direct solution of these equation is not possible. Hence linearization of this equation is essential.

Linearization of Velocity Potential Equation

Consider the steady irrotational flow around the thin aerofoil as shown in Fig. 4.4.

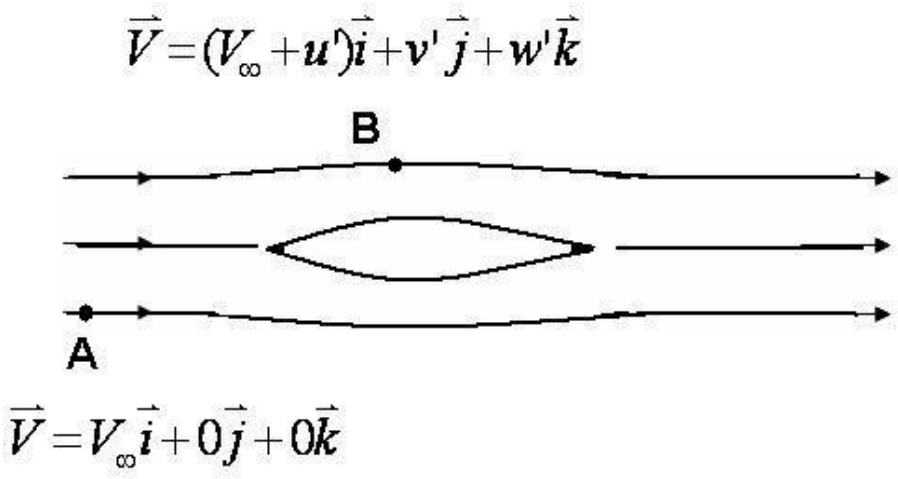

Fig. 4.4. Schematic of the perturbed velocity field.

At location A, velocity is only in x direction. However, presence of body perturbs the components of velocity at location B. Lets represent the general velocity field as,

$$\vec{V}=V_x\vec{i}+V_y\vec{j}+V_z\vec{k}$$

here, $V_x=V_\infty+u'$ and u', v', w' are the perturbed velocites in the x, y and z directions respectively such that.

$$V_y=v'$$
$$V_z=w'$$

Since the velocity field is irrotational, we can represent the velocity field using gradient of velocity potential as,

$$\nabla\Phi=\vec{V}=(V_\infty+u')\vec{i}+v'\vec{j}+w'\vec{k}$$

Let the perturbed velocity field be presented by perturbed velocity potential, ϕ. Hence,

$$\frac{\partial\phi}{\partial x}=u' \quad \frac{\partial\phi}{\partial y}=v' \quad \frac{\partial\phi}{\partial z}=w'$$

Therefore,

$$\Phi(x,y,z)=V_\infty x+\phi(x,y,z)$$

Such that,

$$V_x=\frac{\partial\Phi}{\partial x}=V_\infty x+u'=V_\infty x+\frac{\partial\phi}{\partial x}$$
$$V_y=\frac{\partial\Phi}{\partial y}=\frac{\partial\phi}{\partial y}=v'$$

Source from Computational Fluid Mechanics and Heat Transfer by Tannehill John C, Anderson Dale A, Pletcher Richard H

$$V_z = \frac{\partial \Phi}{\partial z} = \frac{\partial \phi}{\partial z} = w'$$

and

$$\Phi_{xx} = \frac{\partial^2 \phi}{\partial x^2} = \phi_{xx}, \quad \Phi_{yy} = \frac{\partial^2 \phi}{\partial y^2} = \phi_{yy}, \quad \Phi_{zz} = \frac{\partial^2 \phi}{\partial z^2} = \phi_{zz}$$

We can use these expression in the known velocity potential equation.

$$\left(1-\frac{\Phi_x^2}{a^2}\right)\Phi_{xx} + \left(1-\frac{\Phi_y^2}{a^2}\right)\Phi_{yy} + \left(1-\frac{\Phi_z^2}{a^2}\right)\Phi_{zz}$$
$$-2\frac{\Phi_x\Phi_y}{a^2}\Phi_{xy} - 2\frac{\Phi_x\Phi_z}{a^2}\Phi_{xz} - 2\frac{\Phi_y\Phi_z}{a^2}\Phi_{yz} = 0$$

This expression in the form of perturbed velocity potential can be written as,

$$\left[a^2 - \left(V_\infty + \frac{\partial \phi}{\partial x}\right)^2\right]\frac{\partial^2 \phi}{\partial x^2} + \left[a^2 - \left(\frac{\partial \phi}{\partial y}\right)^2\right]\frac{\partial^2 \phi}{\partial y^2} + \left[a^2 - \left(\frac{\partial \phi}{\partial z}\right)^2\right]\frac{\partial^2 \phi}{\partial z^2}$$
$$-2\left(V_\infty + \frac{\partial \phi}{\partial x}\right)\frac{\partial \phi}{\partial y}\frac{\partial^2 \phi}{\partial x \partial y} - 2\left(V_\infty + \frac{\partial \phi}{\partial x}\right)\frac{\partial \phi}{\partial z}\frac{\partial^2 \phi}{\partial x \partial z} - 2\frac{\partial \phi}{\partial y}\frac{\partial \phi}{\partial z}\frac{\partial^2 \phi}{\partial y \partial z} = 0$$

or,

$$\left[a^2 - (V_\infty + u')^2\right]\frac{\partial u'}{\partial x} + \left[a^2 - v'^2\right]\frac{\partial v'}{\partial y} + \left[a^2 - w'^2\right]\frac{\partial w'}{\partial z}$$
$$-2(V_\infty + u')v'\frac{\partial v'}{\partial y} - 2(V_\infty + u')w'\frac{\partial u'}{\partial z} - 2v'w'\frac{\partial v'}{\partial z} = 0$$

But we know that, total enthalpy is constant in flow field. We can use this fact to represent the speed of sound encountered in the above equation as,

$$\because h_0 = const.$$
$$h_0 = h_\infty + \frac{V_\infty^2}{2} = h + \frac{V^2}{2} = h + \frac{(V_\infty + u')^2 + v'^2 + w'^2}{2}$$
$$\frac{a_\infty^2}{\gamma - 1} + \frac{V_\infty^2}{2} = \frac{a^2}{\gamma - 1} + \frac{(V_\infty + u')^2 + v'^2 + w'^2}{2}$$
$$a^2 = a_\infty^2 - \frac{\gamma - 1}{2}\left(2u'V_\infty + u'^2 + v'^2 + w'^2\right)$$

Using this expression and further simplification, Eq. 2.11 can be written as,

$$\left(1 - M_\infty^2\right)\frac{\partial u'}{\partial x} + \frac{\partial v'}{\partial y} + \frac{\partial w'}{\partial z}$$

$$= M_\infty^2\left[(\gamma+1)\frac{u'}{V_\infty}+\left(\frac{\gamma+1}{2}\right)\frac{u'^2}{V_\infty^2}+\left(\frac{\gamma-1}{2}\right)\left(\frac{v'^2+w'^2}{V_\infty^2}\right)\right]\frac{\partial u'}{\partial x}$$

$$+M_\infty^2\left[(\gamma-1)\frac{u'}{V_\infty}+\left(\frac{\gamma+1}{2}\right)\frac{v'^2}{V_\infty^2}+\left(\frac{\gamma-1}{2}\right)\left(\frac{w'^2+u'^2}{V_\infty^2}\right)\right]\frac{\partial v'}{\partial x}$$

$$+M_\infty^2\left[(\gamma-1)\frac{u'}{V_\infty}+\left(\frac{\gamma+1}{2}\right)\frac{w'^2}{V_\infty^2}+\left(\frac{\gamma-1}{2}\right)\left(\frac{u'^2+v'^2}{V_\infty^2}\right)\right]\frac{\partial w'}{\partial x}$$

$$+M_\infty^2\left[\frac{v'}{V_\infty}\left(1+\frac{u'}{V_\infty}\right)\left(\frac{\partial u'}{\partial y}+\frac{\partial v'}{\partial x}\right)+\frac{w'}{V_\infty}\left(1+\frac{u'}{V_\infty}\right)\left(\frac{\partial u'}{\partial z}+\frac{\partial w'}{\partial x}\right)+\frac{u'w'}{V_\infty}\left(\frac{\partial w'}{\partial y}+\frac{\partial v'}{\partial z}\right)\right]\frac{\partial v'}{\partial x}$$

The equation (4.1) is the exact equation for steady irrotational flow around the thin configurations.

We can simplify this equation, since the perturbed velocities, u', v' and w' are small in comparison with the freestream velocity V_∞.

Hence,

$$\frac{u'}{V_\infty}, \frac{v'}{V_\infty} \text{ and } \frac{w'}{V_\infty} << 1$$

So, $\left(\frac{u'}{V_\infty}\right)^2\left(\frac{v'}{V_\infty}\right)^2\left(\frac{w'}{V_\infty}\right)^2 <<< 1$

This approximations leads to two facts,

1. Except for the Transonic flows (Flows having Mach number in the range 0.8 to 1.2)

$$M_\infty^2\left[(\gamma+1)\frac{u'}{V_\infty}+\cdots\right]\frac{\partial u'}{\partial x} << \left(1-M_\infty^2\right)\frac{\partial u'}{\partial x}$$

2. If Mach number of the flow is less than 5.0

$$M_\infty^2\left[(\gamma+1)\frac{u'}{V_\infty}+\cdots\right]\frac{\partial u'}{\partial x} << \left(1-M_\infty^2\right)\frac{\partial u'}{\partial x}$$

$$M_\infty^2\left[(\gamma-1)\frac{u'}{V_\infty}+\cdots\right]\frac{\partial v'}{\partial y} << \frac{\partial v'}{\partial y}, \quad M_\infty^2\left[(\gamma-1)\frac{u'}{V_\infty}+\cdots\right]\frac{\partial w'}{\partial z} << \frac{\partial w'}{\partial z}$$

$$M_\infty^2\left[(\gamma-1)\frac{v'}{V_\infty}\left(1+\frac{u'}{V_\infty}\right)\left(\frac{\partial u'}{\partial y}+\frac{\partial v'}{\partial x}\right)+\cdots\right] << 1 \quad (\approx 0)$$

For these two facts we get,

$$\left(1-M_\infty^2\right)\frac{\partial u'}{\partial x}+\frac{\partial v'}{\partial y}+\frac{\partial w'}{\partial z}=0$$

Or,

$$\left(1-M_\infty^2\right)\frac{\partial^2\phi}{\partial x^2}+\frac{\partial^2\phi}{\partial y^2}+\frac{\partial^2\phi}{\partial z^2}=0$$

This is the linear equation and this approximation is valid for steady irrotational subsonic and supersonic flows under the assumption of small perturbation.

Supersonic flow over a cone

The flow over a cone is a two-dimensional axisymmetric problem. It is also referred to as "Quasi-Two dimensional Problem". This is so, because, the cone under consideration is aligned symmetrically about the z-axis or along the direction of V_∞, as shown in the Fig.4.5

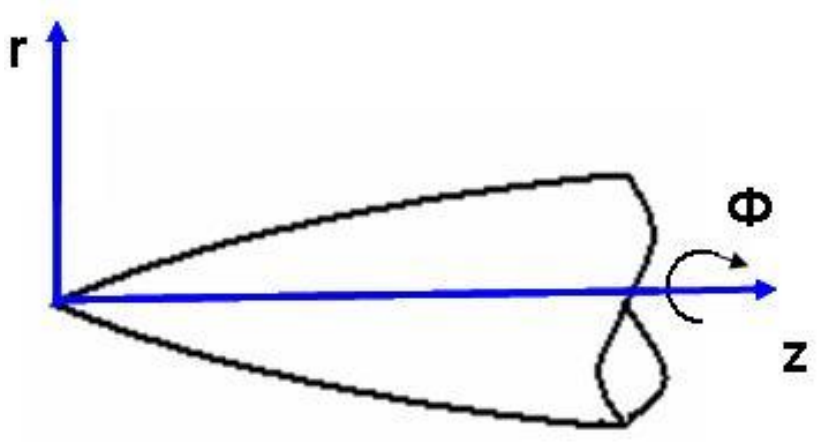

Fig. 4.5: Geometry in consideration and the fluid flow direction

The supersonic flow over a cone is of great practical importance in applied aerodynamics. The nose cones of many high-speed missiles and projectiles are approximately conical, are the nose regions of the fuselages of most supersonic airplanes.

In the particular problem of supersonic flow over a cone, consideration is given to a sharp right circular cone with zero angle of attack. Consider a cone on the (r, ϕ, Z) co-ordinate system, as shown in Fig. 4.5 which is symmetric about the Z axis and extends to infinity with a semi-vertex cone angle θ. The supersonic flow with freestream velocity V_∞ is considered along the Z axis, such that the angle of attack is 0o. Typical flowfield for supersonic flow over cone is as shown in Fig. 2.6. For such a supersonic flow over the surface of the cone, it is expected that a oblique shock wave attached to the tip of the cone is formed. Further, the shape of the shock wave formed is also conical.

A streamline from the supersonic freestream discontinuously deflects as it passes through the shock, and then curves continuously downstream of the shock, becoming parallel to the cone surface asymptotically at infinity. Further, it is also assumed that the pressure and all the other flow properties are constant along the surface of the cone. Since the cone surface is simply a ray from the vertex, consider other such rays between the cone surface and the shock wave, as shown by the dashed line in Fig 4.6. Hence assumption of constancy of flow properties can be extended along these rays as well. Therefore properties variation takes place as the fluid moves from one ray to the next.

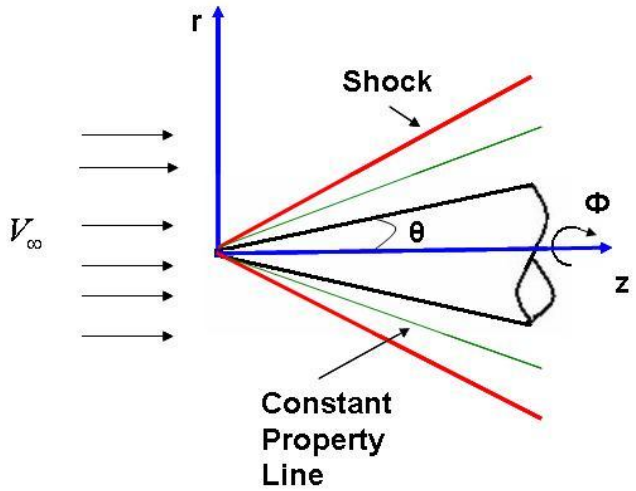

Fig.4.6: Flowfield in the presence of supersonic flow over a cone.

Mathematical Formulation for Supersonic flow over cone

Consider Fig. 4.7. For the terminologies of the derivation in concerned with supersonic flow over cone. At any angular location in the flow field, the radial and normal components of velocity are Vr and Vθ, respectively. Understanding the flowfield around the cone necessarily means solving for the

Source from Computational Fluid Mechanics and Heat Transfer by Tannehill John C, Anderson Dale A, Pletcher Richard H

flowfield between the body and the shock wave by calculating these velocity components. Since the flow field is symmetric about the z axis all properties are independent of Φ.
So,

$$\frac{\partial}{\partial \phi} = 0$$

Further, since we have assumed that the flow properties are constant along a ray from the vertex

$$\frac{\partial}{\partial r} = 0$$

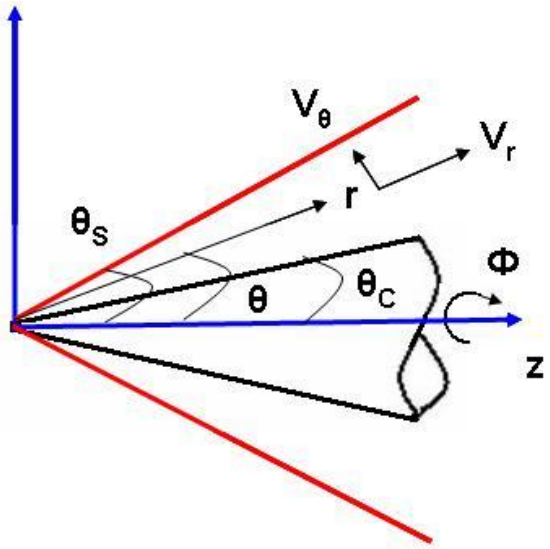

Fig. 4.7: Schematic for terminologies regarding derivation for supersonic flow over cone.

From the equation of continuity, we get

$$\nabla.(\rho V) = 0$$

But, since the geometry is symmetric about the z axis and extends to infinity, the scale on the Z-axis can be neglected while considering the spherical co-ordinate system to analyze the problem. Hence the mass conservation equation can be written as,

$$\nabla.\rho(V) = \frac{1}{r^2}\frac{\partial}{\partial r}(r^2 \rho V_r) + \frac{1}{r\sin\theta}\frac{\partial}{\partial \theta}(\rho V_\theta \sin\theta) + \frac{1}{r\sin\theta}\frac{\partial(\rho V_\phi)}{\partial \phi} = 0$$

$$\frac{1}{r^2}[r^2\frac{\partial(\rho V_r)}{\partial r} + (\rho V_r)(2r)] + \frac{1}{r\sin\theta}[\rho V_\theta \cos\theta + \sin\theta\frac{\partial(\rho V_\theta)}{\partial \theta}] + \frac{1}{r\sin\theta}\frac{\partial(\rho V_\theta)}{\partial \phi} = 0$$

$$\frac{2\rho V_r}{r} + \frac{\rho V_\theta}{r}\cot\theta + \frac{1}{r}(\rho\frac{\partial V_\theta}{\partial \theta} + V_\theta\frac{\partial \rho}{\partial \theta}) = 0$$

$$2\rho V_r + \rho V_\theta \cot\theta + (\rho\frac{\partial V_\theta}{\partial \theta} + V_\theta\frac{\partial \rho}{\partial \theta}) = 0$$

This is the continuity equation for the axisymmetric flow over the cone.

For this axi-symmetric flow, there is increase in the entropy across the shock, but the change in entropy is zero in the region between the shock and the cone since post shock flow is isentropic ,i.e, $\nabla s = 0$ .Further, the flow in this region is steady and adiabatic, hence $\Delta h_o = 0$.

Therefore, from Crocco's equation, $V \times (\nabla \times V) = \nabla h_0 - T \times \nabla s$,we find that ($V \times (\nabla \times V) = 0$ i.e., the conical flowfield is irrotational.
Hence,

$$\nabla \times \mathbf{V} = \frac{1}{r^2 \sin\theta} \begin{vmatrix} \mathbf{e}_r & r\mathbf{e}_\theta & (r\sin\theta)\mathbf{e}_\phi \\ \frac{\partial}{\partial r} & \frac{\partial}{\partial \theta} & \frac{\partial}{\partial \phi} \\ V_r & rV_\theta & (r\sin\theta)V_\phi \end{vmatrix} = 0$$

$$\nabla \times V = \frac{1}{r^2 \sin\theta} \{e_r [\frac{\partial}{\partial \theta}(rV_\phi \sin\theta) - \frac{\partial}{\partial \phi}(rV_\theta)] - re_\theta [\frac{\partial}{\partial r}(rV_\phi \sin\theta) - \frac{\partial (V_r)}{\partial \phi}] + (r\sin\theta) e_\phi [\frac{\partial}{\partial r}(rV_\theta) - \frac{\partial V_r}{\partial \theta}]\} = 0$$

Applying the axisymmetric conical flow constant as, $\frac{\partial}{\partial \phi} = 0$ and, we can get as

$$\frac{\partial}{\partial r}(rV_\phi \sin\theta) - \frac{\partial (V_r)}{\partial \phi} = 0$$

$$r\frac{\partial}{\partial r}(V_\phi \sin\theta) = 0$$

This simplifies the irrotatinality constant to,

$$V_\theta = \frac{\partial V_r}{\partial \theta}$$

Unit process is one or more grouped operations in a manufacturing system that can be defined and separated from others.

Flow through duct

The procedure for using the method of characteristic lines are to numerically calculate the flow in a duct is as follows:

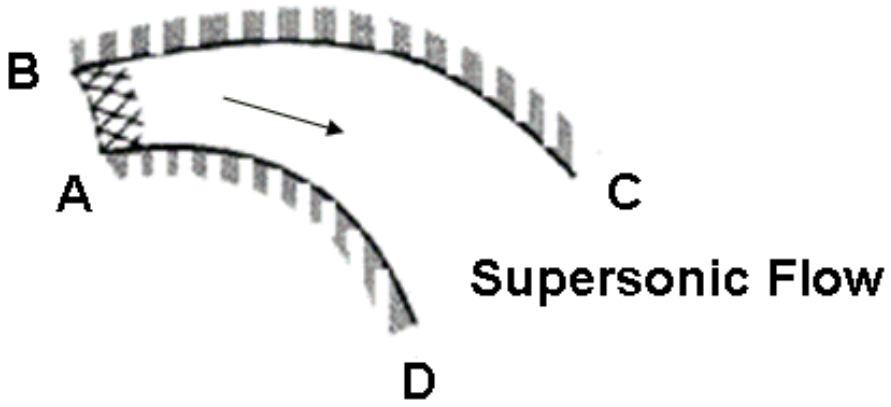

Fig. 4.8. Supersonic flow through duct

The conditions on some initial line must be specified, e.g., conditions on the line AB in Fig. 4.8 must be specified. The shape of the walls, e.g., AD and BC in Fig. 4.8, must be known.

Using the initial values of the variables on line A, determine the stagnation pressure, temperature, etc. Starting with a series of chosen points on line AB, march the solution forward to the points defined by the intersection of characteristics with each other or with the wall as indicated. At each point, use the calculated values of v and θ to get flow variables. A computer program based on this procedure can be easily developed.

Nozzle Design

Supersonic nozzles are used in a variety of engineering applications to expand a flow to desired supersonic conditions. Supersonic nozzles can be divided into two different types: gradual-expansion nozzles and minimum-length nozzles (Fig. 4.9).

Gradual-expansion nozzles are typically used in applications where maintaining a high-quality flow at the desired exit conditions is of importance (e.g., supersonic wind tunnels). For other types of applications (e.g., rocket nozzles), the large weight and length penalties associated with gradual-expansion nozzles make them unrealistic; therefore minimum-length nozzles, which utilize a sharp corner to provide the initial expansion, are commonly used.

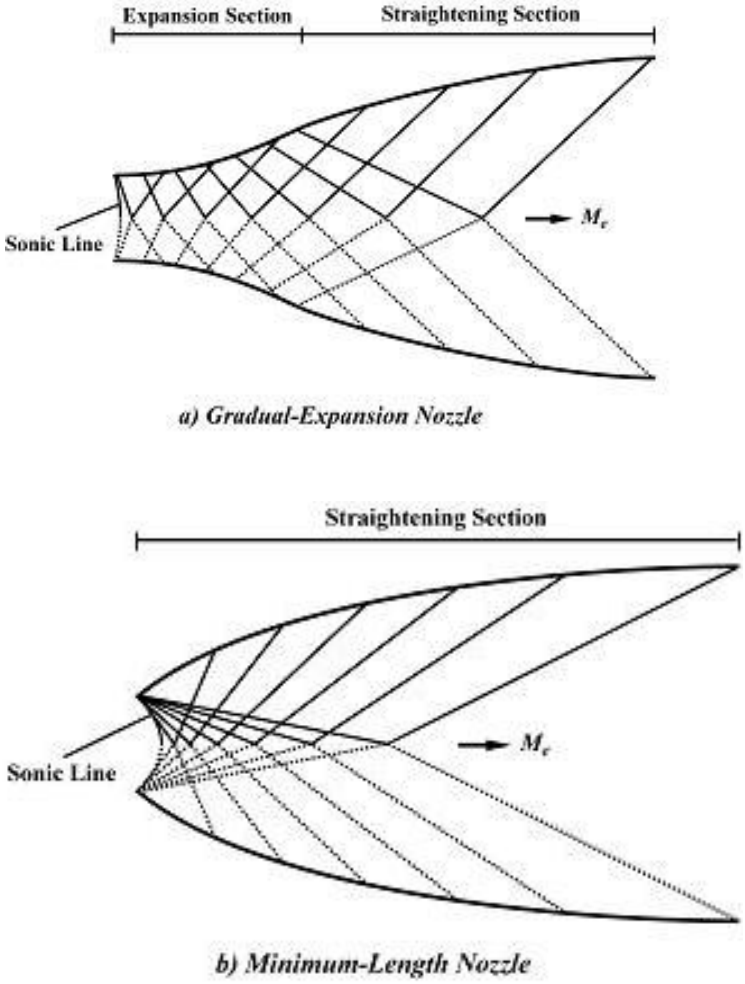

Fig. 4.9 Types of nozzles

For both gradual-expansion and minimum-length nozzles, the flow can be divided into simple and non-simple regions. A non-simple region is characterized by Mach wave reflections and intersections. In order to meet the requirement of uniform conditions at the nozzle exit, it is desirable to minimize the non-simple region as much as possible. This can be performed by designing the nozzle surface such that Mach waves (e.g., characteristics) are not produced or reflected while the flow is straightened.

The Method of Characteristics is therefore applied to allow the design of a supersonic nozzle which meets these requirements. In the present work, design of both gradual-expansion nozzle and minimum-length nozzle is demonstrated.

The boundary layer on the nozzle and side walls has a displacing effect which reduces the effective height and width of the nozzle. Allowance for this is to be made by adding a correction for boundary layer. The side walls should also diverge to allow for their boundary layers.

Method of characteristics is & Method of waves

The method of characteristics deals with a continuous velocity field, the computation being made at the lattice points of a network of characteristics. The wave method deals with a patch work field of cells of uniform flow, with discontinuities between them. Accuracies in the two methods are similar, being dependent on the fineness of the mesh

Computation with waves is convenient only in plane flow, since it depends on the theorem that the strength of a wave does not change after intersections and reflections. In axially symmetric flow and in general 3-D flow the strength of a wave varies continuously.

The wave method is more intuitive in plane flow than the characteristic method and is usually preferred. In some problem it is more convenient – because of the idea of wave cancellation to determine a boundary shape.

Design of Minimum-Length Nozzle (MLN)

It should be noted that for this two-dimensional nozzle configuration, flow symmetry implies that only half of the nozzle is physically required, assuming that the characteristic reflections in the non-simple region are maintained. Therefore, we can make the assumption of a half-symmetric minimum-length nozzle, in which a nozzle flap is extended from the symmetry plane such that it meets the length requirement for the last characteristic intersecting the nozzle surface (Fig.4.10).

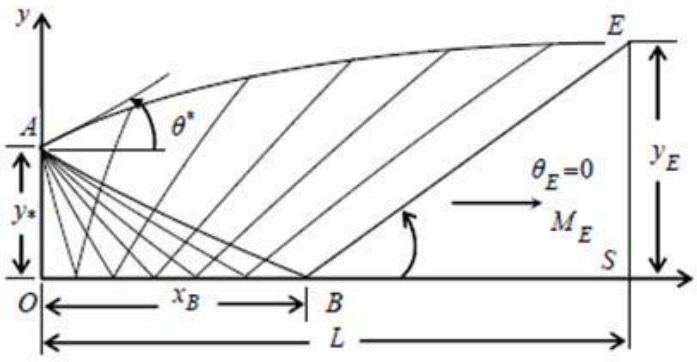

Fig. 4.10. Schematic of characteristic lines for MLN.

Implementation of Method of Characteristics

The two-dimensional Method of Characteristics is a relatively simple analytical model for analyzing supersonic two-dimensional flow. This analysis is performed by considering the characteristic lines in the flow. Points along each characteristic have five important properties: M (Mach number), θ (flow angle), ν (Prandtl-Meyer function), and x and y (position). For the assumption of steady, supersonic, we know that,

$$\theta \pm \vartheta = Constant$$

The constant for summation can be said to be K+ and for subtraction to be K-. These constants are the Riemann invariants, which are constant along the characteristics C+ and C-.

Design of Gradual expansion nozzle

The steps involved in this calculation are precisely same as those used for the minimum length nozzle except for the fact that the expansion fan at the sharp corner is now replaced by a series of right running characteristic lines originating from the arc of the circle. One major assumption that has been made here is that a characteristic originating from any point on the expansion section is always reflected from the axis in such a way that it reaches the straightening portion of the nozzle. Multiple reflections of characteristic lines within the smooth expansion portion of the nozzle would make the problem much complicated without really improving the results much.

UNIT – IV
PANEL METHODS

In most of these cases the geometry was approximated by flat, zero-thickness surfaces and for additional simplicity the boundary conditions were transferred, too, these simplified surfaces (e.g., at z = 0).The application of numerical techniques allows the treatment of more realistic geometries and the fulfillment of the boundary conditions on the actual surface. In this the methodology of some numerical solutions will be examined and applied to various problems. The methods presented here are based on the surface distribution of singularity elements, which is a logical extension of the analytical methods presented in the earlier chapters. Since the solution is now reduced to finding the strength of the singularity elements distributed on the body's surface this approach seems to be more economical, from the computational point of view, than methods that solve for the flowfield in the whole fluid volume (e.g., finite difference methods). Of course this comparison holds for inviscid incompressible flows only, whereas numerical methods such as finite difference methods were basically developed to solve the more complex flowfields where compressibility and viscous effects are not negligible.

Basic Formulation

Consider a body with known boundaries S_B , submerged in a potential flow, as shown in Fig. 5.1. The flow of interest is in the outer region V where the incompressible, irrotational continuity equation, in the body's frame of reference, in terms of the total potential is

$$\nabla \cdot V = 0$$

Following Green's identity, we can construct the general solution to above Equation by a sum of source σ and doublet μ distributions placed on the boundary SB
Here the vector n points in the direction of the potential jump μ, which is normal to SB and positive outside of V (Fig. 5.1), and V∞ is the free-stream potential.

This formulation does not uniquely describe a solution since a large number of source and doublet distributions will satisfy a given set of boundary conditions. Therefore, a choice has to be made in order to select the desirable combination.

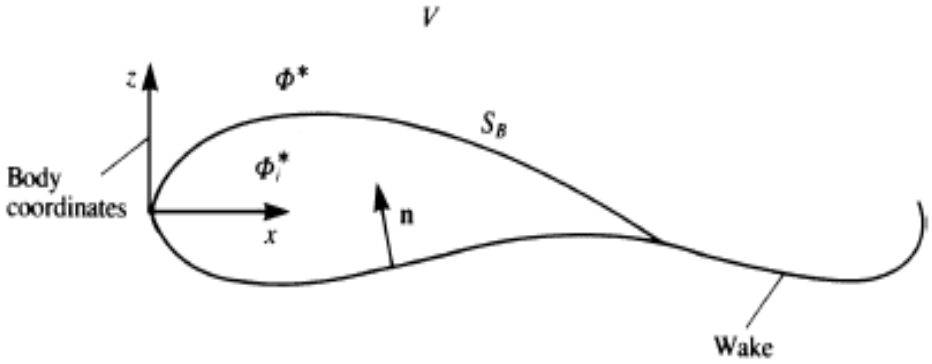

Figure 5.1 Potential flow over a closed body.

of such singularity elements. It is clear from the previous examples that for simulating the effect of thickness, source elements can be used, whereas for lifting problems, antisymmetric terms such as the doublet (or vortex) can be used. To uniquely define the solution of this problem, first the boundary conditions of zero flow normal to the surface must be applied. In the general case of three-dimensional flows, specifying the boundary conditions will not immediately yield a unique solution because of two problems. First, a decision has to be made in regard to the "right" combination of source and doublet distributions.

Second, some physical considerations need to be introduced to fix the amount of circulation around the surface S_B. These considerations deal mainly with the modeling of the wakes and fixing the wake shedding lines and their initial orientation and geometry.

The Boundary Conditions

The boundary condition for equation can directly specify a zero normal velocity component on the surface S_B, in which case this "direct" formulation is called the Neumann problem. It is possible to specify on the boundary, so that indirectly the zero normal flow condition will be met, and this "indirect" formulation is called the Dirichlet problem. Of course, a combination of the above boundary conditions is possible, too, and this is called a mixed boundary condition problem.

An additional approach would be to search for a singularity distribution that creates enclosed streamlines, equivalent to the geometry of the surface S_B. This method is useful in two dimensions, where the stream function W is well defined but for complex, three-dimensional geometries the implementation of this method is difficult and will not be dealt with here.

Physical Considerations

The above mathematical formulation, even after selecting a desirable combination of sources and doublets, and after fulfilling the boundary conditions on the surface SB , is not unique.

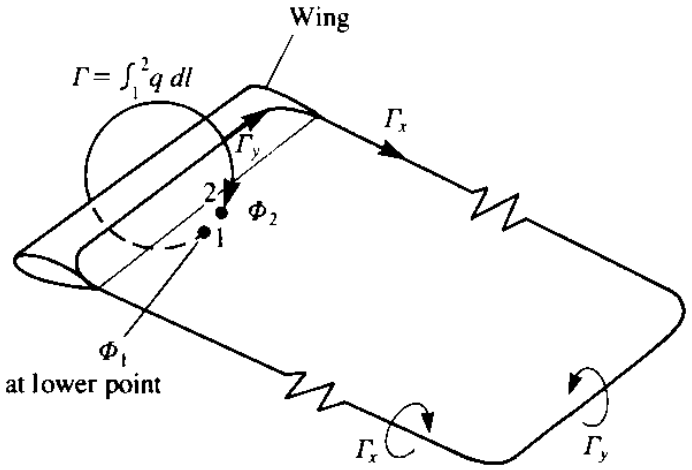

Figure 5.2 Vorticity system created by a finite wing in steady forward flight.

Previous examples showed that for describing the flow over thick bodies without lift the source distribution was sufficient, but for the lifting cases the amount of the circulation was not uniquely defined. Let us examine the case of a lifting wing, as viewed from a large distance (Fig. 5.2).

For simplicity, the bound vortex is represented by a concentrated vortex line with the strength T (=Tx = Ty). According to the Helmholtz theorems a vortex line cannot start in a fluid and we can write which for the simple case of Fig. 5.2 implies that the problem is modeled by one constant- strength, closed vortex line. Also, the amount of the bound circulation is where point 1 lies under and point 2 is above the (very) thin wake. These two arguments clearly demonstrate that for the three dimensional lifting problem there is a need to model a wake, since the bound vorticity needs to be continued beyond the wing.

Also, as shown in Fig. 5.2, for the wing to have circulation T at a spanwise location,a discontinuity in the velocity potential near the trailing edge must exist:

$$\delta 2 - \delta 1 = T$$

where δ1 is under and δ2 is above the wake. Now we are in a position where the additional physical conditions, required for a unique solution, can be established in relation to a wake model. This model has to specify two additional conditions:

- To set the wake strength at the trailing edge.
- To set its shape and location.

Wake Strength

The simplest solution to this problem is to apply the two-dimensional Kutta con- dition along the three-dimensional trailing edge (as shown in Fig. 5.3) such that

$$\gamma T.E. = 0$$

Since, for example, in the two-dimensional case $\partial\mu(x)/\partial x = -\gamma(x)$ the above condition can be rewritten for the trailing-edge line, such that μ is constant in the

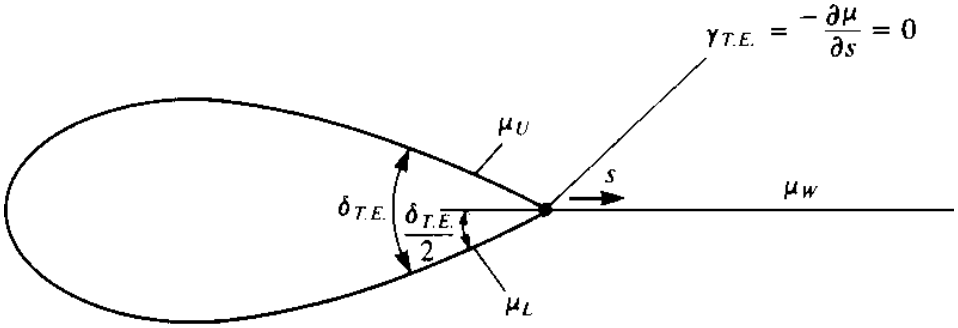

Figure 5.3 Implementation of the Kutta condition when using surface doublet distribution.

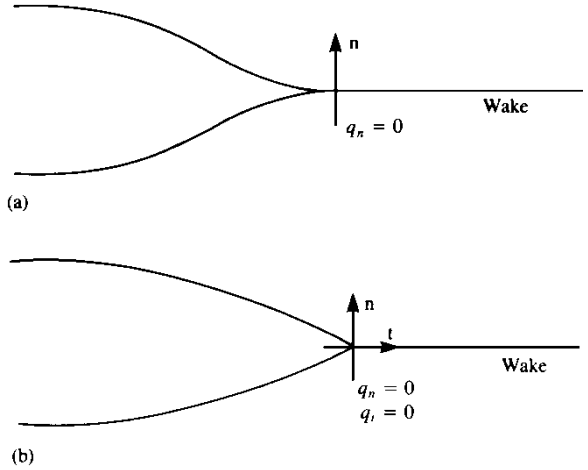

Figure 5.4 Possible conditions that can be applied at (a) cusp and (b) finite angle trailing edges

trailing edge. In such situations this point is not necessarily a stagnation point and if the velocity formulation is used then only the qn = 0 condition can be used. In the case that the trailing edge has a finite angle (Fig. 5.4b), then in order to have a continuous velocity at this point the condition $q_t = 0$ can also be used.

Wake Shape

In two dimensions, the trailing vortex segment of the wake is ignored since it has zero vorticity (in steady flow) and it is sufficient to specify the location of the trailing edge where the Kutta condition is met. In three dimensions, the wake influence is more dominant and its geometry clearly affects the solution. To distinguish between the models for bound circulation (which generate the lift) and the circulation shed into the wake, it is logical to assume that the wake should not produce lift – since it is not a solid surface. As an example, let us recall the formulation for the force F generated by a vortex sheet γ. The Kutta–Joukowski theorem for lift states that

$$\mathbf{F = \rho q \times \gamma}$$

For a three-dimensional case 6F = 0 only if the local flow is parallel to γ (we assume γ /=0). So the condition for the wake geometry is

$$\mathbf{q \times \gamma W = 0} \qquad \textbf{or}$$

$\gamma_W \parallel \mathbf{q}$

that is, the vorticity vector is parallel to the local velocity vector.

An equivalent representation of the wake by a thin doublet sheet is obtained by noting that $\gamma W = -\nabla \mu W$. If no force is produced by this lifting surface then equation becomes

$$q \times \nabla \mu W = 0$$

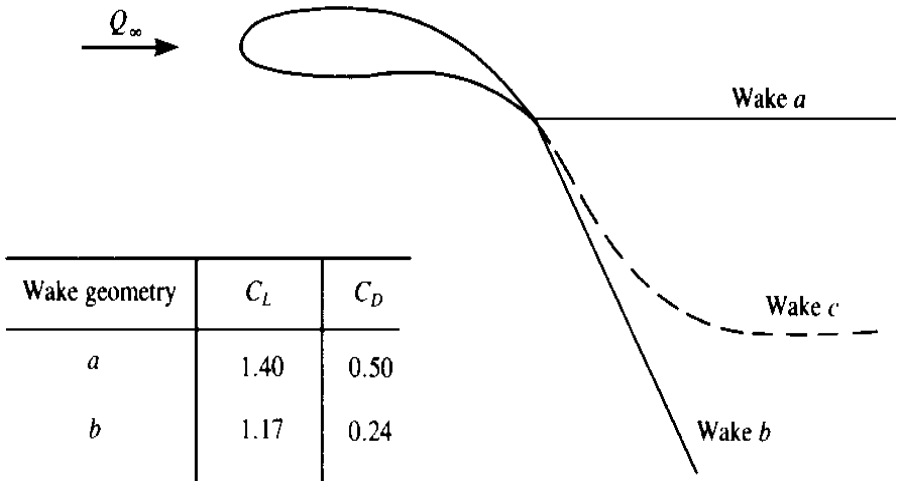

Wake geometry	C_L	C_D
a	1.40	0.50
b	1.17	0.24
c	1.22	0.33

Figure 5.5 Effect of prescribed wake geometry on the aerodynamics of an AR = 1.5 wing.

So the condition for the wake panels, in terms of doublets, is

$$\mu W = \text{const.}$$

and the boundaries of these elements (which are really the vortex lines) should be parallel to the local streamlines, as in equation. This condition is difficult to satisfy exactly since the wake location is not known in advance. In most cases it is sufficient to assume that the wake leaves the trailing edge at a median angle δT.E./2, as shown in Figs. 5.3 and 5.4, whereas for portions of the wake far from the trailing edge, additional effort is required to satisfy the condition of equation.

As an example of the dependence of the solution on the wake initial geometry, the results for a cambered rectangular wing of aspect ratio 5.5 are shown in Fig. 5.5. The solution was obtained by a first-order panel method (VSAERO9.3) with 600 panels per semispan and the corresponding lift and drag coefficients are tabulated in the inset to the figure (incidentally, case c is the closest to experimental results).

$\delta^* = \delta\infty$

Reduction of the Problem to a Set of Linear Algebraic Equations

At this point it is assumed that the problem is unique and that a combination of source/doublet distributions has been selected along with a wake model and the Kutta condition. For the following example $\delta^* = \delta\infty$ along with equation. for the source strength will be used and a constant-strength rectilinear panel is assumed.

The body's surface (see Fig. 5.6) is now divided into N surface panels and into NW additional wake panels. The boundary condition (either Neu-mann or Dirichlet) will be specified at each of these elements at a collocation point (which for the Dirichlet boundary condition must be specified inside the body where $\delta^* = \delta\infty$, e.g., at a point under the center of the panel). In most cases, though, the point may be left on the surface without moving it inside the body.

Rewriting, for example, the Dirichlet boundary condition for each of the N collocation points.

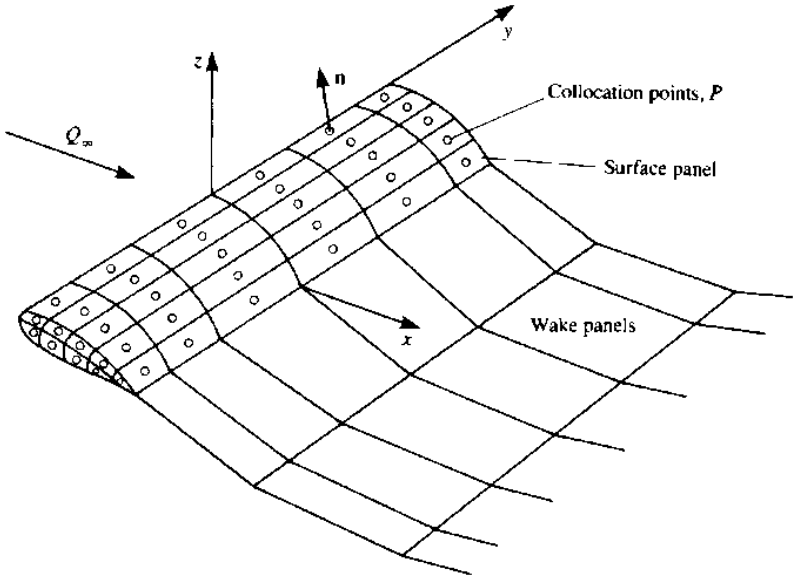

Figure 5.6 Approximation of the body surface by panel elements.

That is, for each collocation point P the summation of the influences of all k body panels and 4 wake panels is needed. The integration in Equation is limited now to each individual panel element representing the influence of this panel on point P. For a unit singularity element (σ or μ), this influence depends on the panel's geometry only. The integration can be performed analytically or numerically, prior to this calculation, and for example for a constant-strength μ element shown in Fig. the influence of panel k (defined by the four corners 1, 2, 3, and 4) at point P is and for a constant-strength σ element

Aerodynamic Loads

Once Equation is solved the unknown singularity values are obtained (μk in this example). The velocity components are evaluated now in terms of the panel local coordinates (l, m, n) shown in Fig. 5.8. The two tangential perturbation velocity components are where the differentiation is done numerically using the values on the neighbor panels.

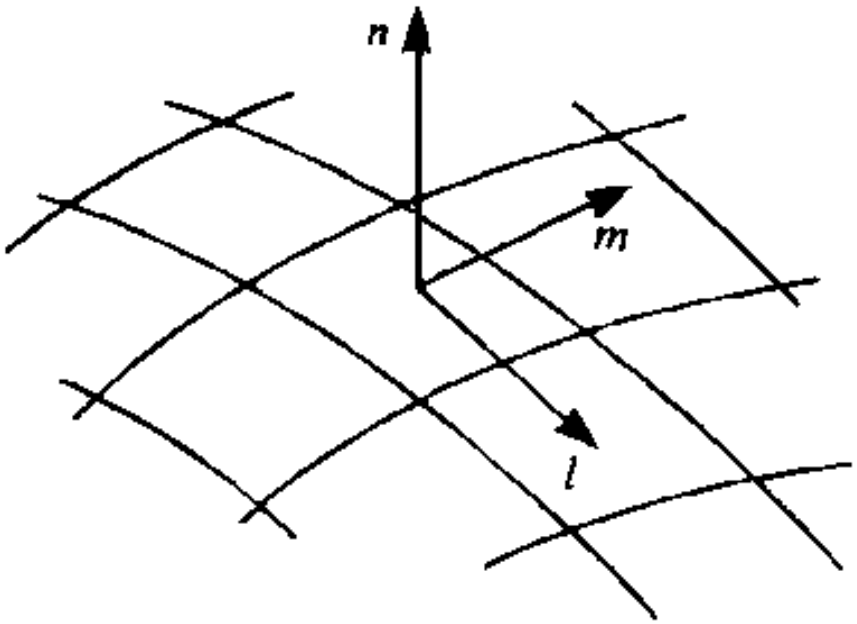

Figure 5.8 Panel local coordinate system for evaluating the tangential velocity components.

Preliminary Considerations, Prior to Establishing, Numerical Solutions Prior to establishing a numerical solution

a. **Type of singularity that will be used:** The options usually include sources, doublets, and vortices or any combination of the above.
b. **Type of boundary conditions:** Velocity or velocity-potential formulation may be used and the corresponding Neumann, Dirichlet, or a combination of such boundary conditions must be selected.
c. **Wake models:** How and where the Kutta condition will be specified. Also, the shape of the wake is controlled by Equation and can be set by Programmer-specified shape based on intuition or on flow visualizations.

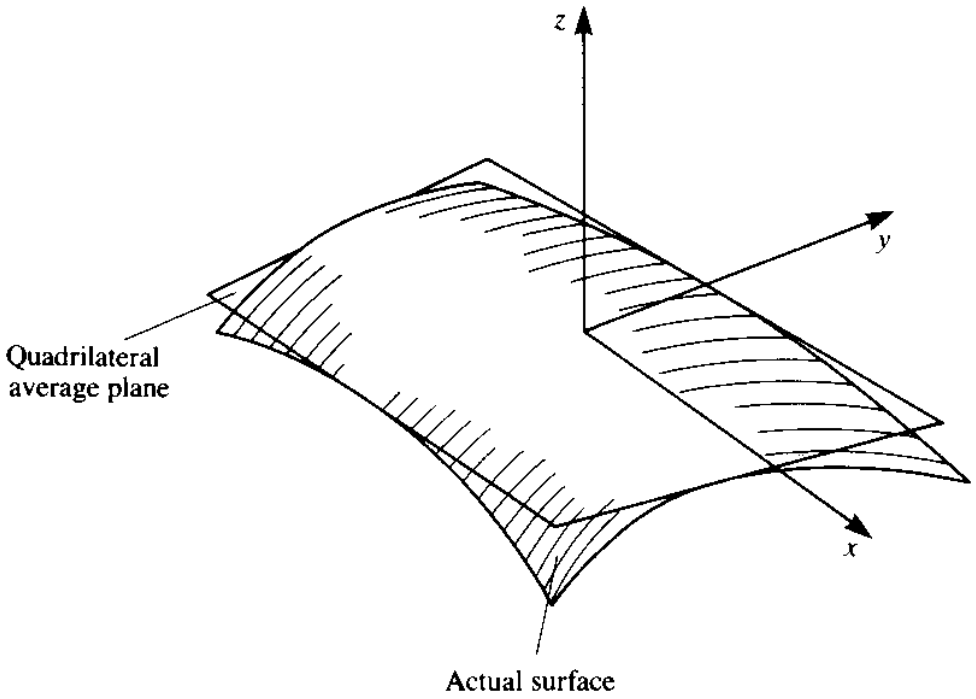

then this is a zero-order approximation of μ. Similarly, a first-order (or linear) approximation is

$$\mu = a0 + b1x + b2\,y$$

and a second-order (or parabolic) polynomial approximation is

$$\mu = a0 + b1x + b2\,y + c1x^2 + c2xy + c3\,y^2$$

(Here the coefficients *a, b, c* are constants, too, and of course are different from the coefficients of the surface approximation).

Considerations of numerical efficiency: It is clear from the brief discussion on discretization that the computation of the influence coefficients is elaborate. Many methods divide such calculations into near and far field where the far field calculation treats the element as a point singularity (and not as a surface distribution).

Typically, the near field is assumed if the distance to a point P is less than 2.5–5 times the larger diagonal of the panel. On the other hand because of the 1/r characteristics of the singularity elements, when $r \rightarrow 0$ the value of $1/r \rightarrow \infty$; therefore, when the point P is too close to the panel (or to a vortex line) cutoff distances are usually applied. (Only the aerodynamic aspects of the numerics are discussed here; other important aspects, e.g., the matrix solver efficiency, are not.)

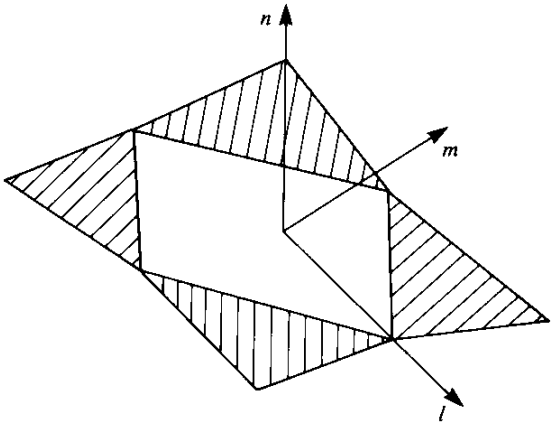

Figure 5.9 Description of a nonplanar panel element by a set of flat sub elements.

Steps toward Constructing a Numerical Solution

When establishing a numerical solution for potential flow a sequence similar to the following is recommended.

a. Selection of Singularity Element

The first and one of the most important decisions is the type of singularity element or elements that will be used. This includes the selection of source, doublet, or vortex representation and the method of discretizing these distributions (zero-, first-, second-order, etc.). Also, all of the questions raised in the previous section need to be answered before the actual formulation of the solution can be constructed. Once these decisions have been made an influence routine, similar to the model needs to be established. This influence computation is a direct function of the element geometry and such a routine outputs the velocity components and the potential (6u, 6v, 6w, 68) induced by the element. In general, the implementation which represents the core of most numerical solutions. Therefore, in the next chapter some of the more frequently used singularity elements will be formulated.

b. Discretization of Geometry (and Grid Generation)

Once the basic solution element is selected, the geometry of the problem has to be subdivided (or discretized), such that it will consist of those basic solution elements. In this grid generating process, the elements' corner points and collocation points are defined. The collocation points are points where the boundary conditions, such as the zero normal flow on a solid surface, will be enforced. Figure 5.10a shows how the cambered thin airfoil at an angle of attack can be discretized by using the lumped-vortex element. In this case the camber line is divided into five panels and the locations of the collocation points and of the vortex points are shown in the figure. Similarly, the subdivision of a three-dimensional body into planar surface elements is shown in Fig. 5.10b.

It is very important to realize that the grid does have an effect on the solution. Typically, a good grid selection will enable convergence to a certain solution when the density is increased (within reason). Moreover, a good grid selection usually will require some pre- liminary understanding of the problem's fluid dynamics, as will be shown in some of the forthcoming examples.

c. Influence Coefficients

In this phase, for each of the elements, an algebraic equation is derived at the collocation point. To generate the coefficients in an automatic manner, a unit singularity strength is assumed and the element influence routine is called at each of the collocation points (by a DO loop).

d. Establish RHS

The right-hand side of the matrix equation is the known portion of the free-stream velocity or the potential and requires mainly the computation of geometric quantities (e.g.,−Q∞α).

e. Solve Linear Set of Equations

The coefficients and the RHS of the algebraic equations were obtained in the previous steps and now the equations are solved by standard matrix techniques.

f. Secondary Computations: Pressures, Loads, Off-Body Velocity, Etc.

The solution of the matrix equation results in the singularity strengths and the velocity field and any secondary information can be computed now. The pressures will be computed by Bernoulli's equation, and the loads and aerodynamic coefficients by adding up the contributions of the elements.

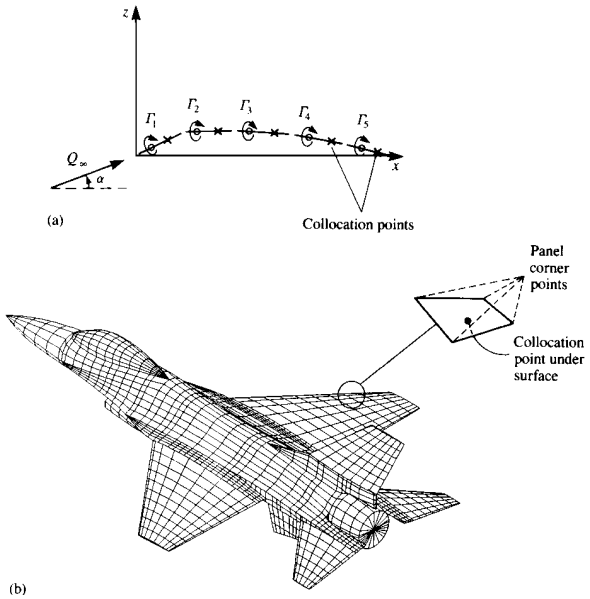

Figure 5.10 Discretization of (a) the geometry of a thin airfoil by using the lumped vortex element and of (b) a three-dimensional body using constant-strength surface doublets and sources.

In the following example, the essence of the above steps will be clarified.

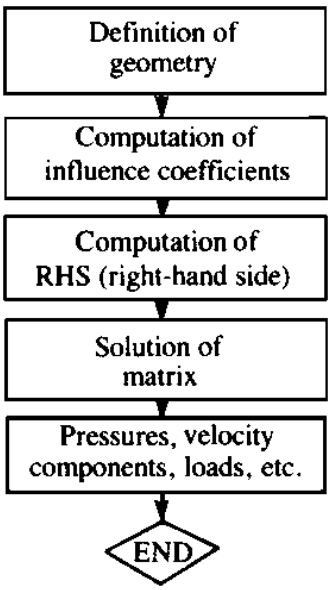

Figure 5.11 Typical flow chart for the numerical solution of the surface singularity distribution problem.

Example: Solution of Thin Airfoil with the Lumped-Vortex Element

As a first example for demonstrating the principle of numerical solutions, let us consider the solution for the symmetric, thin airfoil. Because the airfoil is thin, no sources will be used, while the doublet distribution will be approximated by two constant- strength doublet elements (μ1, μ2 pointing in the −z direction). This element is equivalent to two concentrated vortices at the panel edges (see Fig. 5.13). However, the geometry of the "lumped-vortex" model was developed, and by placing the vortex at the quarter chord and the collocation point at the three-quarter chord point of the panel the Kutta condition is automatically satisfied. Using this knowledge the equivalent discrete- vortex model (with only two elements) for the airfoil is shown in Fig. 5.13. Also, for the thin lifting surface only the Neumann (velocity) boundary condition can be used, because of the zero thickness of the airfoil. (Note that the doublet representation in Fig. 5.12 clearly indicates the existence of a starting vortex, also shown in Fig. 5.13, at a large distance behind the airfoil.)

a.Selection of Singularity Element

For this very simple example the lumped-vortex element is selected and its influence is derived in terms of the geometry involved. Such an element is depicted in Fig. 5.14a; it consists of a concentrated vortex at the panel quarter chord and a collocation point and

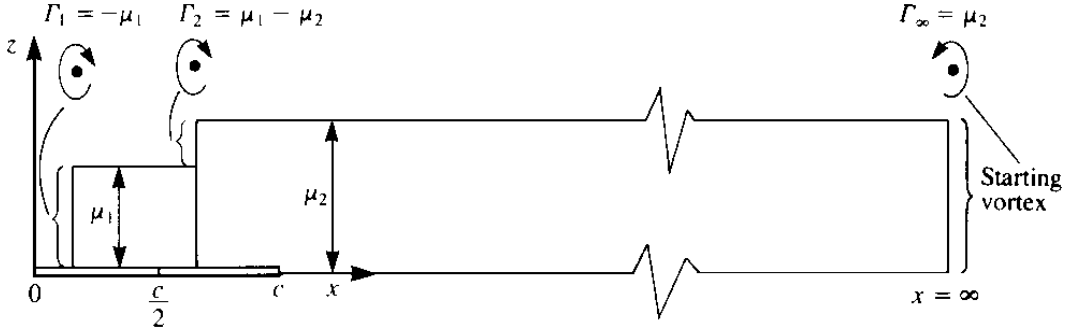

Figure 5.12 Constant-strength doublet element representation of the flat plate at an angle of attack (using two doublet panels pointing in the −z direction).

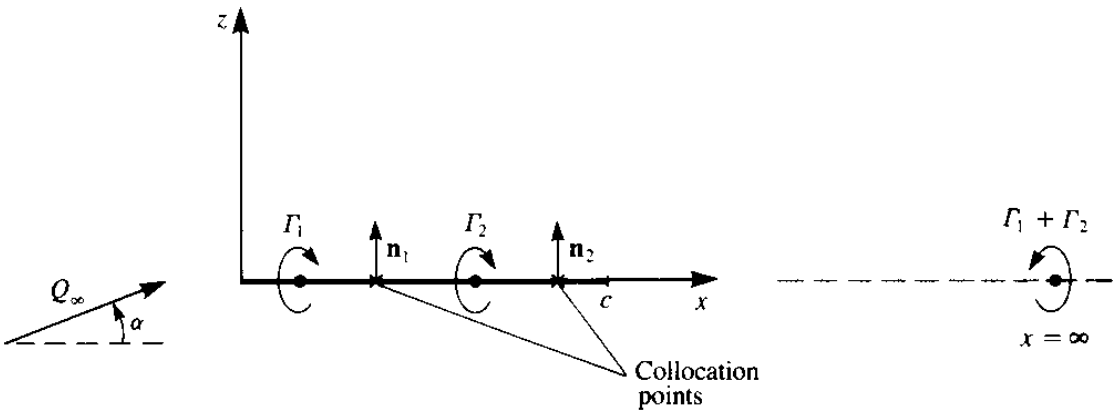

Figure 5.13 Equivalent discrete-vortex model for the flow over a flat plate at an angle of attack (using two elements).

normal vector n at the three-quarter chord. It is important to remember that this element is a simplification of the two-dimensional continuous solution and therefore accounts for the Kutta condition at the trailing edge of the airfoil.

If the vortex element of circulation T is located at (x0, z0), then the velocity induced by this element at an arbitrary point P(x, z), according to the analysis.

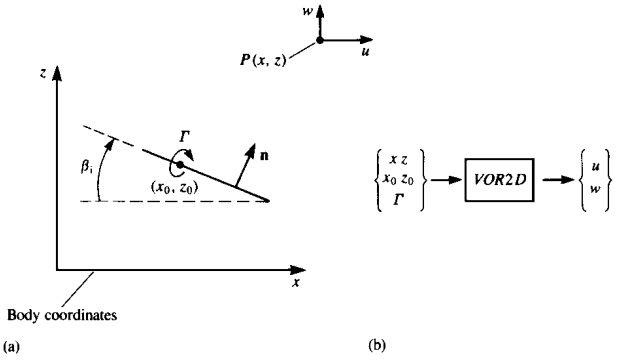

Figure 5.14 Nomenclature and flowchart for the influence of a panel element at a point *P*.

This can be programmed as an influence coefficient subroutine in the manner shown in Fig. 5.14b. Let us call this routine VOR2D.

$$(u, w) = \text{VOR2D}(T, x, z, x0, z0)$$

b. Discretization of Geometry and Grid Generation

For this example, the thin airfoil case is being solved (Fig. 5.17). For simplicity, only two elements will be used so that no computations are necessary. At this phase the geometrical information on the grid has to be derived. This can be automated by computer routines for more complex situations, but for this case the vortex point locations are

$$(x01, z01) = (c/8, 0)$$
$$(x02, z02) = (5c/8, 0)$$

and the collocation points are

$$(xc1, zc1) = (3c/8, 0)$$
$$(xc2, zc2) = (7c/8, 0)$$

The normal vectors n must be evaluated at the collocation points, and for an arbitrary element i we write

$$ni = (\sin \beta i, \cos \beta i)$$

where the angle βi is defined in Fig. 5.14a. In this particular case, when the airfoil has no camber and is placed on the z = 0 plane, both normals are identical:

$$n1 = n2 = (0, 1)$$

c. Influence Coefficients

Here the condition requiring zero velocity normal to the airfoil will be enforced.
This boundary condition, according to Equation, is

$$(q + Q\infty) \cdot n = 0$$

The velocity q is induced by the unknown vortices, whereas the free-stream normal com- ponent can be calculated directly and hence is moved to the right-hand side of the equation:

$$q \cdot n = -Q\infty \cdot n$$

Because, in this case, the airfoil was divided into two elements with two unknown vortices of circulation T1, T2, two equations based on the zero flow normal to the airfoil boundary condition will be derived at the collocation points. We define as positive T a clockwise rotation, and calculate the velocity induced by a unit strength vortex at point 1 on collocation point 1.

(u11, w11) = VOR2D(1.0, xc1, z c1, x01, z01)

and the velocity induced at collocation point 1, by a unit vortex at point 2, is

(u12, w12) = VOR2D(1.0, xc1, zc1, x02, z02)

The velocity induced at collocation point 2, by a unit vortex at point 1, is

(u21, w21) = VOR2D(1.0, xc2, z c2, x01, z01)

and the velocity induced at collocation point 2, by a unit vortex at point 2, is

(u22, w22) = VOR2D(1.0, xc2, z c2, x02, z02)

The influence coefficients aij are really the normal component of the flow velocity induced by a unit strength vortex element Tj at collocation point i

$$aij = qij\ (Tj = 1) \cdot ni$$

For the current problem, Equation is applied to collocation point 1 and to vortex point 1. Thus

$$a11 = (u11, w11) \cdot n1$$ similarly, for the second vortex, we have

$$a12 = (u12, w12) \cdot (0, 1)$$

and for the second collocation point, we get

$$a21 = (u21, w21) \cdot (0, 1)$$

Note that the left-hand side of Equation can be described now as

$$q \cdot n = a_{ij} T_j \quad \text{for} \quad i = 1, 2; j = 1,2$$

d. Establish RHS

The solution is based on enforcing the boundary condition of Equation at the collocation points. Since the product $Q\infty \cdot n$ is known it is transferred to the right-hand side of the equation:

$$q \cdot n = -Q\infty \cdot n \equiv RHS$$

It is useful to express the component of the free stream in vector form to allow easy vector operations; for this particular case the right-hand side (RHS) is

$$RHSi = -(U\infty, W\infty) \cdot ni$$

where $(U\infty, W\infty) = Q\infty(\cos \alpha, \sin \alpha)$. Computing the RHS vector for the two collocation points results in

$$RHS1 = -Q\infty \sin \alpha$$
$$RHS2 = -Q\infty \sin \alpha$$

e. Solve Linear Set of Equations

The results of the previous computations can be summarized as

$$a_{ij} T_j = RHSi \quad i = 1, 2; j = 1$$

and explicitly, for this particular case, which can be solved by standard matrix methods.

f. Secondary Computations: Pressures, Loads, Etc.

The resulting pressures and loads can be computed by using the Kutta–Joukowski theorem

$$6L_i = \rho\, Q\infty T_i$$

and by assuming a constant pressure distribution along the element, the pressure difference becomes

$$6p_i = \rho\, Q\infty T_i/a$$

where a is the panel length. The lift and moment about the airfoil leading edge are then non dimensional aerodynamic coefficients are sin α.

These results are similar to those for a zero-thickness symmetrical airfoil and equal to the exact flat plate solution. The method can easily be extended to various camber line shapes and even multi element lifting airfoils.

5.7 Accounting for Effects of Compressibility and Viscosity

The potential flow model presented in this chapter results in a very simple mathematical model that can be transformed into a very efficient and economical numerical solution. This led to the development of three-dimensional "panel codes" for arbitrary geometries, and naturally, modifications were sought to improve these methods beyond the limits of incompressible inviscid flows. Some of these modifications are listed here.

a. Effects of Compressibility

The first and most straightforward modification to an incompressible potential-flow based method is to incorporate the effects of "low-speed compressibility" (e.g., for $M\infty < 0.6$). This modification can be obtained by using the Prandtl–Glauert rule, as developed in Section 4.8. Thus, small-disturbance flow is assumed, and a compressibility factor β If the free stream is parallel to the x coordinate then the x coordinate is being stretched with increased Mach number while the y and z coordinates remain unchanged.

b. Effects of Thin Boundary Layers

When analyzing high Reynolds number flows in Section 5.8, it was assumed that the boundary layer is thin and that the boundary conditions are specified on the actual surface of the body. However, by neglecting the viscosity terms in the momentum equation, the information for calculating the viscous surface friction drag is lost too. It is possible to account for the viscosity effects such as displacement thickness and friction drag by using a boundary layer solution that can be matched with the potential-flow solution. Two of the most common methods for combining these two solutions are as follows.

The first approach is to use a boundary layer solution, usually a two-dimensional model along a streamline, which is quite effective for simple wings and bodies. The solution begins by solving the inviscid potential flow, which results in the velocity field and the pressure distribution. These data are fed into two-dimensional boundary layer solutions that provide the local wall friction coefficient and the boundary layer thickness. The friction coefficient can then be integrated over the body surface for computing the friction drag. If the displacement thickness effect is sought, then a second iteration of the potential flow computation is needed, but now with modified surface geometry. This modification can be obtained by displacing the body panels according to the local boundary layer displacement, and the procedure can be reiterated until a satisfactory solution is obtained.

The second approach to incorporate boundary layer solutions into panel codes is to follow the procedure described above, but to account for the displacement effects by a modification of the boundary conditions instead of a change of the surface geometry. In this case, at each panel the normal flow is given a certain blowing value that accounts for the local boundary layer displacement thickness δ. The formulation can be derived using the properties of the source distribution of Section 4.4, and the incremental "transpiration velocity" is simply added to the source strength obtained from the inviscid model. Here q is the local streamwise velocity component of the potential flow (outside the boundary layer) and the differentiation takes place along a streamlines. Note that as a result of the added transpiration velocity qni = 6σi , the normal velocity component on the actual surface of the body is nonzero.

c. Models for Wake Rollup, Jets, and Flow Separations

The vortices in the thin wake behind lifting wings tend to follow the local velocity induced by the lifting surface and its wakes. Consequently, the condition stated by results in the wake rollup. This condition causes the shape of the wake to be unknown when the boundary conditions for the potential flow are established. Traditionally, the shape of the wake is assumed to be known and after the solution is obtained, the validity of the initial wake shape can be rechecked. Two methods used by two panel codes will be presented to calculate the wake shape (VSAERO-wake relaxation and PMARC-time stepping). Since the wake is modeled by a doublet/vortex distribution, it is possible to extend this method for modeling jets and even shear layers of separated flows.

It was demonstrated in the previous chapters that the solution of potential flow problems over bodies and wings can be obtained by the distribution of elementary solutions. The strengths of these elementary solutions of Laplace's equation are obtained by enforcing the zero normal flow condition on the solid boundaries. In general, as the complexity of the method is increased, the "element's influence" calculation becomes more elaborate. Therefore, in this chapter, emphasis is placed on presenting some of the typical numerical elements upon which some numerical solutions are based. To calculate the induced potential and velocity increments at an arbitrary point P requires information on the element geometry and strength of singularity.